1-1-2010

Novel grain refinement of AZ91E magnesium alloy and the effect on hot tearing during solidfication

Abdallah Elsayed

NOVEL GRAIN REFINEMENT OF AZ91E MAGNESIUM ALLOY AND THE EFFECT ON HOT TEARING DURING SOLIDIFICATION

by

Abdallah Elsayed,

B.Eng, Ryerson University, 2008

A thesis

presented to Ryerson University

in partial fulfillment of

the requirements for the degree of

Master of Applied Science

in the Program of

Mechanical Engineering

Toronto, Ontario, Canada, 2010

AUTHOR'S DECLARATION

I hereby declare that I am the sole author of this thesis or dissertation.
I authorize Ryerson University to lend this thesis or dissertation to other institutions or individuals for the purpose of scholarly research.

_____

Abdallah Elsayed

I further authorize Ryerson University to reproduce this thesis or dissertation by photocopying or by other means, in total or in part, at the request of other institutions or individuals for the purpose of scholarly research.

_____

Abdallah Elsayed

Abdallah Elsayed

NOVEL GRAIN REFINEMENT OF AZ91E MAGNESIUM ALLOY AND THE EFFECT ON HOT TEARING DURING SOLIDIFICATION

Master of Applied Science

Mechanical Engineering

Ryerson University, Toronto, Ontario, Canada, 2010

ABSTRACT

Vehicle weight in the aerospace and automotive industries directly impacts carbon emissions and fuel efficiency. An increase in the use of lightweight materials for structural applications will result in lighter vehicles. Low density materials, such as magnesium (1.74 g/cm^3) are a potential alternative to aluminum (2.70 g/cm^3), to reduce component weight in structural applications.

However, current magnesium alloys still do not have adequate mechanical properties and castability to meet the performance specifications of the automotive and aerospace industries. Grain refinement can significantly improve mechanical properties and reduce hot tearing during permanent mould casting. Recently, Al-Ti-B based grain refiners have shown potential in grain refining magnesium-aluminum alloys such as AZ91E. This study investigates the grain refining efficiency and fading of Al-5Ti-1B and Al-1Ti-3B in AZ91E magnesium alloy and their subsequent effect on hot tearing.

The grain refiners were added at 0.1, 0.2, 0.5 and 1.0 wt.% levels. For the grain refinement and fading experiments, the castings were prepared using graphite moulds with holding times of 5, 10 and 20 minutes. For the hot tearing experiments, castings were produced representing the optimal addition level of each grain refiner. The castings were prepared using a permanent mould with pouring and mould temperatures of 720 and 180 °C, respectively. The castings were characterized using SEM, TEM, optical microscopy and thermal analysis.

For the Al-5Ti-1B grain refiner, the addition of 0.1 wt.% provided a 68 % reduction in grain size as compared to the unrefined AZ91E alloy at a holding time of five minutes. Grain growth restriction by TiB_2 particles was the source of grain refinement. With the addition of Al-5Ti-1B, only a small reduction in hot tearing susceptibility was observed because large $TiAl_3$ particles bonded poorly with the eutectic and blocked feeding channels.

The addition of 1.0 wt.% Al-1Ti-3B provided a grain size reduction of 63 % as compared to the unrefined AZ91E alloy at a holding time of five minutes. The grain refinement with Al-1Ti-3B addition was attributed to a combination of TiB_2 grain growth restriction and AlB_2 nucleating sites. A significant reduction in hot tearing susceptibility was observed with Al-1Ti-3B addition as a result of a higher cooling rate and shorter local solidification time as compared to the AZ91E alloy. The reduction in hot tearing susceptibility was attributed to the good interface between the eutectic and TiB_2 particles. Both grain refiners demonstrated a good resistance to fading during the holding times investigated. In addition, the AZ91E + Al-5Ti-1B and AZ91E + Al-1Ti-3B castings showed much fewer dislocation networks as compared to the untreated AZ91E casting.

The development of efficient Al-Ti-B refiners can also improve castability of magnesium alloys. In addition, the fade resistant Al-Ti-B grain refiners can reduce operating costs and maintain productivity on the foundry floor. Thus, magnesium alloys with Al-Ti-B treatment have the potential for more demanding structural applications in the automobile and aerospace industries.

ACKNOWLEDGEMENTS

First and foremost, I would like to thank my supervisor, Prof. C. (Ravi) Ravindran for his insightful guidance and instruction. His thoughtfulness helped me through my studies, as well as my day to day life.

I also have great appreciation for Prof. B.S. Murty and the Micro-Nano Research Group at IIT-Madras (Chennai, India) for material support and great hospitality during my research visit.

I would also like to thank the technical support staff at Ryerson University; in particular, Mr. Alan Machin, Mr. Joseph Amankrah and Mr. Qiang Li for their help with sample preparation and SEM analysis.

Further, I would like to thank Dr. Sophie Lun Sin, Mr. Francesco D'Elia and the other members of The Centre for Near-net-shape Processing of Materials for experimental help and technical discussion.

Finally, I would like to thank my family and friends for their continuous love and support during the past two years. Their constant encouragement helped me overcome the many challenges I faced throughout my study.

TABLE OF CONTENTS

Page

LIST OF TABLES

LIST OF FIGURES

Page

NOMENCLATURE

Symbol	Description	Units
Greek		
γ_{sl}	Interfacial tension of solid-liquid interface	J/m^2
ΔG_r	Change in free energy with nucleation	J
ΔG_v	Change in free energy of the liquid and solid in liquid (G_2-G_1)	J/m^3
π	Pi	
ΔT	Undercooling	°C
ΔG^*	Critical change in free energy with nucleation	J
γ_{ml}	Interfacial tension between the mould-liquid interface	J/m^2
γ_{sm}	Interfacial tension between the solid-mould interface	J/m^2
θ	Wetting angle	Degrees
σ_y	Yield strength	MPa
σ_o	Friction stress opposing the motion of a dislocation	MPa
δ	Planar disregistry	%
θ_d	Angle between two low index directions in (hkl)	Degrees
ε_b	Strain	m/m
α	Coefficient of thermal expansion	1/°C
ΔT_R	Temperature range of cooling from liquidus to solidus	°C
l	Length of hot spot	m
English		
G_2	Free energy of solid in liquid melt	J
V_s	Volume of solid	m^3
V_l	Volume of liquid	m^3
G_v^s	Free energy of the solid per unit volume	J/m^3
G_v^l	Free energy of the liquid per unit volume	J/m^3
A_{sl}	Surface area of the solid-liquid interface	m^2
G_1	Free energy of liquid	J
r	Radius of nucleus	m

r^*	Critical radius of nucleus	m
L_v	Latent heat of fusion per unit volume	J/m^3
T_m	Melting point of the liquid	°C
k_y	Unpinning constant	$Nm^{-5/2}$
d	Average grain size	µm
s and n	Representation of the substrate and the nucleated crystal, respectively	
(hkl)	Low index plane	
[uvw]	Low index directions in (hkl)	
$d_{[uvw]}$	Lattice spacing along direction [uvw]	nm
Q	Growth-restriction factor	K
m	Liquidus slope	K/wt.%
k	Equilibrium partition coefficient	wt.%/wt.%
C_o	Initial concentration of element	wt.%
a	Lattice parameter	nm
c	Lattice parameter	nm
L	Length of casting	m
t_V	Vulnerable time period when cracks can propagate between grains	s
t_R	Time available for liquid and mass flow	s
v	Degrees of freedom	

Elements

Mg	Magnesium
Al	Aluminum
Zr	Zirconium
Fe	Iron
Mn	Manganese
C	Carbon
O	Oxygen
Cl	Chlorine
Ni	Nickel
Si	Silicon
B	Boron
Ca	Calcium
Ti	Titanium
Y	Yttrium
Nd	Neodymium
Be	Beryllium
Sn	Tin
Zn	Zinc
V	Vanadium

Abbreviations

HCP	Hexagonal close-packed
SEM	Scanning Electron Microscopy
EDX	Energy Dispersive X-ray
CSC_b	Cracking-susceptibility coefficient
BSE	Back-scattered electron
TEM	Transmission Electron Microscopy
LST	Local solidification time
CR	Cooling rate
ANOVA	Analysis of Variance

CHAPTER 1 INTRODUCTION

The quest for increasing fuel economy and reducing carbon emissions in the automotive and aerospace industries has promoted the use of light weight materials such as magnesium (Mg). Magnesium has a density of 1.74 g/cm^3 [1], much lower than the density of aluminum (Al, 2.70 g/cm^3 [2]). A replacement of current Al components with Mg will result in lower vehicle weights and increased fuel efficiencies. Two major drawbacks to Mg alloys are their inadequate mechanical properties relative to Al alloys, and high susceptibility to hot tearing during permanent mould casting.

Grain refinement improves mechanical properties and increases feeding while reducing segregation, porosity and hot tearing [3]. A hot tear is an irreversible crack defect that occurs during the semi-solid stage of solidification as a result of thermal and mechanical stresses. Grain refinement can reduce hot tearing as fine grains during solidification provide more uniform mechanical properties, increased liquid metal feeding and a higher resistance to tear growth.

Numerous potential additions based on carbon, calcium and boron have been examined by previous researchers in hopes of finding an efficient grain refiner with a low tendency of fading. While carbon based additions show significant refinement, the poor wetability between the Mg melt and carbon particles makes addition difficult. Research conducted on other refiners such as calcium and boron do not examine fading and refiner effect on hot tearing susceptibility. In this study, the grain refining potential of two aluminum-titanium-boron based refiners was examined.

Objectives

The purpose of this study was to examine the effectiveness of using Al-5Ti-1B and Al-1Ti-3B for grain refinement and the effects of these grain refiners on reducing hot tearing susceptibility of AZ91E Mg alloy.

Outline of Thesis

To better organize the thesis, the literature review and results were split into two sections. An outline of the thesis is provided below:

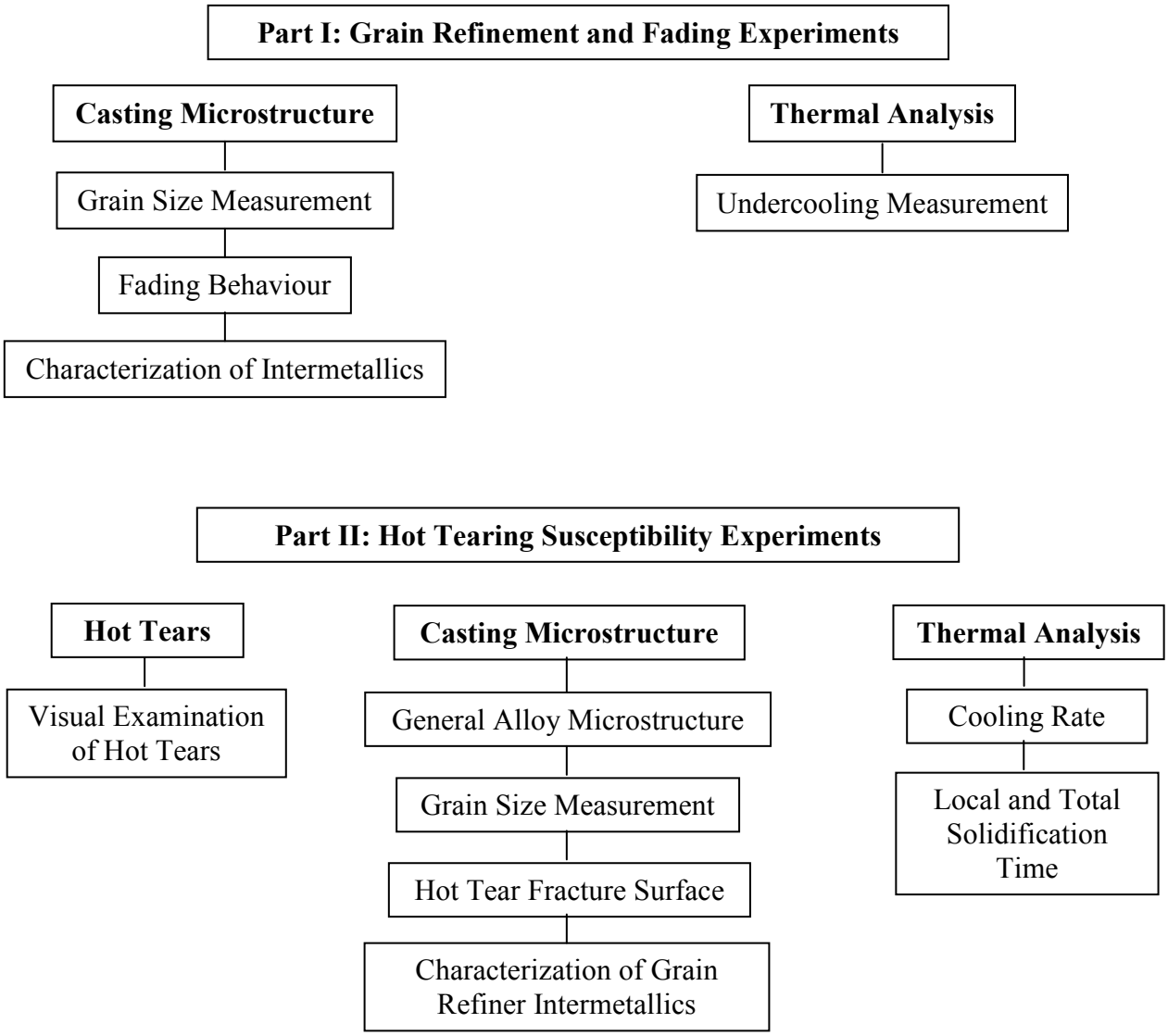
Part I: Grain Refinement and Fading Experiments
Casting Microstructure
Grain Size Measurement
Fading Behaviour
Characterization of Intermetallics
Thermal Analysis
Undercooling Measurement
Part II: Hot Tearing Susceptibility Experiments
Hot Tears
Visual Examination of Hot Tears
Casting Microstructure
General Alloy Microstructure
Grain Size Measurement
Hot Tear Fracture Surface
Characterization of Grain Refiner Intermetallics
Thermal Analysis
Cooling Rate
Local and Total Solidification Time

CHAPTER 2 LITERATURE REVIEW

There are two parts in this chapter. Part I outlines grain refinement of Mg alloys and Part II discusses hot tearing. Part I begins with a discussion on solidification of metals and alloys, as understanding of solidification is vital for any research regarding grain refinement. The closing sections of Part I discuss the principles of grain refinement and fading of Mg alloys free of and containing Al, respectively. The first sections of Part II include research relating to the formation of hot tears, and the chapter concludes with a methodology to reduce the occurrence of hot tears in Mg and Al alloys.

Part I: Grain Refinement of Mg Alloys

2.1 Nucleation of Metals and Alloys

The transformations of liquid metal with a non-crystallographic structure to a crystallographic structure are the first signs of solidification. The two types of nucleation processes possible to initiate solidification of a liquid metal are (1) homogeneous nucleation and (2) heterogeneous nucleation [4].

2.1.1 Homogeneous Nucleation

In homogeneous nucleation, the liquid metal solidifies by the clustering of small groups of atoms called nuclei. In many instances, the transformation of a pure liquid metal to a solid metal does not occur at a single temperature. The melt must be undercooled for the liquid to solid transformation to occur and this undercooling is the driving force for nucleation [4]. The nucleation of a solid is best understood using a diagram similar to Figure 2-1.

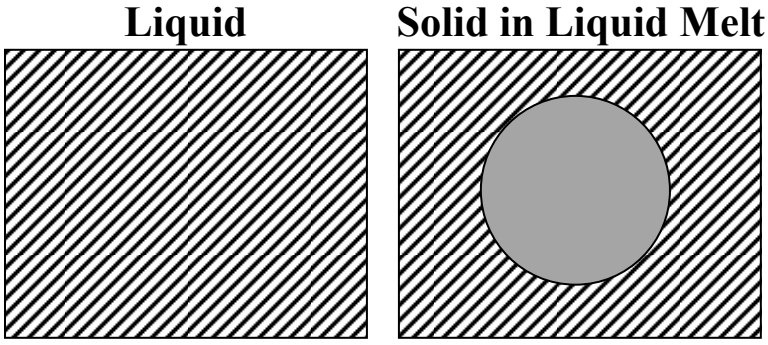

Figure 2-1: Homogeneous Nucleation A) Only Liquid B) Solid in Liquid Melt [4]

Nucleation processes play a key role in the solidification of castings. The beginning of solidification requires a free energy change. The free energy (G_2) of the system in Figure 2-1B can be described as [4]:

$$G_2 = V_s G_v^s + V_l G_v^l + A_{sl}\gamma_{sl} \quad \textbf{(1)}$$

Where:

V_s: Volume of solid

V_l: Volume of liquid

G_v^s: Free energy of the solid per unit volume

G_v^l: Free energy of the liquid per unit volume

A_{sl}: Surface area of the solid-liquid interface

γ_{sl} : Interfacial tension of the solid-liquid interface

The first term in Equation 1, ($V_s G_v^s$), represents the free energy of the solid particle while the second term, ($V_l G_v^l$), represents the free energy of the remaining liquid melt. The last term, ($A_{sl}\gamma_{sl}$), represents the free energy of the solid-liquid interface between the solid particle and the remaining liquid.

Assuming the densities of the liquid and solid are equal, the free energy (G_1) of the liquid (Figure 2-1A) can be expressed as [4]:

$$G_1 = (V_s + V_l)G_v^l \quad \textbf{(2)}$$

The change in free energy associated with nucleation is given by [4]:

$$\Delta G_r = G_2 - G_1 = V_s(G_v^s - G_v^l) + A_{sl}\gamma_{sl} = -V_s(G_v^l - G_v^s) + A_{sl}\gamma_{sl} = -V_s\Delta G_v + A_{sl}\gamma_{sl} \quad \textbf{(3)}$$

Assuming γ_{sl} is isotropic and r represents a spherical nucleus, Equation 3 becomes [4]:

$$\Delta G_r = -\frac{4}{3}\pi r^3 \Delta G_v + 4\pi r^2 \gamma_{sl} \quad \textbf{(4)}$$

Examination of Equation 4 shows that with increasing radius, the volume free energy change ($\frac{4}{3}\pi r^3 \Delta G_v$) tends to favour nucleation while the interfacial energy ($4\pi r^2 \gamma_{sl}$) tends to resist nucleation. A graphical representation of Equation 4 is shown in Figure 2-2.

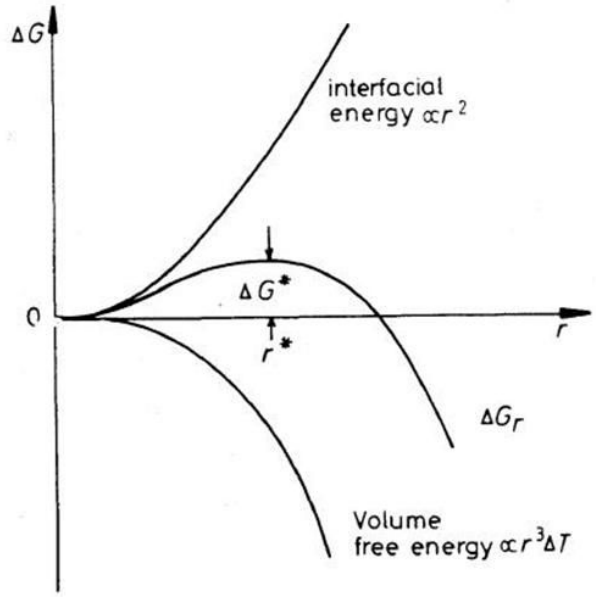

Figure 2-2: Free Energy Curve of Homogeneous Nucleation of Spherical Particle of Radius r [4]

For a given undercooling ΔT, there is a critical radius r^* associated with a maximum free energy ΔG^*. If $r < r^*$, the system lowers its energy by dissolving the embryo. If $r > r^*$, the free energy decreases if the solid grows [4].

The slope of the ΔG_r curve in Figure 2-2 is zero when the free energy of the system equals ΔG^*. By differentiating Equation 4, the critical radius (r^*) can be calculated as [4]:

$$r^* = \frac{2\gamma_{sl}}{\Delta G_v} \tag{5}$$

With a given undercooling (ΔT), ΔG_v is given by [4]:

$$\Delta G_v = \frac{L_v \Delta T}{T_m} \tag{6}$$

Where:

L_v: Latent heat of fusion per unit volume

T_m: Melting point of the liquid

Substitution of (ΔG_v) into Equation 5 (provided in Equation 7 [4]) shows that r^*, and subsequently ΔG^*, can be decreased by increasing the undercooling or by lowering the interfacial surface energy.

$$r^* = \left(\frac{2\gamma_{sl} T_m}{L_v} \right) \frac{1}{\Delta T} \tag{7}$$

2.1.2 Heterogeneous Nucleation

In practice, homogeneous nucleation rarely takes place because of the relatively large activation barrier required for nucleus formation. In heterogeneous nucleation, impurity particles or gaps (undulations) on the mould walls promote crystallization by lowering the activation barrier ΔG^* (reduction of the interfacial energy component of Equation 4). In practice, the dominant mode for nucleation is heterogeneous nucleation. Figure 2-3 depicts how heterogeneous nucleation takes place at a mould wall.

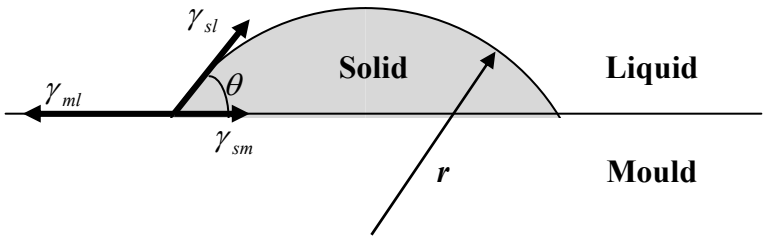

Figure 2-3: Heterogeneous Nucleation on a Mould Wall [4]

With the presence of an impurity particle (or mould wall gap), the critical radius (r^*) required for nucleation is much smaller. Equation 8 models heterogeneous nucleation using a surface tension balance between the solid-mould, mould-liquid and solid-liquid interfaces [4].

$$\gamma_{ml} = \gamma_{sm} + \gamma_{sl} \cos\theta \tag{8}$$

Where:

γ_{ml} : Interfacial tension at the mould-liquid interface

γ_{sm} : Interfacial tension at the solid-mould interface

γ_{sl} : Interfacial tension at the solid-liquid interface

θ : Wetting angle

Rearranging Equation 8 for $\cos\theta$ yields [4]:

$$\cos\theta = \frac{\gamma_{ml} - \gamma_{sm}}{\gamma_{sl}} \quad \textbf{(9)}$$

A mould wall with a small interfacial energy with the solid (low γ_{sm}) would require a small wetting angle to act as a good nucleating site.

2.2 Grain Refinement and Fading

Grain refinement improves mechanical properties and increases feeding while reducing segregation, porosity and hot tearing [3]. Proper selection of grain refiner for industrial use requires adequate grain refinement even at low addition levels and this refining effect must be maintained even with long holding times. In addition, the grain refiner must not adversely affect castability or corrosion resistance. The use of grain refinement is therefore very beneficial to improve the performance of cast products.

This section provides a description regarding how fine grains are able to improve mechanical properties followed by characteristics of good grain refiners. The end of this section closes with an alternative method to reduce grain size by restricting the growth of nucleated grains during solidification rather than providing a site for nucleation as described in Section 2.1.2.

With fine grains, dislocation motion is easily impeded by the large grain boundary area as compared to a coarse grained material. For many materials, the yield strength is a function of grain size [5,6]:

$$\sigma_y = \sigma_o + k_y d^{-1/2} \quad \textbf{(10)}$$

Where:

σ_y : Yield strength

σ_o : Friction stress opposing the motion of a dislocation

k_y : Unpinning constant (measure of to what extent dislocations pile-up at barriers)

d : Average grain size

Thus, a material with a fine grain structure is expected to have higher yield strength than a coarse grained material.

Inoculation involves the introduction of nucleating agents to a melt, either by adding a nucleus, or by generating the nucleus in the melt via a chemical reaction. Some of the characteristics of good grain refiners as outlined by Campbell [7] are:

1. Borides, carbides and intermetallic particles which form metallic or weak covalent bonds are more suitable as grain refiners rather than metal oxides which are strongly covalently bonded [8].
2. The nucleating solid and the grain refiner should have a good lattice match.
3. The grain refiner should not dissolve within the melt.

To determine if a metal/refiner combination results in a good lattice match as suggested by Campbell [7], Equation 11 can be used [9] to calculate the planar disregistry (δ) .

$$\delta_{(hkl)_n}^{(hkl)_s} = \frac{1}{3}\sum_{i=1}^{3} \frac{| d_{[uvw]_s^i} \cos\theta_d - d_{[uvw]_n^i} |}{d_{[uvw]_n^i}} \quad \textbf{(11)}$$

Where:

s and *n*: Representations of the substrate and the nucleated crystal, respectively

(hkl): Low index plane

[uvw]: One of the three low index directions in (hkl)

θ_d: Angle between two low index directions in (hkl)

$d_{[uvw]}$: Lattice spacing along direction [uvw]

A good lattice match would result in a low γ_{sm} that would reduce the wetting angle described in Equation 9. With a smaller planar disregistry, the grain refiner is expected to be a better nucleating particle. For the particle to act as a nucleating site, the planar disregistry should be less than 12 % [9]. Unfortunately, for accurate lattice matching studies, detailed information about the crystallography of the nucleating particles (lattice parameters, crystallographic form, habit plane, etc.) is required which can be difficult to obtain.

As mentioned by Campbell [7], the dissolution of a grain refiner within the melt shortly after addition is undesirable and indicates grain refiner fading. Fading is the loss of grain refiner efficiency after holding of the refiner in the melt for a long period of time. With increasing holding time the added grain refining particles tend to settle or float in the melt due to density

differences. The loss of grain refiner efficiency could also be the result of refining particles agglomerating together.

Another list of characteristics by Murty *et al.* [10] of inoculants to act as effective nucleating particles is as follows:

1. They should have a melting point higher than the alloy being solidified.
2. Sufficient number of nucleating particles should be uniformly distributed.
3. The nucleating particles should be larger than a critical size, which depends on the undercooling of the melt.
4. They should be able to initiate freezing at very small undercooling.

To quickly determine the grain refining efficiency of an added nucleant, cooling curves for the solidifying melt could be analyzed. By comparing the undercooling observed in the refined and un-refined castings, an indirect measure of grain refinement could be obtained. As discussed in Section 2.1.1, the critical radius (r^*) for nucleation could be reduced by increasing undercooling. Therefore, a grain refiner addition that results in a much smaller undercooling than the un-refined alloy would indicate that nucleation in the melt was easy. The relative amount of undercooling could be used as an indicator of grain refiner effectiveness [11].

Another method to enable grain refinement is to add solute elements into the melt that control the growth of the nucleated grains [12]. The added solute tends to diffuse to the solid-liquid interface and increase the concentration of solute elements at the interface. The additional solute builds a constitutionally undercooled zone that promotes solidification at a lower temperature as compared to low solute areas of the melt. The diffusion of solute elements slows down the solidification front and restricts grain growth. This phenomenon can be explained using the growth restriction factor (Q) obtained from binary phase diagrams. The growth restriction factor is defined as [13]:

$$Q = mC_o(k_i - 1) \tag{12}$$

Where:

m : Liquidus slope

k : Equilibrium partition coefficient

C_o : Initial concentration of the solute in the melt

Values of Q are additive for all the solutes in the melt [12]. The higher the value of Q, the higher will be the constitutional undercooling and, consequently, the smaller will be the grain size [13]. A comparison of the Q values of various elements in Mg melts is summarized in Table 2-1.

Table 2-1: Calculated *Q* for Different Solutes in Mg [13]

Solute	Type of System	Q at C_o (K)
Mn	Peritectic	0.32 at 2.01
Ca	Eutectic	6.1 at 1
Al	Eutectic	11.9 at 3
Zr	Peritectic	13.5 at 0.45
Ti	Peritectic	39.5 at 0.006

2.3 Grain Refinement of Mg Alloys Free of Al

A well known grain refiner for Mg alloys free of Al is zirconium (Zr). Zirconium has lattice parameters very similar to those of Mg. The typical lattice parameters for pure Mg and Zr are outlined in Table 2-2.

Table 2-2: Lattice Parameters of Mg and Zr [14].

Element	Structure	Lattice Parameters (nm)
Mg	HCP	a = 0.320 c = 0.520
Zr	HCP	a = 0.323 c = 0.523

A calculation of planar disregistry between Zr and Mg results in only 0.7 % using Equation 11 which is well below the suggested 12 % [9] threshold required for nucleation. Therefore, Zr is an excellent site for nucleation.

In Mg alloys containing Al, a reaction between Zr and Al occurs which nullifies the nucleating potential of Zr [15]. The result is the formation of a Al_2Zr phase as observed by Kabirian and Mahmudi [16] with the addition of Zr to AZ91 Mg-Al alloy. The presence of these particles leads to grain coarsening in the as-cast state but maintained grain sizes during aging because of the thermal stability of Al_2Zr.

Since many commercial Mg alloy systems utilize Al, an alternative grain refiner for Mg-Al alloys must be developed. The following section describes some of the benefits and shortfalls of grain refiners for Mg-Al alloys.

2.4 Grain Refinement of Mg Alloys Containing Al

Unlike Al alloys, where well established, reliable grain refiners are commercially available, a similar universally reliable grain refiner system does not exist for the range of Mg alloys [12]. As a result, numerous potential grain refiners have been developed for Mg-Al alloys and details about each are mentioned in Table 2-3.

Table 2-3: Summary of Grain Refinement Techniques for Mg-Al Alloys

Technique	Mechanism	Advantage/Disadvantage	References
Melt Superheating	Formation of Al-Mn-Fe or Al_4C_3 nucleating particles	**Advantage** • No external additions required **Disadvantage** • Higher energy costs	[12-14,17,18]
Hexachloroethane (C_2Cl_6) Addition	Formation of Al_4C_3 nucleating particles	**Advantage** • Very effective **Disadvantage** • Release of harmful fumes	[17,19,20]
Elfinal Process ($FeCl_2$) Addition	Formation of Al-Mn-Fe nucleating particles	**Advantage** • Very effective **Disadvantage** • Addition of Fe, which reduces corrosion properties	[3]
Carbon Based Grain Refiners (C, Al-C, Ni-C, Si-C)	Formation of Al_4C_3 nucleating particles	**Advantage** • Good wettability with Mg melt **Disadvantage** • Grain refiner production is tedious and difficult	[9,18,19,21-26]
Aluminum-Boron Additions (Al-B)	Addition of AlB_2 nucleating particles	**Advantage** • Effective at small additions **Disadvantage** • No information regarding its fading behaviour	[27]

Silicon Addition	Grain growth restriction	**Advantage** • Effective at small additions **Disadvantage** • Dissolution of Si is difficult in Mg	[28]
Strontium Addition	Unclear	**Advantage** • Effective at small additions **Disadvantage** • Expensive	[28]
Calcium Addition	Grain growth restriction	**Advantage** • Improves creep resistance **Disadvantage** • Reacts with Al to form Al_2Ca	[12,15,29,30]
Al-Ti Based Grain Refiners (Al-Ti-B, Al-Ti-C, Al-Ti-C-Y)	Addition of TiB_2, TiC nucleating particles that may also restrict grain growth	**Advantage** • Readily available **Disadvantage** • Presence of coarse $TiAl_3$ particles	[9,13,31-41]

The above table is a succinct outline of the known grain refinement techniques for Mg-Al alloys. A detailed discussion focusing on historical and newly-developed grain refining additions follows (Sections 2.4.1-2.4.5). With the exception of melt superheating, the grain refinement methods discussed in this thesis focus on additions made to the molten Mg. Other techniques such as ultrasonic vibration are not discussed because of its difficult application in the foundry.

2.4.1 Historical In-situ Carbon Based Grain Refiners

The historical in-situ carbon (C) based grain refiners introduce C into the melt by either melt superheating or hexachloroethane (C_2Cl_6) addition. The added C reacts with the Mg-Al alloy to form nucleating particles.

2.4.1.1 Melt Superheating

The grain refinement method by melt superheating is not fully understood and difficult to implement on a foundry scale. Melt superheating involves heating the melt to 150 to 260 °C above the liquidus temperature and holding the melt at this temperature for an extended period of time (to allow nucleation of refining particles) depending on crucible size and Al content [12]. It has been found that Al, iron (Fe) and manganese (Mn) are essential elements to maximize grain

refinement. With higher Al content, less holding time is required. After holding, the melt is rapidly cooled to the pouring temperature and poured. Extended time at the pouring temperature will result in grain coarsening [12]. The grain refinement is observed to be the result of the nucleation of Al-Mn-Fe compounds or aluminum carbide (Al_4C_3) particles [14]. The presence of C in the melt is believed to originate from the graphite or steel crucibles used for melting, but the theory describing its formation is not clear [13].

Research conducted by Motegi [18] used a AZ91E melt, superheated to 850 °C for 900 s and cooled to a pouring temperature of 600 °C at a rate of 2.5 °C/s. The superheat-treated casting showed a finer grain size than the untreated melt. Aluminum carbide particles were found in the center of grains and on occasion Al-C-O bearing particles as well. The Al-C-O particles could have formed by a reaction of Al_4C_3 and water during polishing, according to Equation 13 [18].

$$Al_4C_{3(s)} + 12H_2O_{(l)} \rightarrow 4Al(OH)_{3(s)} + 3CH_{4(g)} \quad \textbf{(13)}$$

Another possibility is that the Al-C-O bearing particles could be Al_2OC that formed according to Equation 14 [17] with the source of Al_2O_3 being from melt oxidation. However, the formation of Al_2OC by the reaction of Al_4C_3 and Al_2O_3 is not possible in Mg melts with Al concentrations lower than 10 at.% [17], which is the case for AZ91E. Therefore, the possibility of the Al-C-O bearing particles being Al_2OC is low.

$$Al_4C_{3(s)} + Al_2O_{3(s)} \rightarrow 3Al_2OC_{(s)} \quad \textbf{(14)}$$

Two major problems with melt superheating are the added operational costs and more complex handling procedure which make melt superheating difficult to implement on the foundry floor.

2.4.1.2 Hexachloroethane (C_2Cl_6) Addition

Current foundry practice utilizes C_2Cl_6 addition for the grain refinement of Mg-Al alloys. Kumar and Mahanty [19] investigated the effect of C_2Cl_6 addition on the grain size of an Mg-0.5 wt.% Al alloy. The C_2Cl_6 was added at 780 °C and the metal was poured into a graphite mould preheated to 300 °C. The grain size reduction with C_2Cl_6 addition can be seen in Figure 2-4. The results show that only small additions are required for significant refinement. The optimal addition level to minimize grain size was found to be 0.01 wt.% C_2Cl_6, which

resulted in a grain size reduction from 800 to 400 µm (50 % reduction) in the base alloy and C_2Cl_6 treated melts respectively.

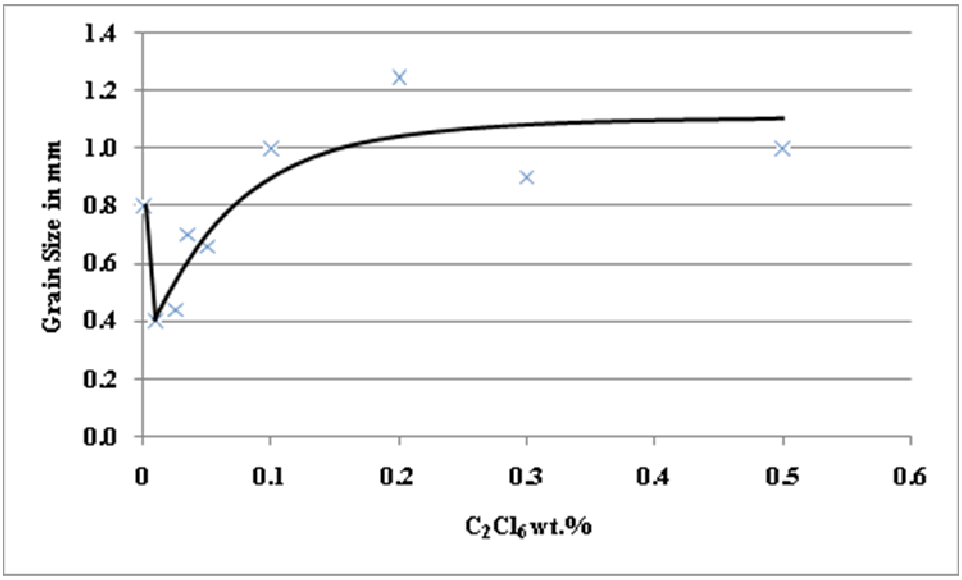

Figure 2-4: Effect of C_2Cl_6 on the Grain Size of Mg-0.5 wt.% Al Alloy [19]

Schwam and Zhu [20] also used melt superheating, in addition to C_2Cl_6 addition, to grain refine AZ91E and AM50A. The Mg alloys were heated to 732 °C, and 0.2 wt.% C_2Cl_6 was plunged into the bottom of the melt using a bell plunger. The Mg alloys were then superheated to 787 °C and held at this temperature for 360 s. The melt was quickly cooled to 732 °C and poured into a permanent mould preheated to 204 °C. With the combined superheat and C_2Cl_6 treatments, the grain size reduced from 330 to 55 µm (83 % reduction) in the AZ91E alloy while only a grain size decrease from 40 to 34 µm (15 % reduction) occurred in the AM50A alloy.

When the C_2Cl_6 was added to the molten Mg-Al alloy, the following reactions occurred [17,20]:

$$C_2Cl_{6(s)} \rightarrow 2C_{(s)} + 3Cl_{2(g)} \quad \textbf{(15)}$$

And at 705 °C,

$$4Al_{(l)} + 3C_{(s)} \rightarrow Al_4C_{3(s)} \quad \textbf{(16)}$$

Unfortunately, the addition of C_2Cl_6 releases dangerous chlorinated hydrocarbons that are harmful to the environment and foundry operators. It is therefore necessary to develop an alternative non-toxic grain refiner. There is extensive published research on grain refinement of

Mg-Al alloys using C_2Cl_6 and it is often used as a benchmark to assess the effectiveness of other grain refiners.

The addition of C_2Cl_6, while effective, is dangerous on the foundry floor. It is then essential to produce a safer, more environmentally friendly grain refiner that can produce the same level of refinement without the release of harmful fumes.

2.4.2 Newly Developed In-situ and Ex-situ Carbon Based Grain Refiners

The ex-situ method of carbon grain refinement involves synthesizing the grain refining particles in a separate alloy and then adding them to the Mg-Al alloy melt. Studies using aluminum-carbon (Al-C) and silicon-carbon (Si-C) alloys are examples of an ex-situ method of carbon grain refinement. Newly developed in-situ methods use C alone or a nickel-carbon (Ni-C) alloy to introduce C into the melt for grain refinement. This section begins with a discussion regarding additions containing carbon or aluminum-carbon (Al-C) then follows with nickel-carbon (Ni-C) additions. Finally, silicon-carbon (Si-C) additions are discussed.

2.4.2.1 Aluminum-Carbon (Al-C) or Carbon Only Grain Refiners

The superheating method (Section 2.4.1.1) and hexachloroethane addition (Section 2.4.1.2) promote the formation of Al_4C_3 particles which act as nucleating particles for Mg grains but are difficult to implement on a foundry scale. Therefore, many researchers such as Guang *et al*. [23], Qian and Cao [26], Motegi [18] and Lu *et al.* [9] developed grain refiners containing Al_4C_3 particles to reduce the grain size of Mg-Al alloys. Qian and Cao [26], Motegi [18] and Lu *et al.* [9] used direct carbon inoculation in order to produce the Al_4C_3 particles while Guang *et al.* [23] developed a Al-1C grain refiner using powder metallurgy. Due to the poor wettability between Al and C and uncontrollable graphite absorption, addition of C to liquid Al was not practical. In the study by Guang *et al.* [23], C and Al powders were ball milled and pressed into 57 mm columns. The grain refiner was then sintered at 710-730 °C for 1-2 h. The microstructure of the grain refiner using optical microscopy is shown in Figure 2-5. The Al-1C grain refiner contained solid Al with layers of Al-C solid solution and Al_4C_3 at the grain boundaries. The formation of the Al_4C_3 is governed by Equation 16.

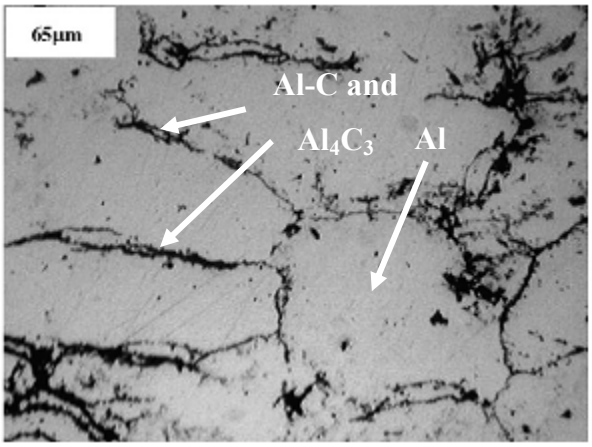

Figure 2-5: Al-1C Grain Refiner [23]

The Al-1C grain refiner was added to AZ31 at 760 °C at addition levels of 1 and 2 wt.%. To isolate the effects of C, additional castings with 1 and 2 wt.% pure Al addition were prepared and compared to the Al-1C treated castings. Without Al-1C grain refiner addition, the grain size of the AZ31 alloy was 580 µm. With an additional 1 and 2 wt.% Al, the grain size decreased to 460 µm (20 % reduction) and 400 µm (31 % reduction) respectively. With the addition of 1 and 2 wt.% Al-1C grain refiner, the grain size decreased to 230 and 140 µm (50 % and 65 % reduction respectively, compared to samples with extra 1 and 2 wt.% Al).

In the study by Qian and Cao [26], the addition of 0.6 wt.% graphite powder directly to Mg and Mg-3Zn did not yield any grain refinement, while the same 0.6 wt.% addition to Mg-3Al showed grain refinement from 400 to 170 µm (58 % reduction) in the base and refined samples respectively. The study by Motegi [18] showed that an optimal addition of 0.06 wt.% C to AZ91E at 750 °C reduced the grain size from 300 to 75 µm (75 % reduction). The study by Qian and Cao [26] illustrated that the Mg alloy must contain Al inorder for C inoculation to provide grain refinement.

The Al_4C_3 particles acted as effective nucleating sites because of their similar lattice geometry to that of Mg as outlined in Table 2-4. Unfortunately, the detection of Al_4C_3 particles at the center of Mg grains is difficult because Al_4C_3 tends to react with water used during sample preparation according to Equation 13. A calculation of planar disregistry between Mg and Al_4C_3 using Equation 11 yields a value of 4.06 % [9], which is well below the upper limit of 12 %. The results indicate that Al_4C_3 is a very effective grain refiner for Mg-Al alloys.

Qian and Cao [26] and Motegi [18] also detected Al-C-O based particles (suggested to be Al_2OC) after carbon inoculation and believed that Al_2OC may also be responsible for grain refinement do to the similar lattice geometry to Al_4C_3 and Mg. The lattice geometry of Al_2OC is also included in Table 2-4. As discussed in Section 2.4.1.1, the Al-C-O bearing particles are actually $Al(OH)_3$ particles that formed as a result of sample contact with water during polishing. The Al-C-O particles were also observed by Lu *et al.* [9] and were considered to have formed because of a reaction with water.

Table 2-4: Lattice Parameters of Mg, Al_4C_3 and Al_2CO [26]

Substance	Crystal Structure	Lattice parameter	
		a (nm)	c (nm)
Mg	Hexagonal	0.320	0.520
Al_4C_3	Rhombohedral, but indexed in a hexagonal unit cell	0.333	0.250
Al_2CO	Hexagonal	0.317	0.508

Guang *et al.* [23] and others demonstrated that effective alternative grain refiners avoiding hexachloroethane can be developed. The reason as to why carbon inoculation has not replaced current hexachloroethane addition is because of conflicting experimental observations with regards to [19]:

1. The amount of inoculant required for grain refinement.
2. The temperature at which the inoculation should be carried out.
3. The time of holding to ensure a uniform dispersion of the nucleating particles.

The conflicting experimental observations and uncertainty in their grain refinement mechanisms warrants the development of alternative grain refiners.

2.4.2.2 Nickel-Carbon (Ni-C) Grain Refiner

A common criticism of carbon inoculation is the difficulty in controlling the carbon content because of the low wettability of C in Mg melts [21]. As previously mentioned in Section 2.4.2.1, many researchers developed Al-C based grain refiners for a better control of C addition. The study by Ding and Liu [21] utilized a Ni-1.6 wt.% C grain refiner to gain an

improved control of C addition owing to high dissolution of C in nickel (Ni). The Ni was to act as a carrier to introduce C into the Mg melt.

The Ni-1.6 wt.% C grain refiner was prepared using pure graphite and Ni. The Ni and C were heated to 1500 °C and held at this temperature for 30 minutes. Two different preparation procedures were used for the grain refiner. One procedure allowed the grain refiner to solidify slowly in the furnace (slowly solidified grain refiner). The other procedure required the grain refiner to be blown into a copper mould and solidified rapidly (rapidly solidified grain refiner). In the slowly solidified grain refiner the graphite was seen as graphite flakes, approximately 5-10 μm long within the Ni matrix. In the rapidly solidified grain refiner, the graphite was seen as nodularized particles approximately 1-6 μm in diameter.

Both Ni-1.6 wt.% C grain refiners were added to a Mg-3 wt.% Al alloy at 760 °C which had an un-refined grain size of 260 μm. The grain refiner was held in the Mg-3 wt.% Al melt for 1.5 hours to ensure complete dissolution. The melt was poured into a cylindrical steel mould.

The grain size results are summarized in Table 2-5.

Table 2-5: Summary of Grain Size Measurements with Ni-C Grain Refiner Addition [21]

Condition	Grain Size (μm)
Mg-3 wt.% Al	260
Mg-3 wt.% Al + 1 wt.% Ni	290 (base point)
Mg-3 wt.% Al + 1 wt.% (Ni-1.6 wt.% C) flaky-graphite	170 (41 % reduction)
Mg-3 wt.% Al + 1 wt.% (Ni-1.6 wt.% C) nodular-graphite	110 (62 % reduction)

With scanning electron microscopy (SEM) analysis, Ni-Al based particles with trace amounts of C and O were observed within the Mg grains. It is unlikely that a Ni-Al particle was the nucleant because of the dissimilar lattice structure to Mg. Ding, and Liu [21] suggested that Ni would dissolve into the melt, releasing C that combines with Al to form Al_4C_3 particles (Equation 16). The nodular-graphite grain refiner was more effective than the flaky-graphite grain refiner because the former contained smaller, more uniform shaped particles that would distribute themselves easily while being resistant to agglomeration. The flaky-graphite grain refiner had a coupled eutectic structure which resulted in long, chained particles while the nodular-graphite grain refiner had a divorced structure that resulted in small, circular particles.

The detection of the Al_4C_3 particles was difficult because of the high reactivity of Al_4C_3 with water according to Equation 13.

The study by Ding and Liu [21] was very novel in finding an alternative carrier to better introduce C into the melt without using Al. Unfortunately, the added Ni reacted with Al to form unwanted Ni-Al particles that may be harmful to the mechanical properties of the Mg alloy despite the grain refinement observed.

2.4.2.3 Silicon-Carbon (Si-C) Grain Refiner

Silicon carbide addition has also been identified as an effective nucleating particle for Mg grains. The research conducted by Easton *et al.* [22] used SiC particle addition to grain refine Mg-Al alloys with concentrations of 1, 2, 3, 6 and 9 wt.% Al. The planar disregistry (Section 2.2) between Mg and SiC is only 4 % [25].

The Mg-Al melts were prepared in a steel crucible at 700 °C and the SiC was added via a Mg-0.15 wt.% SiC alloy. The melt was stirred vigorously and then held for five minutes before a sample was poured into a steel mould preheated to 200 °C. Another 0.15 wt.% SiC was added to the same melt, for a total of 0.3 wt.% SiC and once again stirred, held for five minutes and poured into a steel mould preheated to 200 °C.

The results indicated that SiC is a good grain refiner for Mg melts with low Al content. To maintain comparison with the current study on AZ91E which has a nominal Al concentration of 9 wt.%, the focus of the results will be the effect of SiC addition on the Mg-9 wt.% Al alloy. The un-refined alloy had a grain size of 130 μm. With 0.15 wt.% SiC, the grain size decreased to 100 μm (23 % reduction) while with 0.30 wt.% SiC, the grain size further decreased to 83 μm (36 % reduction). With the addition of SiC there were also clusters of Mg_2Si at the grain boundaries. It is believed that the SiC particles reacted with the Al in the melt to form a Al_4C_3 layer that acted as a nucleating particle [9]. The reaction would occur according to Equation 17. The observation of Al_4C_3 particles was not seen most likely because of the dissolution of the particles upon contact with water [22].

$$3SiC_{(s)} + 4Al_{(l)} \rightarrow Al_4C_{3(s)} + 3Si_{(s)} \quad \textbf{(17)}$$

The released Si would react to form the Mg_2Si particles observed at the grain boundary regions. The addition of SiC showed to be a moderately effective nucleating particle for Mg-9 wt.% Al, but the explanation about SiC reacting with Al to form Al_4C_3 leads the authors to

believe that a more substantial grain refining effect would be achieved if the Al_4C_3 particles were added directly into the melt.

A study conducted by Liu *et al.* [24] was similar to the study by Easton *et al.* [22] where SiC powders were used for grain refinement, but unlike the study by Easton *et al.* [22] the SiC powders would not react with Al contained within the Mg alloy to form Al_4C_3 particles. Instead a grain refiner that already contained the Al_4C_3 was developed using SiC powders. Silicon carbide powders (10 µm) were added to liquid Al at 950 °C in a medium frequency induction furnace. The Al-SiC mix was held at 950 °C for 15 minutes, then air cooled to 750 °C with mechanical stirring and finally poured into a permanent mould.

The grain refiner was added to AZ31, AZ63 and AZ91 Mg alloys for comparison. The effects of the Al-SiC-Al_4C_3 grain refiner on the grain size of AZ31 are presented in Figure 2-6. An equivalent amount of Al was also added to the AZ31 alloy for comparison.

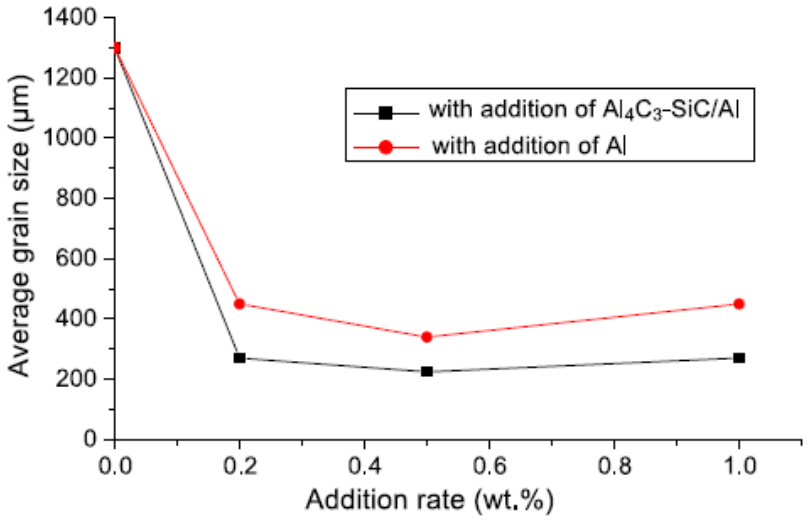

Figure 2-6: Influence of Al_4C_3-SiC/Al and Al on the Average Grain Size of AZ31 [24]

The average grain size decreased from 450 µm to approximately 270 µm (40 % reduction, compared to Al enriched sample) with just 0.2 wt.% addition of the Al-Al_4C_3-SiC grain refiner. The results also suggested that the additional Al content aids in grain refinement but is not the only factor in reducing the alloy grain size. With the addition of 0.5 wt.% Al-Al_4C_3-SiC grain refiner to AZ63, the grain size decreased from 300 to 200 µm (33 % reduction) and further decreased to 180 µm at an addition level of 1.0 wt.%. However, almost no variation of average

grain size was observed in the AZ91 alloy with the addition of 0.5 wt.% or even 1 wt.% of the grain refiner [24]. The transformation of SiC particles to Al_4C_3 was governed by Equation 17 and reported to occur at temperatures above 850 °C [24]. Using EPMA, Liu *et al.* [24] determined that the phase responsible for nucleation was a combination of Al_4C_3 and Si at the surface of the SiC particles [24].

The grain refinement was attributed to heterogeneous nucleation of Mg by Al_4C_3 particles. With further addition of grain refiner, the grain size remained relatively constant as observed in Figure 2-6. This may be a result of the latent heat of crystallization. When a relatively small number of grains appear in the melt as a result of heterogeneous nucleation, the latent heat released would not significantly raise the melt temperature. When a large number of grains begin to form as a result of excess grain refiner addition, the latent heat can significantly increase the local melt temperature and remelt some of the newly formed nuclei. The result is a levelling off of grain refinement with excess grain refiner addition [24]. The levelling off of grain refinement is a phenomenon common to all grain refiners that promote heterogeneous nucleation. The results of Liu *et al.* [24] show that further work is required to improve the efficiency of Al_4C_3-SiC/Al grain refiners to better refine AZ91 and other high Al content Mg alloys.

2.4.3 Aluminum-Boron (Al-B) Grain Refiner

Grain refiners utilizing KBF_4 salt have been developed to determine if an Al-B based grain refiner, containing AlB_2 particles were capable of acting as sites for nucleation in Mg-Al alloys. One study by Suresh *et al.* [27] consisted of adding an Al-4B grain refiner to AZ91 Mg alloy to observe any reduction in grain size and any increases in strength and ductility.

The experimental procedure consisted of adding the Al-4B grain refiner to AZ91 at 740 °C and stirring the melt for 10 minutes to allow for reaction of the Mg alloy and the added grain refiner [27]. The melt was then poured into cast iron moulds preheated to 300 °C.

The major results concerning grain size and mechanical properties are shown in Table 2-6. With increasing Al-4B grain refiner addition the grain size decreased. The optimal addition level to minimize grain size was 0.032 wt.% boron (B) with a grain size decrease from 100 μm to 30 μm (70 % reduction). At the optimal addition level (0.032 wt.% B), the yield strength increased from 95 to 110 MPa, the tensile strength improved from 180 to 226 MPa and the ductility rose from 3.3 to 4.8 % as compared to the base AZ91 alloy.

Table 2-6: Grain Size and Mechanical Properties with the Addition of Al-4B to AZ91 [27]

Alloy	Grain Size (µm)	Yield Strength (MPa)	Tensile Strength (MPa)	Ductility (% Elongation)
AZ91	100	95	180	3.3
AZ91 + 0.008 wt.% B	70	102	197	3.9
AZ91 + 0.02 wt.% B	45	107	211	4.4
AZ91 + 0.032 wt.% B	30	110	226	4.8
AZ91 + 0.04 wt.% B	30	113	229	4.9

The AlB_2 particles appeared as blocky structures approximately 4-8 µm in size. These particles were found in the centers of grains indicating their ability to act as sites for heterogeneous nucleation (Figure 2-7). The AlB_2 particles also met the necessary requirements to act as good nucleating particles such as [10,26]:

1. Similarity between the crystal structures of the base material and grain refiner.
2. Non-dissolution of the grain refining particle in the liquid base material.

The lattice parameters of pure Mg are a = 0.320 nm and c = 0.520 nm, while those of AlB_2 are a = 0.301 nm and c = 0.325 nm. Also, AlB_2 has a resistance to fading because the melting point of AlB_2 is 892 °C, well beyond the typical holding temperatures of Mg alloys (650 to 750 °C) [27].

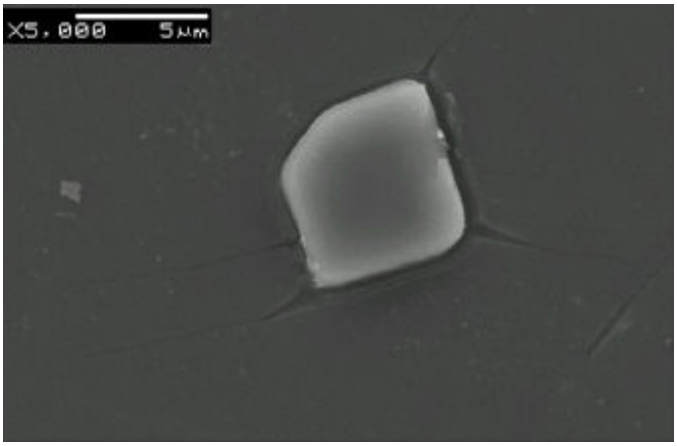

Figure 2-7: AlB_2 Particle in AZ91 Casting (0.032 wt.% B) [27]

The AlB_2 particle addition resulted in significant grain refinement of AZ91 Mg alloy without sacrificing strength and ductility. Unfortunately, during this study the effect of holding time on the grain refining ability of AlB_2 was not considered, and holding time needs to be studied with industrial application in view.

2.4.4 Grain Refinement by Calcium Addition

The effect of calcium (Ca) addition to Mg-Al melts is of particular interest to researchers because Ca provides a high constitutional undercooling at the advancing solid-liquid interface during solidification [12,15]. Traditionally, Ca addition has been used to promote the formation of Al_2Ca, an intermetallic particle that effectively pins grain boundaries and improves the creep resistance of Mg-Al alloys [42,43].

A study by Du *et al*. [29] utilized a Al-15 wt.% Ca grain refiner to refine an Mg-3Al alloy. The Mg-3Al alloy was prepared using commercially pure Mg and Al and the Al-15 wt.% Ca grain refiner was stirred into the melt for one minute at 750 °C. With increased Ca concentration, the grain size continually decreased. The smallest grain size observed using 0.5 wt.% Ca was 160 μm as compared to 520 μm in the unrefined alloy (69 % reduction). The source of the grain refinement was attributed to the high segregating power of Ca. In the same study Du *et al.* [29] added a combination of Ca and C to try to further decrease the as-cast grain size. The smallest grain size was observed using 0.2 wt.% C and 0.2 wt.% Ca. The grain size decreased from 520 to 110 μm (78 % reduction) in the refined and un-refined castings respectively. The authors observed Al-C-O particles similar to others [18,26] and also observed Al-C-O-Ca particles within the casting. As previously discussed in Section 2.4.1.1 the formation of the Al-C-O particles could be a two step reaction of C and Al to form Al_4C_3 and then a reaction of Al_4C_3 and oxygen (O, from water used during grinding/polishing) to form the Al-C-O particle. The possibility that the Al-C-O particle being Al_2CO is low because the Al content is below 10 at.% which was required for its formation [17]. Du *et al.* [29] provided three possible explanations for the formation of the Al-C-O-Ca particles:

1. A quaternary compound of Al, C, O and Ca could have formed all at once.
2. The Al-C compound could have formed first and became absorbed onto the Al-Ca compounds.

3. Carbon could have reacted with the surface of the Al-Ca particles to form the Al-C-O-Ca particles.

The authors indicated that the most probable formation route was either the second or third mechanism. An SEM image and corresponding EDS spectra of the Al-C-O-Ca particle shown in Figure 2-8 helps justify their reasoning. In either mechanism, the added Ca and C tended to react with each other, possibly reducing the potency of C, Ca or both. The results of Ca addition alone and a combined C and Ca addition look promising, although further research is required to determine the effects of the Al-C-O-Ca intermetallics.

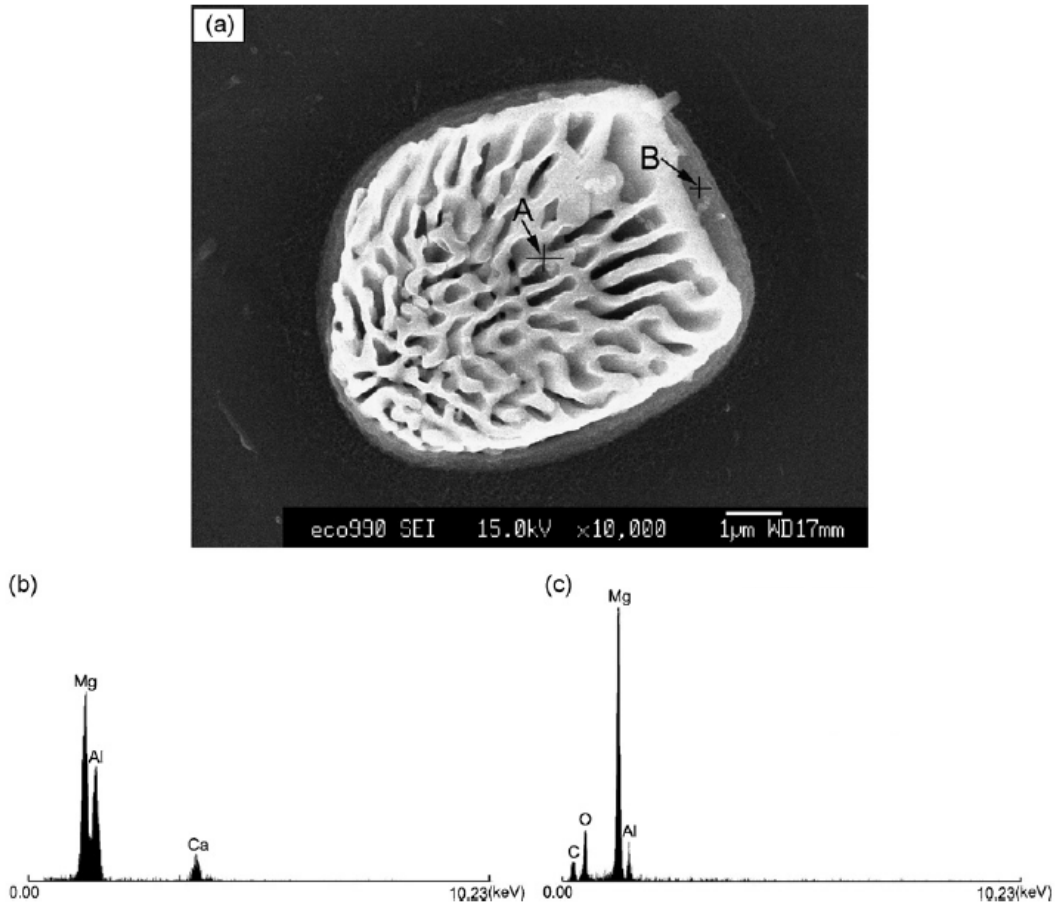

Figure 2-8: a) High Magnification SEM Image of Al-C-O-Ca Intermetallic Particle b) EDS Spectra Measured for an Inner Part (denoted by A) c) and an Outer Part (denoted by B) [29]

The effect of Ca addition on the microstructure and mechanical properties of AZ91D with Ca additions was studied by Li *et al.* [30] in a separate study. The addition of Ca produced Al_2Ca

particles at the grain boundaries and refined the grain size by grain growth restriction. The addition levels investigated were 0.1, 0.3, 0.5, 0.8 and 1.0 wt.% Ca. With increasing Ca addition the grain size continually decreased. The smallest grain size observed was 14.5 μm using 1.0 wt.% Ca as compared to 21 μm in the unrefined alloy (30 % reduction). The Ca was added as a Mg-30 wt.% Ca grain refiner at 730 °C and stirred for two minutes.

Despite the decrease in grain size, the grain refined castings had lower mechanical properties than the unrefined AZ91D. The results are shown in Figure 2-9. The addition of Ca to AZ91D had a two-fold effect. The increase in yield strength is attributed to grain refinement. However, the presence of brittle Al_2Ca particles at the grain boundaries is cited as the source of the decrease in ultimate tensile strength and elongation. With its drawbacks, Ca addition would be unsuitable for the foundry industry.

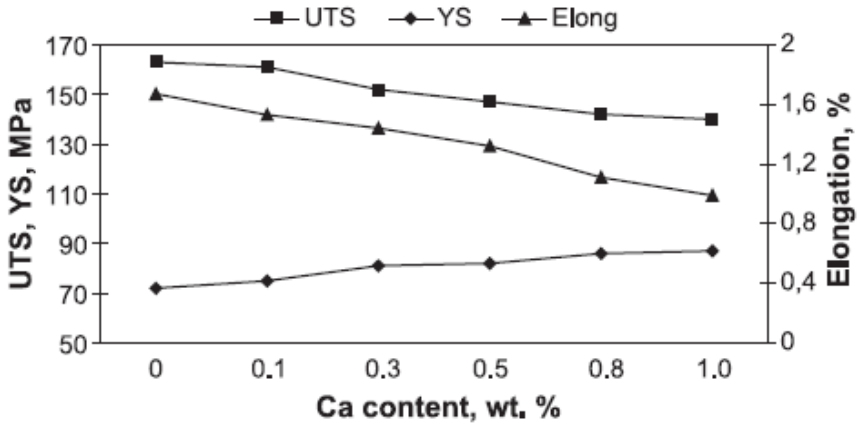

Figure 2-9: Tensile Properties of AZ91D with Different Ca Contents [30]

2.4.5 Aluminum-Titanium Based Additions

This section summarizes research conducted using Al-Ti based additions. The grain refiners have an Al matrix and titanium (Ti) is added in concentrations ranging from 1 to 5 wt.%. Section 2.4.5 begins by describing the effect of Al-Ti additions containing B or C on Mg-Al alloys. Furthermore, studies on Al-Ti-B-C based grain refiners are also discussed and this section concludes with a novel Al-Ti-C-Y grain refiner.

2.4.5.1 Aluminum-Titanium-Boron (Al-Ti-B) Grain Refiners

The literature on the use of Al-Ti-B grain refiners in Mg melts is limited. Fortunately, there is extensive knowledge on the use of Al-Ti-B based grain refiners in Al alloys. As reported by

Vinod Kumar *et al.* [44], Al-1Ti-3B and Al-5Ti-1B are common grain refiners for Al alloys prepared by reaction of K_2TiF_6 and KBF_4 salts in molten Al at 800 °C for 60 minutes. The refiners were added in compositions of 0.2, 0.5 and 1.0 wt.% to an Al-Si alloy and parts of the melt were poured at regular intervals of 0, 2, 5, 30, 60 and 120 minutes into a graphite mould. The research conducted by Vinod Kumar *et al.* [44] emphasizes the importance of fading behaviour of the Al-Ti-B based refiners with holding time. Fading is the loss of potency of a grain refiner, as it is held in the melt before pouring. The decreasing effectiveness of the grain refiner with increasing holding time is attributed to settling, agglomeration or contamination of the grain refining particles. Microstructure analysis of the Al-Ti-B grain refiners revealed the presence of $TiAl_3$ and TiB_2 particles. The TiB_2 particles within the Al-Ti-B grain refiners are of interest to the current study because of its similar lattice geometry to Mg [34].

The edge-to-edge model describes a good grain refiner as one where the contact between a row of atoms in the refining particle and a row of atoms in the nucleating substrate will result in minimal strain energy along their respective closed packed directions and planes. The contact will also result in a minimal misfit between interatomic spacings [40]. Crystallographic studies [34] using the edge-to-edge model showed that TiB_2 is a potential nucleant for Mg. Generally, the misfit between the directions should be less than 10 % while the misfit between the planes should be less than 6 % [40] which is lower than the required planar disregistry of 12 % using Equation 11 [9]. A similar crystallographic study revealed that the smallest planar disregistry (Equation 11) between Mg and TiB_2 was 5.6 % [34]. The use of Al-Ti-B grain refiners commonly used for Al alloys can then be used for Mg alloys because of the presence of TiB_2 particles.

To determine the potential grain refining effect of Al-Ti-B grain refiners with Mg, Wang *et al.* [37] developed a Al-4Ti-5B grain refiner for an AZ31 Mg alloy. The high concentration of B in the grain refiner was to ensure the formation of a large number of TiB_2 particles. The microstructure of the grain refiner contained 1-2 μm TiB_2 particles and 5-10 μm AlB_{12} particles. The B had a higher affinity to Ti and forms TiB_2. Once all the Ti was exhausted, the remaining B reacted with Al to form AlB_{12}. The grain size of AZ31 with and without Al-4Ti-5B addition is outlined in Table 2-7. The grain refinement was attributed to TiB_2 particles acting as nucleating sites for Mg grains.

Table 2-7: Grain Size of AZ31 Treated with Al-4Ti-5B Grain Refiner [37]

Grain Refiner Concentration (wt.%)	Grain Size (µm)
0	1100
0.1	400
0.2	200
0.3	80
0.5	100

Using powder sintering, a Mg-50 wt.% TiB_2 grain refiner was developed and added to an AZ91D melt to observe its effects on grain refinement. Without addition, the base AZ91D alloy had a grain size of 240 µm while the highest addition level of 1.8 at.% provided a grain size of 50 µm (79 % reduction). Titanium bearing particles were found at the center of grains using SEM and energy dispersive X-ray (EDX) analysis as shown in Figure 2-10. As a consequence, heterogeneous nucleation of Mg grains by TiB_2 particles was also described as the source of grain refinement in a study by Liu *et al.* [33].

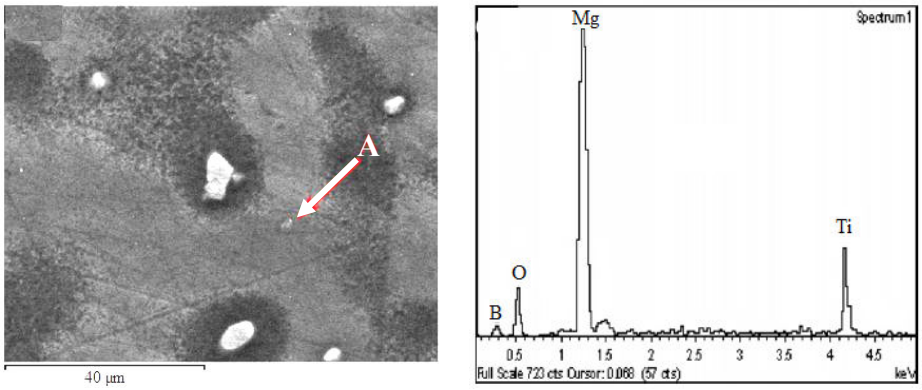

A) B)

Figure 2-10: A) SEM Image of Mg Grain Center B) EDX Spectrum of Ti Particle A [33]

Powder sintering was also used by Wang *et al*. [36] to determine the effect of altering the Ti and B ratio during grain refiner synthesis to obtain an optimal proportion of TiB_2 particles while avoiding the formation of coarse and brittle $TiAl_3$ particles. An Al-TiB_2 alloy was synthesized by sintering elemental powders of Al, Ti and B. The powders were ball milled, compacted and heated to form cylindrical samples. Two different Ti:B ratios were examined including Ti:B = 1:2 and Ti:B = 1:2.5 and $TiAl_3$ particles were only present in the former ratio. Therefore, $TiAl_3$ particles can be eliminated by using a Ti:B ratio greater than 2.5.

Cao *et al.* [31] performed a similar study to Wang *et al*. [36], except they prepared a Al-TiB_2 alloy and mixed the still molten Al-TiB_2 alloy to molten Mg. The Ti:B ratio was maintained at 1:2. As expected, some $TiAl_3$ particles were present but were eliminated by holding the Al-TiB_2 alloy in the molten state. Clusters of TiB_2 were found to settle along grain boundaries indicating segregation of TiB_2 particles. A similar settling of TiB_2 particles along grain boundaries was also observed in the study by Wang *et al.* [38] regarding TiB_2 particle addition to AZ91 Mg alloy. The results from Cao *et al.* [31] and Wang *et al.* [38] contradict the results of Qiu *et al.* [34] and Zhang *et al.* [40] who predict TiB_2 particles to be found at the centre of grains as nucleating particles.

2.4.5.2 Aluminum-Titanium-Carbon (Al-Ti-C) Grain Refiners

The use of Al-Ti-B grain refiners to refine Al-Si alloys, such as Al-7 wt.% Si, has been difficult, as noted by Vinod Kumar *et al.* [44]. Silicon in Al-Si alloys tends to react with the $TiAl_3$ particles to form a titanium-silicide compound at the surface of $TiAl_3$. As a result, the effectiveness of $TiAl_3$ to act as a nucleating site was poisoned. Therefore, to further the research described in Section 2.4.5.1, Vinod Kumar *et al.* [44] looked into an alternative Al-Ti-C grain refiner and compared it to Al-Ti-B refiners. The aim of the study was to determine which refiner type (Al-Ti-C or Al-Ti-B) could provide adequate grain refinement without fading. Two Al-Ti-C grain refiners were prepared with compositions of Al-5Ti-0.8C and Al-5Ti-1.2C by the reaction of K_2TiF_6 salt and graphite powder with molten Al at 1200 °C for 60 minutes. The Al-5Ti-0.8C grain refiner contained 0.5 to 1 μm TiC particles and plate like $TiAl_3$ particles in an Al matrix. The Al-5Ti-1.2C grain refiner only contained TiC in the Al matrix [45]. The addition of only 0.1 wt.% of either Al-5Ti-0.8C or Al-5Ti-1.2C can grain refine Al-7 wt.% Si to the same degree as 1.0 wt.% Al-1Ti-3B showing the high nucleating potential of TiC particles. At higher addition levels, the TiC particles would tend to agglomerate. The particle agglomeration would reduce the grain refining effect of Al-5Ti-0.8C and Al-5Ti-1.2C.

Qiu *et al.* [34] examined if TiC particles could nucleate Mg grains using the edge-to-edge model. Qiu *et al.* [34] compared the lattice misfit between Mg, TiB_2 and TiC particles to determine which Ti bearing particle was best suited for grain refinement. Important crystallographic data of each phase are listed in Table 2-8.

Table 2-8: Crystallographic Data for Mg, TiB_2 and TiC [34]

Phase	Structure	Lattice Parameters (nm, 25 °C)	Lattice Parameters (nm, 650 °C)	Closed Packed Directions	Closed Packed Planes
Mg	Hexagonal	a = 0.320 c = 0.520	a = 0.326 c = 0.530	$[2\bar{1}\bar{1}0]$ $[2\bar{1}\bar{1}3]$ $[1\bar{1}00]$	(0002) $(01\bar{1}1)$
TiB_2	Hexagonal	a = 0.303 c = 0.322	a = 0.304 c = 0.323	[0001] $[2\bar{1}\bar{1}0]$ $[1\bar{1}00]$	(0001) $(1\bar{1}00)$
TiC	Cubic	a = 0.432	a = 0.432	[110] [112]	(111)

By examining orientation relationships between the closed packed directions on closed packed planes between Mg and potential nucleating particles, it was determined that TiB_2 was a more potent nucleating particle than TiC.

Although TiC particles were observed to be more beneficial than TiB_2 in Al melts [44], the scenario appears to be different for Mg alloys. There has been some research using a combined TiB_2-TiC addition, but its use focused on developing Mg composites rather than developing an effective grain refiner.

A study by Zhang *et al.* [41] used TiB_2 and TiC powders in Mg to develop a Mg-TiB_2-TiC composite. A master alloy was prepared using a sintering technique of Ti, Al and B_4C powders all less than < 75 μm. The powders were ball milled, mixed, compacted and allowed to react at 1127 °C for 20 minutes under an argon atmosphere. The sintered block was added to commercial purity Mg at 750 °C and stirred for 5 minutes at 250 RPM to homogenize the melt. In the Mg composite was the presence of Mg, $Mg_{17}Al_{12}$, TiB_2 and TiC phases. The good lattice matching between TiB_2 and Mg favours a strong interface and TiC has good wettability with Mg resulting in an increase in yield and tensile strengths, but a decrease in ductility as compared to AZ91. The yield and tensile strength of AZ91 was 82 and 233 MPa respectively, while the Mg-TiB_2-TiC composite had a yield and tensile strength of 95 and 298 MPa respectively. The ductility of AZ91 was 6 % while that of the composite was 2.4 %. The decrease in ductility was attributed to the brittle nature of theTiB_2 and TiC ceramic particles. The research by Zhang *et al.* [41] showed that good wettability between TiC and Mg was possible.

The elimination of $TiAl_3$ in a Al-Ti-B alloy by carbon addition to form TiC was accomplished by Wang *et al*. [35]. The Al-Ti-B alloy was produced by ball milling and sintering pure powders of Al, Ti and B. The aim of the study was to add the Al-Ti-B alloy to Mg to form a Mg-TiB_2 composite. Upon casting, the Mg-TiB_2 microstructure also contained coarse $TiAl_3$ flakes which can have harmful effects on the ductility of the composite.

A second master alloy was prepared to eliminate the coarse $TiAl_3$ particles [35]. By adding C to the powder mix, formation of the $TiAl_3$ phase was suppressed and a TiC phase formed. The Ti addition had a higher affinity to C rather than Al. The master alloy was examined for any Al_4C_3 particles, but none were found. An increasing addition of C further increased the presence of TiC and decreased the presence of $TiAl_3$ and TiB_2 particles. Upon addition of the new Al-Ti-B-C alloy to Mg, the only phases observed were TiB_2, TiC, $Mg_{17}Al_{12}$ and Mg. A successful Mg-TiB_2-TiC composite was produced with good interfacial bonding between all the phases and the coarse, brittle $TiAl_3$ phase was suppressed. Since the study focused on developing a Mg-TiB_2-TiC composite, there was no grain size measurement with the addition of the TiB_2 and TiC particles but useful information regarding what phases would be present with the combined addition of Ti, B and C was explained.

2.4.5.3 Aluminum-Titanium-Carbon-Yttrium (Al-Ti-C-Y) Grain Refiners

Xu *et al*. [39] used a Al-Ti-C-Y grain refiner to reduce the grain size of AZ31 Mg alloy. Elemental powders of Al (99.9 %), Ti (98.0 %), graphite (99.9 %) and yttrium (Y, 99.8 %) were mixed and pressed into cylindrical samples 20 mm in diameter and 15 mm in length. An Al melt was prepared in a graphite crucible at 800 °C and the powder samples were added to the melt and allowed to sit for 10 minutes. After stirring with a graphite mixer for 15 minutes, the melt was poured into a steel mould to make Al-Ti-C-Y ingots. Addition levels of 0.5 wt.%, 1.0 wt.% and 1.5 wt.% of Al-Ti-C-Y were investigated. The AZ31 melt was prepared using induction melting of Mg, Al and Zn and Al-Ti-C-Y grain refiner addition was made at 730 °C.

The Al-Ti-C-Y grain refiner consisted of large, rod-like $TiAl_3$, rounded TiC and strip like Al_3Y particles all within an Al matrix as shown in Figure 2-11. There was no presence of Al_4C_3 particles observed in the Al-Ti-C-Y grain refiner. The addition of 1.0 wt.% Al-Ti-C-Y grain refiner provided the largest reduction in grain size and an addition of 1.5 wt.% grain refiner increased the casting grain size due to the agglomeration of TiC nucleating particles. The grain

size was 580 μm in the base AZ31 alloy and reduced to 170 μm with 1.0 wt.% addition of Al-Ti-C-Y (71 % reduction). The grain morphology also changed from coarse dendritic to fine equiaxed upon Al-Ti-C-Y addition.

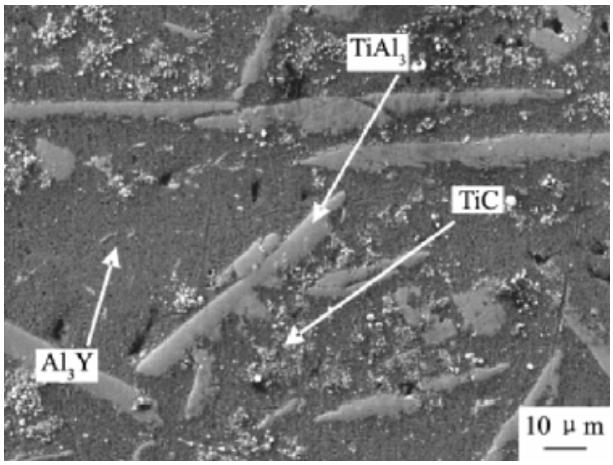

Figure 2-11: Microstructure of Al-Ti-C-Y Grain Refiner [39]

The (111) set of planes of the TiC particles has a very similar atomic arrangement to that of the Mg basal plane (0001) [39]. Therefore, the TiC particles acted as sites for nucleation. The Al_3Y particles were found at the grain boundaries indicating their potential in restricting grain growth [32].

The Al-Ti-C-Y grain refiner shows good potential in reducing the casting grain size but the high cost of Y makes the grain refiner difficult to implement on the foundry scale. The presence of the large $TiAl_3$ particles would also be detrimental to mechanical properties and castability.

A contribution to the grain refining potential of Al-Ti based grain refiners stems from the high growth restriction factor (Q, Section 2.2) value of Ti. As indicated in Table 2-1 (Section 2.2), the Q value for Ti is much larger (39.5 K) than other solutes that are added to Mg melts. The growth restriction effect of Ti is unfortunately limited by its low solubility (0.006 wt.%) in Mg melts. The Q value for Zr (13.5 K) is lower than that of Ti, but the higher solubility of Zr (0.45 wt.% as compared to 0.006 wt.% for Ti) in Mg makes it a better choice to grain refine Mg alloys free of Al from a constitutional viewpoint [13].

The Al-Ti based grain refiners show potential to reduce the grain size of Mg-Al alloys but precautions have to be made to avoid coarse $TiAl_3$ particles. Previous literature suggests that

TiB_2 is more potent than TiC and that systems containing Y, while effective, can be expensive to manufacture. This study suggests that focus should be laid on Al-Ti-B grain refiners because of their high potency and commercial availability in the Al industry.

The literature regarding the grain refinement of Mg-Al alloys encompasses many different additions such as TiB_2, TiC, AlB_2, Al_4C_3, Ca and others. Of all the grain refiners mentioned, the Al-Ti-B based systems appear to be the most reliable in producing consistent grain refinement. The use of Al-Ti-B type grain refiners in Mg alloys has not attracted much attention and the mechanisms are not clear. It is also interesting that none of the previous literature examined the fading of the grain refiners despite its high value in the grain refinement of Al alloys. Therefore, for this thesis, Al-Ti-B based grain refiners were examined with an emphasis on the fading behaviour in Mg-Al melts.

Part II: Hot Tearing

The first sections of Part II provide the generalities of hot tearing, including definition, theory of formation, methods of testing and methods to alleviate its occurrence. The end sections of Part II contain literature about the influence of processing parameters, alloy type, grain refinement and elemental additions.

2.5 Hot Tearing of Alloys

Hot tearing also known as “hot shortness” is a very common and serious defect encountered during casting [46]. It is known that hot spots and a restraint are required for hot tear formation [46], but its understanding is further compounded because it couples several phenomena including, but not limited to: alloy composition, gas content, solidification conditions and part geometry [47].

There is general agreement that the presence of lower melting temperature phases within the metal greatly increases the probability of hot tearing [46]. This section begins with a definition of hot tears and theories regarding their formation. The next section discusses methods of testing for hot tearing. Finally, the last section describes ways to reduce the occurrence of hot tears.

2.5.1 Definition and Identification of Hot Tears

A hot tear is a tensile failure of a metal casting during solidification where the metal is still semisolid and unable to withstand severe mechanical and thermal stresses [7,46]. The mechanical stresses are a result of geometry constraints from the mould walls and the thermal stresses arise from the volumetric contraction of the casting during cooling. The major characteristics of hot tears are as follows [7]:

1. They form ragged, branching cracks.
2. The main tear and its offshoots follow intergranular paths.
3. The failure surface reveals a dendritic morphology.
4. The failure surface is heavily oxidized.
5. Their location is often at a hot spot, and where contraction strain from adjoining extensive thinner sections may be concentrated.
6. They do not always appear under apparently identical casting conditions.

2.5.2 Theories on Hot Tear Formation

It is important to consider interdendritic and grain boundary areas during solidification since hot tears follow intergranular paths. Hot tears also require a site for nucleation which makes the presence of inclusions important. The amount of inclusions from one casting to the next can make the difference of a crack forming and one that does not form [7].

When the temperature of the melt cools past the solidus temperature, the metal develops a condition of essentially continuous liquid films. The strength and ductility of the casting at this stage is very low, making the casting very fragile. As a result, tearing can then be similar to the separation of liquid films [46].

Pellini conducted strength tests of solidifying steel to examine their behaviour during near hot tear conditions [46]. Tensile type experiments on solidifying castings showed a considerable reduction in area even 15 °C below the solidus temperature. The considerable reduction in area is a contradiction to common belief that the liquid film stage shows near zero ductility. For pure metals, the duration of the liquid film stage during solidification is on the order of seconds. For alloys that have segregating phases the liquid film condition exists for a time period on the order of minutes due to the wider solidification temperature range [46]. The following factors can promote the extension of liquid films that can lead to hot tear formation [46]:

1. Long regions of the casting undergoing contraction.
2. Fast cooling in areas undergoing contraction.
3. Thin sectioned hot spot regions undergoing extension.

Pellini states that hot tearing occurs sometime between dendrite coherency and when the melt becomes solid, but the flow of liquid metal can effectively heal the fracture and prevent hot tear formation [46]. The strain theory predicts that for fracture to occur while the metal is semi-solid the strain rates must be very high since the strain on the metal is uniform over the semi-solid area. At the later stages of solidification the strain over the liquid film regions is highly concentrated and more likely to cause tearing [46]. If a tear does form, it appears to grow in steps rather than as one continuous crack. This phenomenon could be a result of composition and temperature variations of the liquid films resulting in non-continuous failure of the casting [46]. If the liquid film regions are thick, the casting will be better able to accommodate strain and resist hot tearing [48]. The strain theory predicts that hot tears form when strains are concentrated in thin liquid film regions. As a result, hot tearing can be described as a highly localized process.

Using the strain theory of hot tearing, a mathematical expression to determine the strain in a hot spot during solidification can be described as [7]:

$$\varepsilon_b = \frac{\alpha \Delta T_R L}{l} \tag{18}$$

Where:

ε_b: Strain

L: Length of casting

α: Coefficient of thermal expansion

ΔT_R: Temperature range of cooling from liquidus to solidus

l: Length of hot spot

Grain size plays an important role in the localization of strain, and therefore is also considered in the strain theory. Coarse grains may localize hot spots on one grain boundary, resulting in a high concentration of strain. On the contrary, finer grains may promote a more homogeneous distribution of strain by localizing the hot spot over many grain boundaries. The

number of grains in a length l of the hot spot is l/a, for grains of diameter a. A modified version of Equation 18 can be written as [7]:

$$\varepsilon_b = \frac{\alpha \Delta T_R La}{l^2} \tag{19}$$

Equation 19 suggests that the best way to reduce hot tearing is to increase the hot spot length which requires design changes to the mould. The coefficient of thermal expansion α, and ΔT are heavily influenced by the alloy and therefore are uncontrollable factors. The grain diameter however is the only parameter that can be modified to reduce hot tearing without significant process and design changes.

The strain theory does describe the importance of grain diameter in hot tearing but does not include information about the time duration at which the metal is at a hot tear susceptible condition. An alternative theory regarding hot tear formation was proposed by Clyne and Davies [7] who assumed that hot tearing was a result of uniaxial tension, occurring during the last stage of solidification. In the early stages of solidification where liquid and mass feeding is present, the strain applied to the casting can be easily accommodated. In the last stage of solidification the grains are unable to move relative to one another and strain is difficult to accommodate. Clyne and Davies define a cracking-susceptibility coefficient, CSC_b [7,48] as:

$$CSC_b = \frac{t_V}{t_R} \tag{20}$$

Where:

t_V: Vulnerable time period when cracks can propagate between grains

t_R: Time available for liquid and mass flow

The difficulty arises in determining both t_V and t_R for a given metal-mould system. Both t_V and t_R are assumed to be multiples of the time duration for which the melt passes through a fraction liquid range. For t_R, the time period is assumed to occur between 0.1 and 0.6 fraction liquid, while for t_V, the time period occurs between 0.01 and 0.1 fraction liquid. The cracking susceptibility coefficient in Equation 20 is in good agreement with experimental observations using Al-Si alloys. The effect of increasing concentration of Si in Al on the hot tearing susceptibility of Al-Si alloys was investigated and the results were compared to those predicted by Equation 20 [7]. The agreement with Al-Mg alloys was poor but improved with modified

CSC_b limits [7]. Equation 20 was also tested on Mg-Zn and Mg-Al alloys and predicts that the peak hot tearing susceptibility of Mg-Zn alloys is 1.7 times greater than that for the peak Mg-Al alloy. The poorer hot tearing resistance of Mg-Zn alloys is attributed to the larger freezing range as compared to Mg-Al alloys. Large freezing range alloys are more prone to hot tearing because of their tendency to form large, long-lasting networks of liquid films [46].

By combining Equation 19 with Equation 20, a modified cracking susceptibility coefficient can be obtained [7]:

$$CSC_b = \frac{\alpha \Delta T_R La}{l^2} \cdot \frac{t_V}{t_R} \tag{21}$$

Equation 21, while useful, has yet to be tested [7]. It helps include many factors during solidification, such as grain diameter, temperature range to solidification and time duration where the casting is likely to form hot tears, but further research is required to include the effects of inclusions and composition variations.

2.5.3 Methods of Testing for Hot Tears

One common method of examining hot tearing susceptibility of alloys is through mould design. Two of the most frequently used moulds are the I-beam (dog-bone) and ring mould [7]. These are described hereafter.

2.5.3.1 I-beam (dog-bone)

The most common form of the I-beam mould involves a downsprue and runner that feed into a "T" shaped end restraint. During solidification, the contraction of the T-junction is restricted and hot tears are likely to form at the intersection of the runner and downsprue. Many variations include placing multiple runners on one downsprue with each runner leading to an end restraint. Figure 2-12 is a typical I-beam mould used to examine the effect of increasing casting length on hot tearing. The hot tearing susceptibility of an alloy can be compared to other alloys by the longest casting length that can be produced free of hot tears. An alloy that can produce very long castings without tearing would be more resistant to hot tearing than an alloy that produces a shorter maximum casting length under the same pouring and mould temperatures.

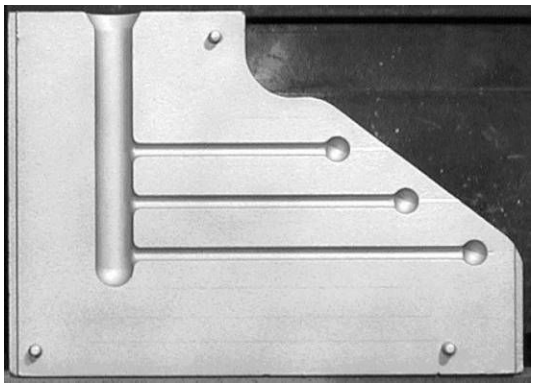

Figure 2-12: I-beam Mould to Examine Hot Tears [49]

Many researchers include load cells in the end restraint of the mould to measure the force exerted by the solidifying casting [50]. The melt solidifies on a threaded bolt which is connected to a load cell and data acquisition system. Problems with obtaining repeatable results often arise because the melt does not solidify onto the bolt in the same manner for each trial.

Li *et al.* [30] used a modified I-beam mould to test hot tearing susceptibility of Mg alloys. The mould is shown Figure 2-13. The mould consisted of tensile shaped samples with various section diameters. An alloy with a high resistance to hot tearing would produce small diameter tensile samples without showing any signs of tearing.

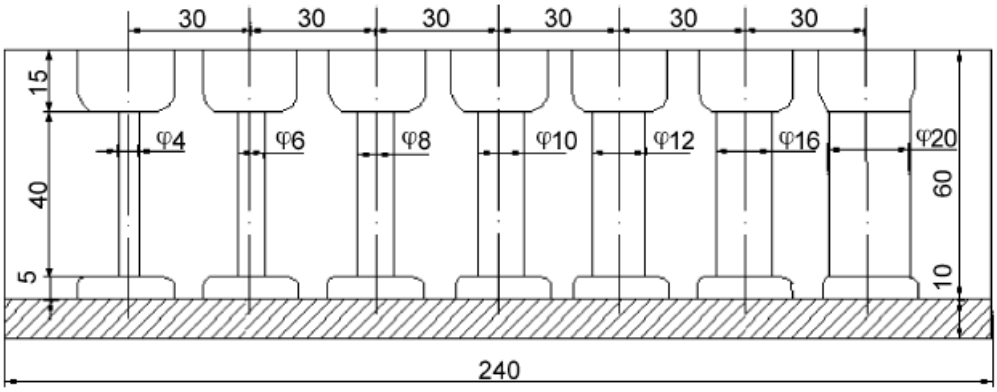

Figure 2-13: Schematic of Mould for Hot Tearing Susceptibility (Dimensions in mm) [30]

2.5.3.2 Ring Mould

In the ring mould configuration, the melt is poured into a sand or permanent mould with a doughnut shaped cavity. Upon solidification, the metal contracts onto the center core and hot tears form from the inner diameter of the casting and expand towards the outer diameter. Alloys

are compared according to the number and length of the cracks present after solidification. One advantage of the ring mould is that it very simple to use and produces a large number of cracks to examine and assess [7]. Unfortunately, the hot tears can form at any location along the diameter of the center core, unlike the I-beam moulds, which concentrate hot tears in one particular location.

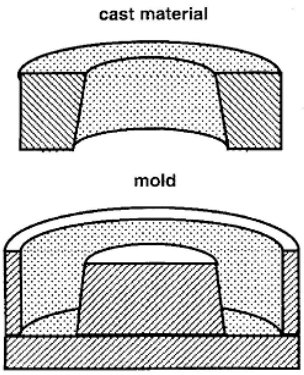

Figure 2-14: Ring Mould to Asses Hot Tearing [51]

2.5.4 Methods to Alleviate Hot Tearing

Mould design is a critical factor in reducing hot tearing. Sharp corners should be avoided as they act as stress concentrations and can trigger hot tear formation. Other methods to reduce hot tearing in mould design include providing curves in gates and quickly removing any internal steel cores to avoid forming a metal constraint [7]. If the design is fixed, then chilling or reducing the contracting length can be used to avoid hot tearing.

2.5.4.1 Chilling

The introduction of chills in hot spot regions enables the melt to solidify rapidly. As a result, the melt remains semi-solid for a shorter period of time and is therefore less prone to hot tear formation. Difficulties arise since chills must be included into the casting process. Hence, care is required to avoid blocking feeding channels.

2.5.4.2 Reduction of Contracting Length

This method involves the addition of feeder boxes to the center of long sections undergoing contraction. In the mould shown in Figure 2-12, a feeder box in the center of one of the horizontal casting sections helps accommodate strain by increasing the length of the hot spot and

reducing the contracting length [7]. Both are important parameters to reduce hot tearing as previously described in Equation 18. The following sections go into more detail regarding the hot tear formation in Al and Mg alloys and the effect of process parameters, elemental additions and grain refinement.

2.6 Research Regarding Hot Tearing Formation and Evaluation

A fundamental study by Metz *et al.* [52] examined the relationship between the response to imposed strain of a solidifying Al alloy and the formation of hot tears. The examined alloys were Al-4 wt.% Si and Al-4wt.% Cu. The experimental setup examined the shear deformation of the alloys during solidification. An examination of coarse grain castings at the tips of hot tears showed that dendrite arms separated during deformation, but were filled by an influx of liquid, indicating that hot tears can be healed if feeding is sufficient [52]. The highly dendritic network made the alloy susceptible to hot tearing. The behaviour of the coarse grain castings could be classified into three domains:

1. **<0.25 fraction solid**
   There was no measureable resistance to flow.
2. **~0.25 fraction solid**
   The dendrites formed a network which resists deformation.
3. **0.25-0.4 fraction solid**
   There was little increase in resistance with increasing strain and this continued until the casting was completely solid.

For the castings grain refined using 0.25 wt.% Ti, the strength of the alloy did not develop until about 0.40 fraction solid. The fine grained castings had a high hot tearing resistance not necessarily because the castings were “stronger”, but because the castings were better able to accommodate local strains due to the smaller grain size and columnar to equiaxed change in grain morphology [52].

In a study by Suyitno *et al*. [53], the factors contributing to hot tearing were described by implementation into a computer simulation based on the direct chill casting of a Al-4.5 wt.% Cu alloy. The simulation was split into four components by Suyitno *et al*. [53], each representing one stage of solidification. The four stages of solidification were:

1. Nucleated crystals float freely and the material behaves as a liquid.
2. The nuclei are close and come together to form a porous network and the solidification shrinkage strain is easily countered by the liquid flow and solid arrangement.
3. The deformation of the solidified body caused by the solidification shrinkage and external strains is not fully counteracted by the liquid flow and solid movement, hot tears are usually initiated.
4. The grains are strongly interconnected, so that deformation of the solidified body will not result in further defects.

The simulation used a series of models to compare the feeding and deformation plus shrinkage rate of the casting.

If insufficient feeding during solidification is present and a pore reaches a certain diameter, then a hot tear would result. Otherwise, porosity will result. The input data to the simulation were temperature, cooling rate and strain rate.

The results of the simulation showed that a hot tear would form if the difference between the feeding rate and deformation plus shrinkage rate was above a critical value. The study also ran simulations that investigated the effect of grain size on hot tearing. Smaller grain sizes reduced the developing stress during solidification and hot tearing tendency. Below a certain grain size a tear would not develop. Therefore, the simulation validated the benefits of smaller grains sizes in reducing hot tears.

2.7 Hot Tearing of Aluminum and Magnesium Alloys

The section is divided into two parts. The first part involves literature describing the influence of process parameters such as mould and pouring temperature, and alloy type on hot tearing of Al and Mg alloys. The second part outlines the effect of grain refinement and different element additions on hot tearing susceptibility of Al and Mg alloys.

2.7.1 Influence of Processing Parameters and Alloy Type

2.7.1.1 Aluminum Alloys

An examination of the hot tearing resistance of wrought Al alloys AA1050, AA3104 and AA5182 was conducted by Lin *et al.* [48] using a constrained rod casting mould similar to

Figure 2-12. Lin *et al.* noted that in multi-component alloys the following characteristics were observed regarding their hot tearing behaviour [48]:

1. Alloys prone to hot tearing tend to have wide freezing ranges.
2. Hot tear alloys have little eutectic content that surround the grains.
3. Fine grained alloys promote good interdendritic feeding, low interlocking stresses and tear healing.
4. Alloys with interdendritic liquid with a high surface tension impede interdendritic channel feeding which increases hot-tear resistance.
5. The size, shape, strength and distribution of second phases have an effect on grain boundary strength and brittleness of the hot tearing alloys.

The castings were poured into a mould preheated to 200 °C and coated with graphite. The pouring temperature was 120 °C above the liquidus of each alloy. Aluminum alloy AA1050 had the highest hot tearing resistance while alloys AA5182 and AA3104 had the second and third highest hot tearing resistance respectively. All the hot tears were intergranular in nature. The microstructure of the AA1050 alloy contained dendrites covered in the eutectic phase which was a sign of feeding in the interdendritic regions. Aluminum alloy AA5182 had the longest freezing range but a smaller grain size than AA3104 and was ranked second in terms of hot tearing susceptibility. Lin *et al.* [48] concluded that freezing range and grain size play a role in hot tearing. Areas ahead of the tear tips contained concentrations of second phases, giving indications of tear healing. The hot tearing phenomenon was explained using Saveiko's liquid film theory which is a function of volumetric shrinkage, deformation of the solid matrix and surface tension of the liquid film. For a tear to grow, it has to generate enough force to make two solid interfaces. The tear must overcome molecular adhesion forces between the liquid and the solid [48].

2.7.1.2 Magnesium Alloys

One study investigating the effects of varying mould and pouring temperatures on the hot tearing susceptibility of AZ91D noted that poor feeding through interdendritic regions could result in porosity and can easily become the source for hot tears [54].

The hot tearing experiments were conducted using an I-beam shaped mould similar to Figure 2-12. Pouring and mould temperatures ranging from 680-720 °C and 140-380 °C, respectively, were examined.

Optical examination of the hot tear castings revealed that the crack width was largest at the top and bottom surfaces, closest to the mould wall because of the high solidification cooling and contraction at the mould-metal interface. The tears were thinner at the center region of the casting bar because of the lower cooling rate that could better accommodate the metal contraction and heal any initiating tears. The difference in tear width from the edges to the center of the castings indicated that thermal gradients were present in the casting bars and also played a role in hot tearing.

An increase in pouring temperature only marginally reduced hot tearing when the mould temperature was above 220 °C. The reduction in hot tearing was a result of the formation of larger $Mg_{17}Al_{12}$ intermetallic particles that would sit at the grain boundaries and would be responsible for filling any initiating hot tears. At mould temperatures below 220 °C, the relatively cooler mould would thermally shock the incoming melt and promote the formation of hot tears.

For a fixed pouring temperature, a higher mould temperature enabled a lower cooling rate. The casting section had a more uniform temperature gradient and thermal contraction gradients decreased. Also, at higher mould temperatures the lower cooling rate changed the partially divorced eutectic structure which contained a mix of alpha-Mg and $Mg_{17}Al_{12}$ eutectic to a fully divorced structure consisting of a homogeneous $Mg_{17}Al_{12}$ eutectic. A fully divorced eutectic phase can better accommodate hot tears than a divorced eutectic phase because of the removal of alpha-Mg stress concentrations [54].

Similar to the study by Bichler *et al.* [54], the effect of mould temperature on the hot tearing of AZ91 Mg alloy was also investigated by Sadayappan *et al.* [49]. In addition to AZ91 Mg alloy, experiments were also conducted on AE44, AE63, AE35, AJ62, MRI 201S, MRI 202S and MRI 206S alloys. The purpose of the study was to perform a comparison of the hot tearing behaviours with respect to alloy type and mould temperature.

The mould used for the study is shown in Figure 2-12. The rod castings were 1 cm in diameter and the anchor was 2 cm in diameter. The longer the casting rod length, the greater the

stress and the more likely hot tears would form. The minimum mould temperatures to eliminate hot tearing were determined for each of the alloys examined. The results are shown in Table 2-9.

Table 2-9: Minimum Temperatures to Eliminate Hot Tears [49]

Alloy	Mould Temperature for No Hot Tearing (° C)
AZ91	≥ 335
MRI 206S	≥ 340
AJ62	≥ 380
MRI 202S	≥ 390
AE63	≥ 395
AE44	≥ 395 (1 crack)
MRI 201S	≥ 420
AE35	≥ 415 (3 cracks)

The AZ91, AJ62 and AE alloys were grain refined using 0.3 wt.% hexachloroethane and the MRI alloys were refined using 6.5 wt.% of a Mg-15 wt.% Zr grain refiner. The MRI 201S alloy also received additional refinement using 1.3 wt.% Mg-22 wt.%Y-1.3 wt.% Nd alloy. Of all the alloys investigated, AZ91 had the highest resistance to hot tearing. Creep-resistant AE35 had the most severe hot tearing susceptibility demonstrated by three cracks even at a mould temperature of 415 °C. Alloys with high Al and low beryllium (Be) contents in their chemistry such as AZ91, MRI206S and AJ62 performed better than the AE alloys. The high Al content was found to help with grain refinement and the low Be content did not interact with the added grain refiners [49]. Image analysis of the castings also revealed that the hot tears were ragged in shape indicating intergranular fracture [49]. This intergranular nature of hot tears was also noted by Campbell [7].

A comparison of the hot tearing performance of different Mg alloys using the same mould geometry (Figure 2-12) was also conducted by Pekguleryuz *et al.* [55] using AZ91D, AZ91E, AM50A, AS21, AS41B and AE42 alloys. All the castings were produced using a mould temperature of 400 °C and a pouring temperature 100 °C above the liquidus of each alloy. The castings were ranked based on the characteristics of the tears that were present after ejection. Castings that showed full hairline cracks or were half broken were considered to be highly susceptible to hot tearing, while castings that only showed short hairline cracks were considered to have high hot tearing resistance. A summary of the results obtained by Pekguleryuz *et al.* [55] is presented in Table 2-10.

Table 2-10: Summary of Qualitative Castability of Mg Alloys [55]

Alloy	Qualitative Castability
AZ91D	Very good
AZ91E	Very good
AM50A	Moderate
AS21	Low
AS41B	Moderate
AE42	Low-to-moderate

The results were very similar to the observations of Sadayappan *et al*. [49] where AZ91D had the highest hot tearing resistance, while AE42 was the most susceptible to tearing. One explanation for the high hot tearing resistance of the AZ91D alloy was the high concentration of eutectic at the grain boundaries that could adequately provide feeding at the later stages of solidification.

The research by Bichler *et al.* [54], Sadayappan *et al.* [49] and Pekguleryuz *et al.* [55] helped establish baseline investigations into the hot tearing of Mg alloys. Further research is required to observe the effects of grain refinement on the hot tearing of Mg alloys. This is examined in Section 2.7.1.2.

2.7.2 Influence of Grain Refinement and Elemental Additions

Adequate grain refinement is expected to be helpful in preventing crack initiation, as first described in and Equation 19 and Equation 21.

Grain refinement can help reduce hot tearing by two mechanisms. The first involves the transformation of dendritic grain structure to a smaller and more globular grain structure. When the metal is in the semi-solid temperature range during solidification, the presence of globular grains are better able to slide over each other and accommodate any casting deformation that could lead to hot tears. Secondly, un-refined alloys have more dendritic grains that entrap liquid between the dendrite arms when coarsening. The trapped liquid is then not able to accommodate feeding to intergranular regions that could prevent hot tears [47].

Since hot tearing phenomenon varies greatly depending on the alloy system, it is unreasonable to expect that grain refinement of any kind would work for all alloy cases. Although this thesis focuses on the effect of grain refinement on the hot tearing of Mg alloys, it

is still worthwhile to look into the research conducted regarding Al alloys because of its similar thermal properties to Mg and the wealth of research available.

The effect of elemental additions is also included in this section because, in some studies, it has been used in combination with grain refiners. Whereas in other studies, the hot tearing results are explained by examining the effect of elemental additions on the grain size of the castings.

Investigation into reducing hot tearing by grain refinement would be very advantageous on the foundry scale, since no changes to the pouring and feeding methods have to be implemented. Grain refinement may not only reduce or even eliminate hot tears, but may also produce a casting with higher strength and promote its use in more demanding structural applications.

2.7.2.1 Aluminum Alloys

The effect of grain refinement on hot tearing of wrought Al alloys was performed by Lin *et al.* [48]. Grain refinement was accomplished using an Al-5Ti-1B grain refiner with addition levels of 0.0035, 0.0045 and 0.012 wt.% Ti for the AA1050 alloy, and 0.014 wt.% Ti for the AA3104 and AA5182 alloys. With grain refinement, there was a more even distribution of the eutectic phase which facilitated the accommodation of volumetric contraction within the casting. The finer grain sizes also resulted in a larger amount of eutectic at the grain boundaries. For all cases a smaller grain size was observed with Al-5Ti-1B addition that lead to a decrease in hot tearing. The grain refinement delayed the dendrite coherency allowing more time for interdendritic fluid flow. The grain refinement was most effective on the AA5182 Al alloy which had the largest non-equilibrium freezing range out of AA1050, AA3104 and AA5182. Hot tearing was still present in some alloys despite the grain refinement because of the presence of brittle second phases that would act as stress risers [48].

A study to reduce the hot tearing resistance of long freezing Al-1 wt.% Sn alloy was investigated by Karunakar *et al.* [56]. The study varied both pouring temperature and Al-5Ti-1B grain refiner addition.

Even at the highest grain refiner addition level of 3 wt.%, hot tears remained. The addition of tin (Sn) increased hot tearing while the presence of Ti and Fe reduced hot tearing.

With Fe addition, a leaf-like Al-Sn-Fe phase formed that held adjacent grains together and prevented hot tearing. It was found by Dodd [56] that hot tearing was most noticeable when the alloy composition resulted in a large freezing range and only a small portion of eutectic was

present. Furthermore, Davies [56] looked at the influence of various additions on the hot tearing of Al-Sn, Al-Cu, Al-Mg and Al-Zn alloys and concluded that hot tearing can be reduced with grain refinement [56].

A ring type mould was used to examine hot tearing susceptibility [56]. Sand casting was used for the experiments and the mould pattern consisted of a downsprue connected to a H-shaped feeding system, resulting in four rings per pour. The ring centers contained steel cores that constrained metal solidification. As the poured metal cooled, it contracted radially and was constrained by the steel cores, resulting in hot tears. The lengths of the hot tears were measured as the average sum of the cracks in all the four rings. Addition levels of 0 to 3.0 wt.% Al-5Ti-1B grain refiner were used. The effects of Fe addition was also investigated using an Al-30 wt.% Fe alloy with concentrations of 5 and 6 wt.%.

The results from Karunakar *et al.* [56] indicated that, with increased Al-5Ti-1B addition (increased grain refinement), the average hot tear length decreased, but was not completely eliminated. With the addition of both Al-5Ti-1B and Al-30 wt.% Fe alloys, the average hot tear length further decreased. Only 3 wt.% Al-5Ti-1B and 6 wt.% Al-30 wt.% Fe addition was able to completely eliminate hot tearing. With the combined addition of Al-5Ti-1B and Al-30 wt.% Fe, a leaf-like Al-Sn-Fe phase formed that anchored the grains together increasing their resistance to hot tearing [56].

In an earlier related study by Datta *et al.* [57] co-authored by Karunakar, the effect of Ni on the hot tearing susceptibility of Al-1 wt.% Sn was investigated. The procedure was similar to the study performed by Karunakar *et al.* [56]. The addition of Ni was made using 15 wt.% of an Al-6 wt.% Ni alloy. The required amount of Ni was added to the Al-Sn alloy and the temperature of the melt was raised to 900 °C for ten minutes. After pouring and solidification, the casting had absolutely no cracking. Examination under a scanning electron microscope revealed an Al-Sn-Ni rich phase that interlocked grains, similar to the effect of Fe addition in the study by Karunakar *et al.* [56]. The composition of Ni in the Al-Sn-Ni phase was approximately 16.62 wt.%. It was found that the Al-Sn-Ni phase would freeze prior to the Al-Sn eutectic and help anchor the grains, resulting in a prevention of hot tear formation [57].

The addition of Al-5Ti-1B grain refiner on the hot tearing susceptibility of permanent mould cast B206 Al alloy was shown to reduce hot tearing by D'Elia and Ravindran [58].

In an unrefined casting, relatively coarse secondary dendrite arms entrapped liquid between the solid grains making it difficult for the available liquid to provide intergranular feeding. In a grain refined structure, the secondary dendrite arms were less branched and the available liquid was able to provide adequate interdendritic feeding to reduce hot tearing.

The study used an I-beam shaped permanent mould identical to the one used in the study by Bichler *et al.* [54]. The pouring and mould temperatures were fixed at 710 and 180 °C, respectively. These conditions were established from previous experiments and resulted in the onset of hot tearing. The addition levels investigated were 0.02, 0.05, 0.1 and 0.25 wt.% Ti.

Figure 2-15 illustrates the effect of grain refiner on grain size for B206. The results show that with Al-5Ti-1B addition the grain size of the casting reduced significantly. The average grain size of the un-refined casting was 680 µm and reached a minimum average grain size of 80 µm after the addition of 0.05 wt.% Ti. The grain size remained constant after further addition of Ti.

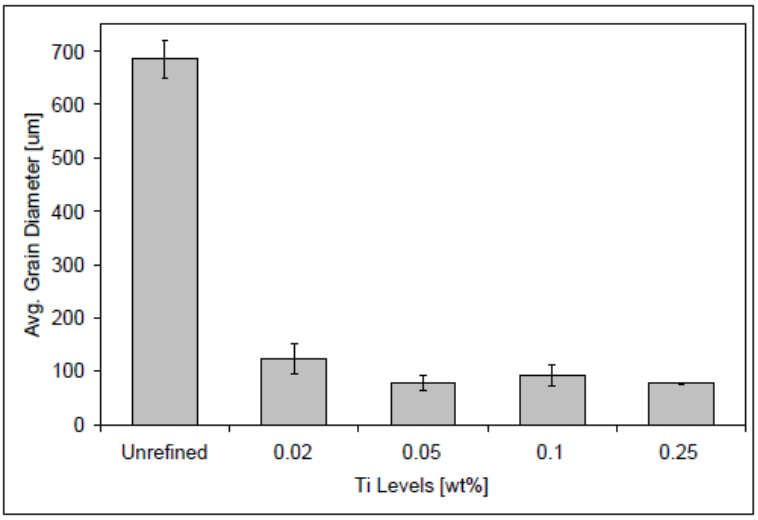

Figure 2-15: Grain Size Measurements of B206 Alloy with Different Levels of Ti [58]

Grain refinement eliminated hot tears in B206 with 0.05 wt.% Ti. The grain refinement eliminated hot tearing by transforming the grain structure from dendritic to globular. The globular grains were better able to rotate amongst each other and accommodate strain during solidification. The small, globular grains also established more uniform feeding throughout the casting, thereby resulting in a reduction of hot tears.

The study by D'Elia and Ravindran [58] demonstrated that adequate grain refinement of B206 Al alloy can completely eliminate hot tearing. The purpose of this thesis is to determine if a similar result can be obtained with AZ91D Mg alloy.

2.7.2.2 Magnesium Alloys

Rare earth additions have been utilized to observe their effects on the hot tearing susceptibility of AZ31, AM60 and AZ91 alloys. Traditionally, rare earth additions to Mg alloys are applied to improve high temperature strength and creep properties. The effect of rare earth additions on the hot tearing resistance of Mg-Al alloys is unclear according to Zheng *et al.* [59].

The rare earth addition was made using a cerium rich mish-metal added to the alloys at 750 °C and subsequently stirred for two minutes. Addition levels ranging from 0 to 1.2 wt.% rare-earth were investigated. The melt was poured into a permanent mould with varying sized tensile sample necks similar to the mould shown in Figure 2-13. The mould temperature was 300 °C.

With increased rare-earth addition, the hot tearing susceptibility of all the alloys increased. Hot tearing was most severe in the AZ31 alloy, followed by the AM60 and AZ91 alloys, respectively. The increased concentration of Al in the alloys was found to improve hot tearing resistance. The hot tear surface showed the presence of well-developed dendrites, indicating that hot tears propagated along grain boundaries. The rare earth additions reacted with the Al in the melt, and at 640 °C formed $Al_{11}RE_3$ intermetallic particles. The $Al_{11}RE_3$ phases blocked feeding channels, promoting hot tear formation. The grain size also increased with rare-earth addition which is known to increase hot tearing susceptibility. As a result, the addition of rare-earths was shown to be ineffective in reducing the hot tearing susceptibility of AZ31, AM60 and AZ91 alloys.

Another study involving Ca addition and hot tearing was conducted by Cao and Kou [50]. The alloys compared during the investigation were as follows:

1. Mg-4 wt.% Al-0.5 wt.% Ca
2. Mg-4 wt.% Al-1.5 wt.% Ca
3. Mg-4 wt.% Al-2.5 wt.% Ca
4. Mg-4 wt.% Al-3.5 wt.% Ca

5. Mg-5 wt.% Al-2.5 wt.% Ca
6. Mg-6 wt.% Al-2.5 wt.% Ca

The mould used to examine the hot tearing susceptibility of the alloys was similar to the mould shown in Figure 2-12. The mould was preheated to 335 °C and the pouring temperature was 125 °C above the liquidus temperature of the alloy. Examination of the hot tearing susceptibility of AZ91 was also made for comparison. Measurements for the contraction of the casting during solidification were also made using a load cell and threaded bolt. Upon solidification, the melt would grip onto a threaded bolt placed inside the anchor location and upon casting contraction, a data acquisition system would record the load applied. A thermocouple was also placed at the hot tear location (intersection of the downsprue and the casting bar).

The intersection between the downsprue and the casting bar was susceptible to hot tearing primarily because of two reasons:

1. The sprue end of the rod was the last area to solidify because of its high volume to surface area ratio.
2. A high stress concentration existed at the sprue end of the rod because of the abrupt reduction in cross-sectional area from the downsprue to the casting rod.

The Mg-4 wt.% Al-0.5 wt.% Ca alloy had the widest freezing range and lowest eutectic content and was the most susceptible to hot tearing. Alloys such as Mg-4 wt.% Al-3.5 wt.% Ca and Mg-6 wt.% Al-2.5 wt.% Ca had very short freezing ranges and a high content of eutectic resulting in a very low susceptibility to hot tearing.

In summary, the hot tearing susceptibility significantly decreased with increasing Ca content but remained relatively constant with increasing Al content. In a separate study, it was found that Ca had an opposite effect on hot tears [60]. With an increase in the concentration of Ca from 0.5 wt.% to 1.0 wt.%, the alloy grain size increased from 284 to 846 μm, respectively, while additional levels of Ca beyond 1.0 wt.% maintained grain size between 600 and 800 μm. In turn, this increase in grain size caused by Ca addition led to a decrease in hot tearing resistance.

A similar increase in hot tearing susceptibility with Ca addition was also found in the study by Li *et al.* [30], first mentioned in Section 2.4.4. With increasing Ca addition, the hot tearing

susceptibility increased. The increase in hot tearing susceptibility was attributed to the different cooling rates of the thermally stable Al_2Ca and $Mg_{17}Al_{12}$ intermetallics at the grain boundaries. The different cooling rates promoted thermal stresses in various regions of the casting and reduced the alloys ability to resist hot tearing [30].

In the Mg castings produced by Sadayappan *et al*. [49], the hot tears appeared as intergranular cracks. According to Cao and Kou [50], any intergranular liquid eutectic during solidification helps heal emerging hot tears. D'Elia *et al*. [58] noted that hot tears were present in castings where large dendrites were present, and feeding of liquid metal in the later stages of solidification was difficult.

The research of Cao and Kou [50] illustrates the influence of alloy solidification range on hot tearing susceptibility. If the solidification range of the alloy can be reduced, then a reduction in hot tearing should result.

The current study aims to use Al-Ti-B based grain refiners to reduce the hot tearing susceptibility of the AZ91E Mg alloy. Proper grain refinement should decrease freezing range, increase liquid metal feeding, and decrease the imposed strain, all leading to a reduction in hot tearing. Aluminum-titanium-boron based refiners have shown potential to provide significant grain refinement, but their application to reduce hot tearing in Mg alloys needs to be examined.

CHAPTER 3 EXPERIMENTAL PROCEDURE

3.1 Materials

This section describes the materials used in this study and outlines the processes required to perform the experiments. The compositions of the Mg alloy and grain refiners used are presented. A detailed description of procedures and equipment utilized to prepare the mould concludes the chapter.

3.1.1 AZ91E Magnesium Alloy

The AZ91E Mg alloy was received as ingots (Meridian Technologies Inc., Strathroy, Ontario). The chemical composition of the AZ91E alloy (batch analysis from the supplier) is presented in Table 3-1.

.

Table 3-1: Composition of AZ91E Alloy (wt.%)

Mg	Al	Zn	Mn	Si	Cu	Fe	Be	Total Others
Bal.	8.7	0.53	0.23	0.05	0.006	0.003	0.0012	0.3

3.1.2 Al-5Ti-1B Grain Refiner

The Al-5Ti-1B grain refiner was received as 11 mm x 146 mm (D x L) rods (KB Alloys Inc., Robards, Kentucky). The chemical composition of the Al-5Ti-1B grain refiner is shown in Table 3-2.

Table 3-2: Composition of Al-5Ti-1B Grain Refiner (wt.%)

Al	Si	Fe	Ti	B	V	Total Others
93.73	0.06	0.1	5	1	0.1	0.1

3.1.3 Al-1Ti-3B Grain Refiner

The Al-1Ti-3B grain refiner was synthesized at the Indian Institute of Technology-Madras (IIT-M). Commercially pure Al (99.7 %) was melted in a high frequency induction furnace (5 kg, 20 kW, made by Inductotherm India Ltd.). The furnace temperature was controlled using a digital controller (Multispan, model MDC-901, temperature range: room-1200 °C) connected to a chromel-alumel thermocouple. The temperature was maintained to +/- 5 °C of the set temperature. The commercial purity Al was first cleaned in acetone to remove any traces of oil

or grease. Titanium and B were added as K_2TiF_6 and KBF_4 salts respectively. The required amounts of KBF_4 and K_2TiF_6 salts were separated into multiple small batches and each batch was wrapped in Al foil. All the wrapped salts were placed into a furnace at 150 °C for 2 hours to remove any moisture. A sample calculation detailing the amount of Al, K_2TiF_6 and KBF_4 required for the preparation of the Al-1Ti-3B grain refiner is presented in Appendix A.1. The commercial purity Al was melted in the induction furnace and brought to a temperature of 800 °C. The melt was degassed using hexachloroethane (1 g for every one 1 kg of Al, product of Greaves Foseco Ltd., India). The exothermic reaction of hexachloroethane and Al increased the melt temperature and both K_2TiF_6 and KBF_4 salts were added simultaneously when the melt temperature decreased to 800 °C. A zirconia coated steel plunger was used to add the salts to the melt. The melt was immediately stirred manually, using a zirconia coated steel stirrer, until the mixture was homogeneous. The melt was allowed to react with the salts for 60 minutes with no additional stirring. The melt was then skimmed and poured into a cylindrical graphite mould 25 mm in diameter and 250 mm in height.

A summary of the processing conditions used to produce the Al-1Ti-3B grain refiner are described in Table 3-3.

Table 3-3: Summary of Processing Conditions Used to Produce Al-1Ti-3B Grain Refiner [61]

Al-1Ti-3B	**Raw Materials**	• Commercial purity **Al** • **K_2TiF_6** and **KBF_4** salts • **Hexachloroethane**
	Reaction Temperature (°C)	800
	Reaction Time (min)	60
	Degassing Temperature (°C)	800
	Degassing Amount (g degasser/kg melt)	1/1
	Addition Procedure	• Both salts added **simultaneously** in small **batches**

The chemical composition of the Al-1Ti-3B grain refiner is presented in Table 3-4.

Table 3-4: Chemical Composition of Al-1Ti-3B Grain Refiner (wt.%) [61]

Al	Si	Fe	Ti	B
Bal.	0.15	0.16	1.00	2.21

3.1.4 Graphite Moulds

The graphite moulds were machined from 70 mm diameter graphite rods (Speer Canada Inc., Kitchener, Ontario). The mould cavity was machined to produce castings with circular bottoms 50 mm tall and 40 mm in diameter. Images of the top view of a graphite mould and casting are shown in Figure 3-1.

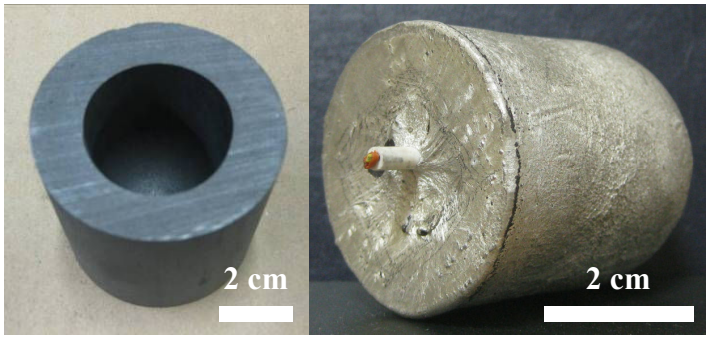

A) **B)**

Figure 3-1: A) Graphite Mould B) Graphite Mould Casting

To obtain thermal data of the solidifying castings, K-type thermocouples (Omega Engineering Inc., Laval, Quebec) were inserted into the solidifying melt immediately after pouring. Low carbon steel fixtures with inner diameters equal to the thermocouple sleeves (3 mm) were used to ensure that the thermocouples were properly located during data acquisition. The steel fixtures were fixed in place using a set screw. The steel fixture/thermocouple assembly was placed atop a 3 mm thick steel plate that covered the melt. Figure 3-2 is a graphical representation of the final assembly of the graphite moulds with the thermocouple depth and mould dimensions.

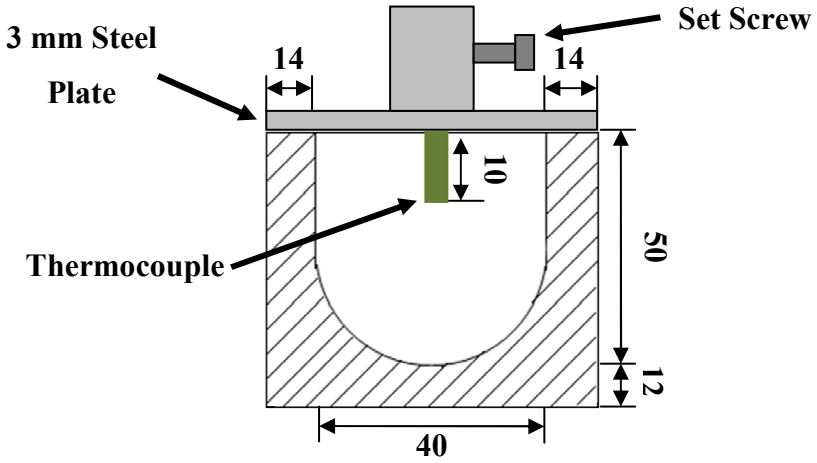

Figure 3-2: Final Assembly for Graphite Moulds (Dimensions in mm)

3.1.5 Permanent Mould to Examine Hot Tearing

The permanent mould used for the hot tearing experiments was custom designed to examine hot tearing. The mould was used for a previous MASc. [62] and PhD. theses [63].

3.1.5.1 Mould Mounting

An image of the permanent mould mounting press is shown in Figure 3-3.

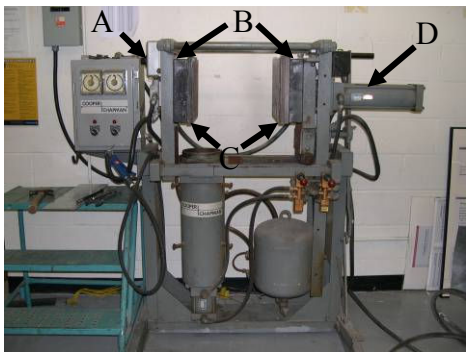

Figure 3-3: Mounting Press A) Temperature Controller B) Strip Heaters C) Mounting Plates D) Pneumatic Cylinder

3.1.5.2 H13 Permanent Mould

The H13 mould is 411 mm x 43.18 mm x 238 mm (L x W x H) in size. A CAD drawing of the dog-bone style permanent mould is shown in Figure 3-4.

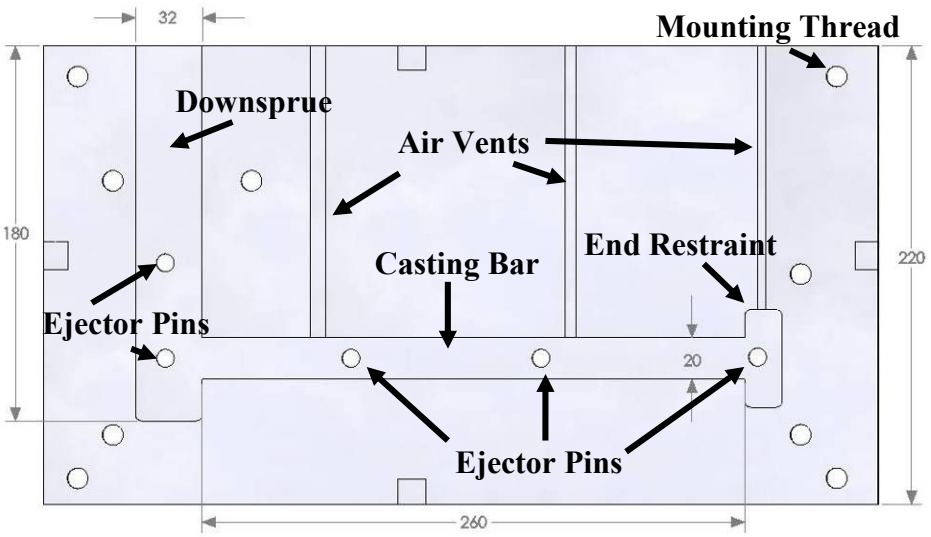

Figure 3-4: H13 Permanent Mould CAD Design (Dimensions in mm)

The permanent mould is similar to the mould design in Figure 2-12 in that it contains a downsprue, casting bar and end restraint. The difference in the mould geometries is that, for this study, the mould corners are sharp 90 ° angles rather than rounded to further promote hot tearing. The mould also contains three air vents to reduce the entrapment of gases. Five 1 cm ejector pins were machined into the mould to help with casting removal and four mounting threads (only one labelled), one at each corner of the mould were used to anchor the mould onto the mounting press. A separate 1.25 cm thick 1020 steel plate was used as the opposite face of the permanent mould.

3.1.5.3 Mould Coating

Boron nitride mould coating was applied on the permanent mould to reduce wear on the mould and ease casting ejection. A compressed air spray gun was used to apply the boron nitride onto the mould surface. The pressure of the gun was regulated between 30-40 kPa to ensure optimum application of coating onto the mould surface and the coating was sprayed on at a distance of approximately 45 cm away from the mould surface.

3.1.5.4 Installation of Thermocouples

Three K-type thermocouples (Omega Engineering Inc., Laval, Quebec) with ceramic sleeves were inserted into slots machined into the bottom surface of the mould to carefully measure the

mould temperature during the hot tearing experiments. The slots extended 75 mm into the mould and the thermocouples were connected to a data acquisition system (Daytronic System 10, DataPAC) to obtain the mould heating profile during casting. An additional three thermocouple slots were also machined for temperature measurement of the solidifying castings. The thermocouples were carefully placed into the casting cavity where the thermocouple tip was at the center of the casting bar section. Steel inserts were used to cover the thermocouple sleeves and fill the thermocouple slots. A thermocouple was placed in the center of the casting bar and one, 25 mm from each end of the casting bar for a total of three locations. Figure 3-5 depicts the locations of the thermocouple probes. The location of the machined slots with the inserts is also shown in Figure 3-5.

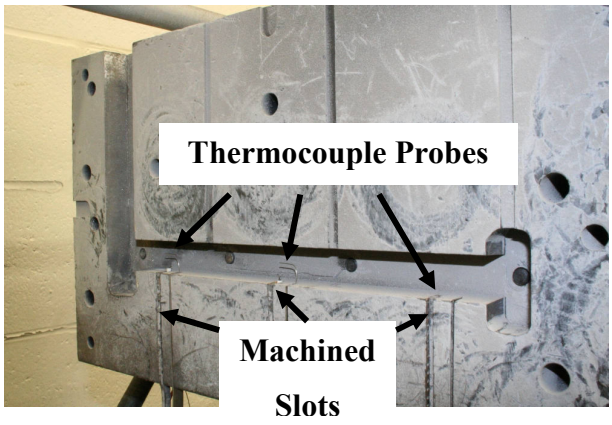

Figure 3-5: Thermocouple Placement in Permanent Mould

3.2 Melting and Addition Procedure

Two different melting procedures were required for this study. The first procedure dealt with experiments investigating grain refinement and fading of AZ91E Mg alloy using the grain refiners and graphite moulds. The second portion of this study focused on the effect of grain refinement on the hot tearing susceptibility of permanent mould cast AZ91E Mg alloy. Both procedures are described in the following sections.

3.2.1 Grain Refinement and Fading Experiments

Approximately 1 kg of virgin AZ91E Mg alloy was preheated for at least 30 minutes in a furnace at 200 °C. The ingots were then added to a low carbon steel crucible and placed into a

custom designed electric resistance melting furnace (PSH Kilns, 5 kW, Oakville, Ontario) set to a temperature of 775 °C. Carbon dioxide was used as a cover gas at a flow rate of 17 m^3/h to prevent oxidation of the melt. Six graphite moulds were then preheated at 750 °C.

The required amount of grain refiner was prepared using a hacksaw and digital scale (Scientech-SP350). The grain refiner was sectioned into pieces weighing 0.3 g or less and placed in the preheating furnace to remove moisture. The melt temperature was checked using a K-type thermocouple coated with boron nitride. Once the melt temperature reached 750 °C, any oxides present on the surface were skimmed using a low carbon steel spoon. The grain refiner was added to the melt and the mixture was stirred for 30 seconds at 200 rpm using a low carbon steel stirrer preheated to 750 °C.

A timer was used to measure the time elapsed after grain refiner addition immediately after stirring ended. After five minutes of holding the AZ91E and grain refiner mixture in the melting furnace, two graphite moulds were removed from the heating furnace and placed a top firebrick. A stainless steel ladle was then used to pour a portion of the melt into the crucibles at a pouring temperature of 720 °C (castings to represent five minutes of holding). After pouring, the graphite moulds were covered with a steel plate, according to the assembly in Figure 3-2. The data acquisition system for thermal measurements was started prior to removal of the graphite moulds from the heating furnace to ensure the entire cooling curve was captured. The melting furnace temperature was lowered to 750 °C to maintain the melt temperature and, after another five minutes of holding (total 10 minutes), the stainless steel ladle was used to produce another two graphite mould castings (castings representing 10 minutes of holding). The same procedure was repeated once more for the final two graphite moulds to represent a holding time of 20 minutes. Any remaining melt was poured into a pig. A summary of the pouring procedure is outlined in Table 3-5.

Table 3-5: Experimental Procedure for Grain Refinement and Fading Experiments

Process	Important Parameters
Preparation of Materials	
I	• **1 kg** of virgin AZ91E ingot • Grain refiner chunks (<**0.3 g** each)
II	• AZ91E ingots and grain refiner were placed in preheating furnace at **200 °C** for **30** minutes.
III	• Graphite moulds were placed in heating furnace at **750 °C**
Melting of Alloy	
I	• AZ91E ingots were placed into melting furnace set at 775°C • **17 m^3/h** of CO_2 cover gas
Addition of Grain Refiner	
I	• Melt temperature was checked using **K-type** thermocouple (**>750 °C**) • Melt was skimmed if necessary
II	• Grain refiner was **added** to melt
III	• Melt was stirred at **200 rpm** for **30** seconds • Timer was started
Pouring	
I	• **Graphite moulds** were removed from heating furnace • Data acquisition was **started**
II	• Ladle was used to pour two castings (five minute samples) • Castings were **covered** (Figure 3-2) • Melting furnace temperature was **decreased** to **750 °C**
III	• I and II were repeated for **10** minute and **20** minute samples

A summary of all the addition levels, holding times and most significant casting parameters used for each grain refiner is outlined in Table 3-6.

Table 3-6: Major Casting Parameters (Grain Refinement and Fading Experiments)

Pouring Temp. (°C)	Mould Temp. (°C)	Holding Times (min)	Al-5Ti-1B Addition Levels (wt.%)	Al-1Ti-3B Addition Levels (wt.%)
720	750	5, 10, 20	0.1	0.1
			0.2	0.2
			0.5	0.5
			1.0	1.0

The pouring temperature of 720 °C was used to match industry practices which maintain temperatures between 680 and 740 °C for permanent mould cast Mg alloys. The high mould

temperature was to ensure that the mould walls did not act as a site for nucleation of grains. Also, the high mould temperature promoted a very slow cooling rate which translated in a large number of temperature measurements recorded by the data acquisition system during solidification. Holding times of 5, 10 and 20 minutes were used during this study to ensure appreciable fading and to ensure effectiveness of CO_2 cover gas.

The addition levels of 0.1, 0.2, 0.5 and 1.0 wt.% were chosen to be similar to research conducted by Vinod Kumar *et al.* [44] which examined grain refinement and fading of Al-7 wt.% Si alloy using Al-Ti-C and Al-Ti-B grain refiners. Any additions beyond 1.0 wt.% were far beyond standard allowable compositional limits of Al in AZ91E.

3.2.2 Hot Tearing Susceptibility Experiments

The procedure used to produce the castings for the hot tearing susceptibility experiments was identical to the procedure used in the grain refinement and fading experiments described in Section 3.2.1. Initially, approximately 800 g of virgin AZ91E Mg alloy was preheated at 200 °C for at least 30 minutes. The ingots were then added to a low carbon steel crucible and placed into a custom designed electric resistance melting furnace (PSH Kilns, 5 kW, Oakville, Ontario) set to a temperature of 765 °C. Carbon dioxide was used as a cover gas at a flow rate of 17 m^3/h to prevent oxidation of the melt. The required amount of grain refiner was prepared and added in the same manner as in Section 3.2.1.

The melt was then removed from the furnace and placed a top fireclay brick adjacent to the permanent mould preheated to 180 °C. The thermocouple was re-inserted into the melt and once the melt temperature dropped to 727 °C the melt was skimmed once again, the data acquisition unit for temperature measurements was started and the melt was poured into the preheated permanent mould. Preliminary experiments determined that a temperature loss of 7 °C occurred during skimming and melt transfer to the preheated permanent mould. The casting was then removed from the permanent mould five minutes after pouring. A summary of the pouring procedure is outlined in Table 3-7.

Table 3-7: Experimental Procedure for Hot Tearing Susceptibility Experiments

Process	Important Parameters
Preparation of Materials	
I	• **800 g** of virgin AZ91E ingot • Grain refiner chunks (<**0.3 g** each)
II	• AZ91E ingots and grain refiner were placed in preheating furnace at **200 °C** for **30** minutes.
Melting of Alloy	
I	• AZ91E ingots were placed into melting furnace set at **765 °C** • **17 m^3/h** of CO_2 cover gas
Addition of Grain Refiner	
I	• Melt temperature was checked using **K-type** thermocouple (**>750 °C**) • Melt was skimmed if necessary
II	• Grain refiner was **added** to melt
III	• Melt was stirred at **200 rpm** for **30** seconds
Pouring	
I	• Data acquisition was **started**
II	• Melt was **poured** directly into permanent mould using low carbon steel crucible
Casting Removal	
I	• Castings were removed **five minutes** after pouring

A summary of all the addition levels, holding times and most significant casting parameters used for each grain refiner are outlined in Table 3-8.

Table 3-8: Major Casting Parameters (Hot Tearing Susceptibility Experiments)

Pouring Temp. (°C)	Mould Temp. (°C)	Al-5Ti-1B Addition Level (wt.%)	Al-1Ti-3B Addition Levels (wt.%)
720	180	Optimal addition level to be determined	Optimal addition level to be determined

A pouring temperature of 720 °C was used for two main reasons. This correlates well with the industry practices which focus between 680 and 740 °C. Further, this pouring temperature ensures consistency with the grain refinement and fading experiments. Previous casting trials [54] found that a mould temperature of 180 °C resulted in a full crack in AZ91E with a pouring temperature of 720 °C. By designating a casting with a hot tear as the baseline, any

additions that result in larger tears would be distinguished as increasing hot tearing susceptibility and any tears smaller than the baseline would represent additions that decreased hot tearing susceptibility. The optimal addition levels were determined from the grain refinement and fading experiments. The logic used to determine the optimal addition levels is discussed in the subsequent chapter.

3.3 Microstructure Analysis

Three different microscopy techniques were used to examine the castings and grain refiners. Each technique required its own set of preparation guidelines and the procedures for each appear in the following order: optical microscopy, scanning electron microscopy and transmission electron microscopy.

3.3.1 Optical Microscopy

For the hot tearing samples, the castings were first solution heat treated at 412 °C for 16 hours with an air quench to dissolve the $Mg_{17}Al_{12}$ eutectic phase. No solution heat treatment was preformed for the graphite castings. All castings were prepared using the procedure described in Table 3-9.

Table 3-9: Casting Grinding and Polishing Procedure for Optical Microscopy

Process	Paper Type	Duration (min)
Grinding		
I	120 Grit SiC	Until Plane
II	320 Grit SiC	2.5
III	600 Grit SiC	2.5
IV	1200 Grit SiC	2.5
Polishing		
I	LECO LECLOTH® w/ 3 micron diamond extender	1, or until mirror surface

Grinding steps I-IV, used water as a lubricant with 5 lb of pressure at a grinding wheel rotation rate of 150 rpm except for step IV which was held by hand. The grinding cloths were replaced every 1.25 minutes. Polishing step I was done by hand with no water lubricant at 200 rpm and the sample was cleaned using ethanol and a blast of compressed air.

The graphite samples were etched by immersing them in a solution of 15 % acetic acid, 10 % distilled water and 75 % ethyl alcohol for two minutes with slight agitation. The hot tearing samples were etched using a solution of 60 % ethylene glycol, 20 % acetic acid, 19 % water and 1 % nitric acid for 10 seconds with slight agitation. Water was used to stop both etching processes and compressed air was used to dry the samples. For the graphite mould castings, grain size measurements were made 10 mm from the bottom surface of the casting. Grain size measurements of the hot tearing samples was done in the casting bar region as indicated by the "Optical Sample" in Figure 3-6. The measurements were made on the face perpendicular to the length of the casting (2.5 cm from the downsprue). The grain size was measured using the linear intercept method over 100 grains immediately after etching. Optical micrographs of the castings were taken using a Leitz optical microscope and Buehler OMNINET® imaging software.

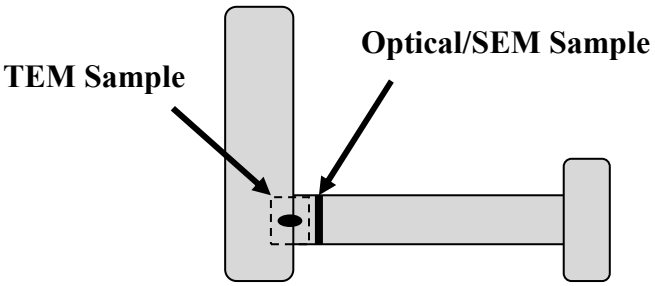

Figure 3-6: Locations of the Samples Used for Optical, SEM and TEM Examination

3.3.2 Scanning Electron Microscopy

For scanning electron microscopy (SEM) examination, the samples were prepared in the same manner as described in Section 3.3.1 and Table 3-9. The SEM analysis was performed on the same sample surface as the grain size measurements for both the graphite mould and hot tearing samples. Etching was limited to samples that showed poor image contrast in the SEM. Scanning electron microscopy analysis was performed on a JOEL-SEM using back-scatter electron (BSE) imaging at a working distance of 11 mm and a potential of 20 kV and a FEI Quanta 200 SEM using a working distance of 8.4 mm and a potential of 30 kV.

3.3.3 Transmission Electron Microscopy

Select castings were prepared for transmission electron microscopy (TEM). For the graphite mould castings, TEM examination was performed on the same sample surface as the grain size measurements and SEM analysis. For the hot tear castings the TEM sample was removed from

the junction of the downsprue and casting bar as described in Figure 3-6. The centre of the casting was examined with the longitudinal axis of the sample running along the casting bar. The samples were prepared using the procedure described in Table 3-10.

Table 3-10: Sample Preparation for Transmission Electron Microscopy

Process	Technique/Tool	Comments
Sectioning		
I	Low speed saw at **200 RPM**, with a **300 g** load	• Rough cut to obtain flat surface
II	Low speed saw at **100 RPM**, with a **100 g** load	• Results in a 500 μm thick flat sample
Grinding*		
I	320 Grit SiC paper at **150 RPM**	• Min. pressure to avoid bending
II	600 Grit SiC paper at **150 RPM**	• Min. pressure to avoid bending
III	1200 Grit SiC paper at **150 RPM**	• Min. pressure to avoid bending • Sample thickness should be < **200 μm** after this step
IV	1/0, 2/0, 3/0 and 4/0 emery paper	• Uni-directional, by hand • Use successively finer papers
Removal		
I	Sample with holder in acetone bath	• Sample detaches from holder • Sample should be < **100 μm**

*The sample was held on a flat steel block using double sided tape for easy handling.

All the sectioning and grinding steps were preformed with flowing water as a lubricant. A Struers Minitom precision cut-off wheel was used for sectioning the sample. The final thinning was performed using a Gatan (Model 691) precision ion polishing system at an energy level of 5 keV, incident angle of 10 ° and current of 30 μA. The samples were then immediately placed into a Phillips CM-12 120 keV TEM vacuum chamber to minimize oxidation on the sample surface.

3.4 Thermal Analysis

Thermal analysis of the solidifying castings was preformed for the grain refinement and fading experiments as well as the hot tearing susceptibility experiments. This section describes the procedure used to obtain thermal data for both portions of the study.

3.4.1 Grain Refinement and Fading Experiments

The data acquisition unit was set to make temperature measurements every 0.2 seconds for six minutes. Two measurements were performed for each casting condition to ensure repeatability and obtain a cooling curve that ranged from above the liquidus temperature to the solidus temperature. The thermocouple was located in the center of the melt as shown in Figure 3-2. The data acquisition unit would output the data into a notepad file that could be easily transferred and manipulated using Microsoft EXCEL®.

3.4.2 Hot Tearing Susceptibility Experiments

The temperature measurements were made in the same manner as in the grain refinement and fading experiments except they were made for five minutes prior to pouring in three different locations on the casting. The temperature measurements were made in the center section of the casting, as described previously in Section 3.1.5.4 and Figure 3-5. Thermocouples would interfere with the metal flow during solidification; therefore, an independent set of castings was produced specifically for thermal analysis.

CHAPTER 4 RESULTS AND DISCUSSION

4.1 Microstructure of Grain Refiners

Scanning electron microscopy of the Al-5Ti-1B and Al-1Ti-3B grain refiners was carried out to observe the particles responsible for grain refinement. The size, shape and distribution of the particles within the grain refiners were also examined.

4.1.1 Al-5Ti-1B

The microstructure of the Al-5Ti-1B grain refiner is shown in Figure 4-1A. Large particles (> 30 μm, A) and fine particles (< 3 μm, B) were observed. An EDX analysis showed that the large particles contained Al and Ti, while the fine particles contained Ti. The large Ti-Al particles were identified as $TiAl_3$ and was expected because the Ti:B ratio in the Al-5Ti-1B grain refiner is greater than 1:2 [36]. The fine Ti bearing particles were compared to the particle morphology observed in the study by Fjellstedt *et al.* [64] and deduced to be TiB_2. Using SEM, the accurate detection of B in small concentrations is difficult due to the low intensity of B and the limitations of EDX analysis. The Al-5Ti-1B grain refiner in Figure 4-1A contained a high concentration of well distributed TiB_2 nucleating particles.

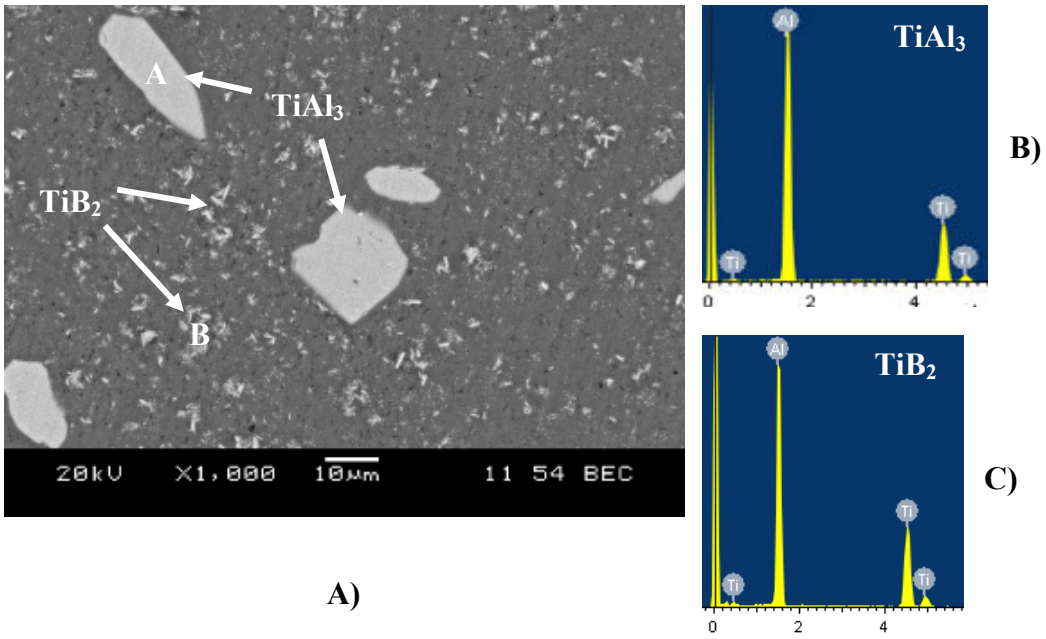

Figure 4-1: A) SEM Image of Al-5Ti-1B Grain Refiner B) EDX Analysis of Particle A and C) EDX Analysis of Particle B

The well distributed TiB_2 particles are expected to promote repeatable grain refinement results when added to AZ91E. The small particle size enables a large number of nucleating sites over a few larger particles at the same Ti and B content.

The formation of the $TiAl_3$ and TiB_2 particles during synthesis can be explained with the following chemical reactions [65]:

$$3K_2TiF_6 + 13Al \rightarrow 3TiAl_3 + 3KAlF_4 + K_3AlF_6 \quad \textbf{(22)}$$

$$2KBF_4 + 3Al \rightarrow AlB_2 + 2KAlF_4 \quad \textbf{(23)}$$

$$AlB_2 + TiAl_3 \rightarrow TiB_2 + 4Al \quad \textbf{(24)}$$

The reactions in Equation 22 and Equation 23 occur simultaneously followed by the reaction in Equation 24. For the Al-5Ti-1B grain refiner, no AlB_2 particles were observed. The AlB_2 particles must have completely reacted with $TiAl_3$ to form TiB_2 during synthesis. In other words, AlB_2 particles were not observed during the SEM analysis.

4.1.2 Al-1Ti-3B

An SEM image of the Al-1Ti-3B grain refiner is shown in Figure 4-2A with corresponding EDX analysis of TiB_2 and AlB_2 particles in Figure 4-2B and Figure 4-2C, respectively. The B

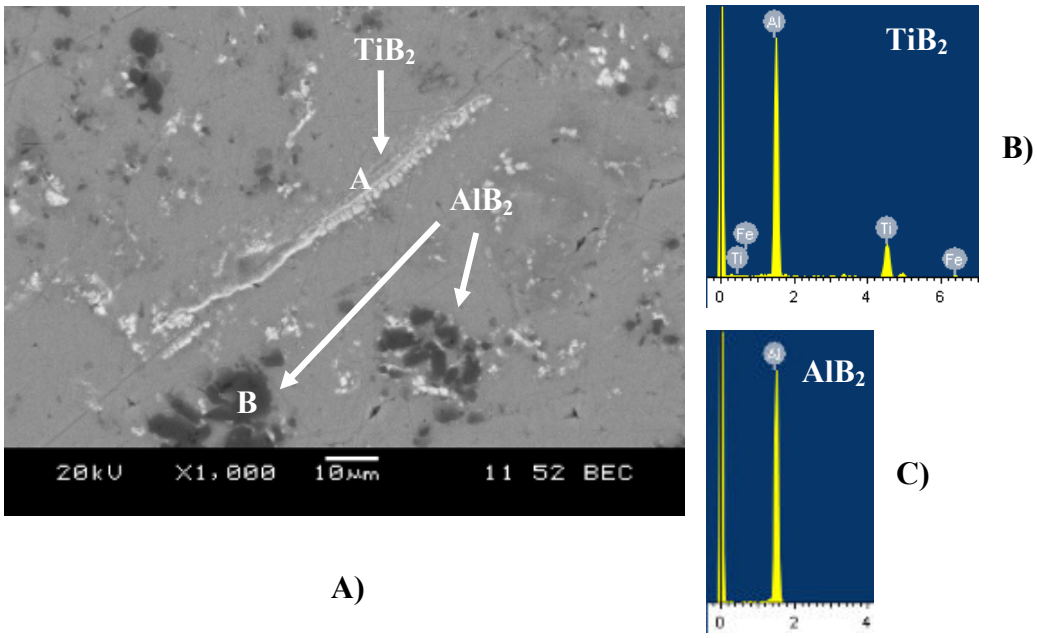

Figure 4-2: SEM Image of Al-1Ti-3B Grain Refiner A) SEM Image of Al-1Ti-3B B) EDX Analysis of Particle A and C) EDX Analysis of Particle B

content within the Al-1Ti-3B grain refiner exceeded the Ti:B ratio of 1:2.5, resulting in a microstructure that contained TiB_2, AlB_2 and no $TiAl_3$ [36]. At location A, The particles are believed to be TiB_2 because of the similarity of their morphology and EDX analysis with the TiB_2 particles in Figure 4-1. At location B, the particles are believed to be AlB_2 by once again comparing with the particles observed by Fjellstedt *et al.* [64]. Aluminum diboride particles formed as a result of the chemical reaction in Equation 23 and reacted with $TiAl_3$ to form TiB_2 according to Equation 24. The $TiAl_3$ particles were the limiting reagent and were exhausted first, leaving only AlB_2 and TiB_2 particles in the Al-1Ti-3B grain refiner.

Aluminum diboride particles can also act as nucleating sites as observed by Suresh *et al.* [27]. A comparison between the Al-5Ti-1B and Al-1Ti-3B grain refiners reveals that the latter has significantly fewer clusters of fine particles which may have hindered its grain refining performance.

The microstructure of the Al-1Ti-3B grain refiner also contained some potassium and fluorine based particles which were K_2TiF_6 and KBF_4 residual salts that did not have sufficient time to react to completion during synthesis. Figure 4-3 depicts the residual salt clustered together with AlB_2 particles. It is not clear if the unreacted salts had any harmful effects on the grain refining performance of Al-1Ti-3B.

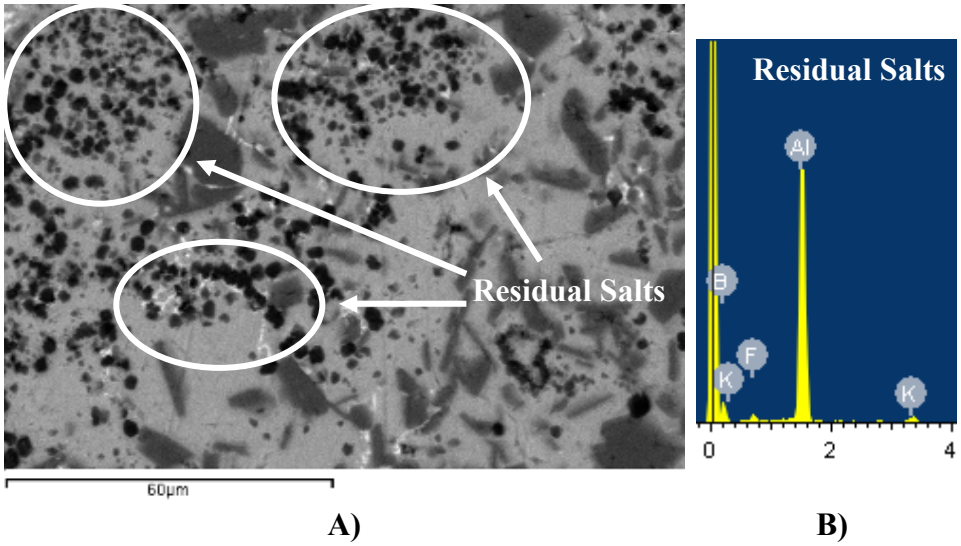

Figure 4-3: SEM Image of Al-1Ti-3B Grain Refiner Showing Residual Salt Particles A) SEM Image of Residual Salt Particles B) EDX Analysis of Salt Particles

Examination of the refiners revealed that Al-5Ti-1B contained fine (< 3 μm) and well distributed TiB_2 particles alongside coarse (> 30 μm) $TiAl_3$ particles with no observed residual salts. The Al-1Ti-3B grain refiner contained a lower concentration of TiB_2 particles with 3-10 μm sized AlB_2 particles. There were some residual K_2TiF_6 and KBF_4 salts, but no $TiAl_3$ particles. The Al-5Ti-1B grain refiner is expected to have the better grain refining performance because of the many potential TiB_2 nucleating particles available. While the Al-1Ti-3B grain refiner has fewer TiB_2 particles, the presence of AlB_2 particles are expected to contribute to grain refinement [27]. The effects of $TiAl_3$ and the unreacted salts on grain refining efficiency are not clear.

Part I: Grain Refinement and Fading Experiments

4.2 Grain Size Measurement

This section summarizes the effect of addition level and holding time on the grain size of AZ91E with Al-5Ti-1B and Al-1Ti-3B addition. The grain size measurements for the baseline AZ91E sample is presented first followed by grain size measurements for the samples treated with Al-5Ti-1B and Al-1Ti-3B, respectively.

4.2.1 AZ91E

An optical micrograph of the base AZ91E alloy is shown in Figure 4-4. The average grain size for AZ91E without any grain refiner addition was 1000 μm. The grain structure was equiaxed and no columnar grains were observed at the edges of the casting. The mould temperature was above (~30 °C) the pouring temperature of the melt. Consequently, solidification proceeded uniformly in all directions.

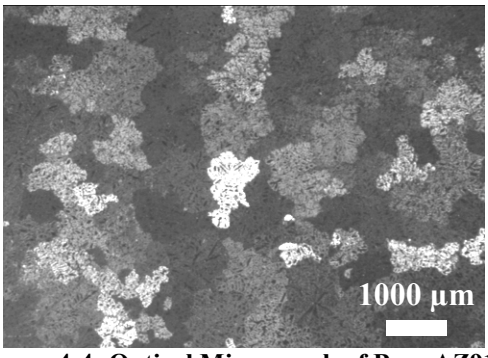

Figure 4-4: Optical Micrograph of Base AZ91E

4.2.2 AZ91E + Al-5Ti-1B

The microstructural changes with increase in holding time for the 0.1 wt.% Al-5Ti-1B addition are depicted in Figure 4-5A. With this addition, a significant grain size reduction from 1000 μm to 323 μm at a holding time of five minutes was observed. The optical micrographs for the remaining addition levels of 0.2, 0.5 and 1.0 wt.% are also in Figure 4-5. Addition levels of 0.1 and 0.2 wt.% provided the largest degree of grain refinement. The addition levels of 0.5 and 1.0 wt.% resulted in grain sizes comparable to the unrefined alloy. All addition levels showed very little signs of fading, indicated by no appreciable grain growth with increasing holding time. A calculation for the addition of the grain refiners is provided in Appendix A.2.

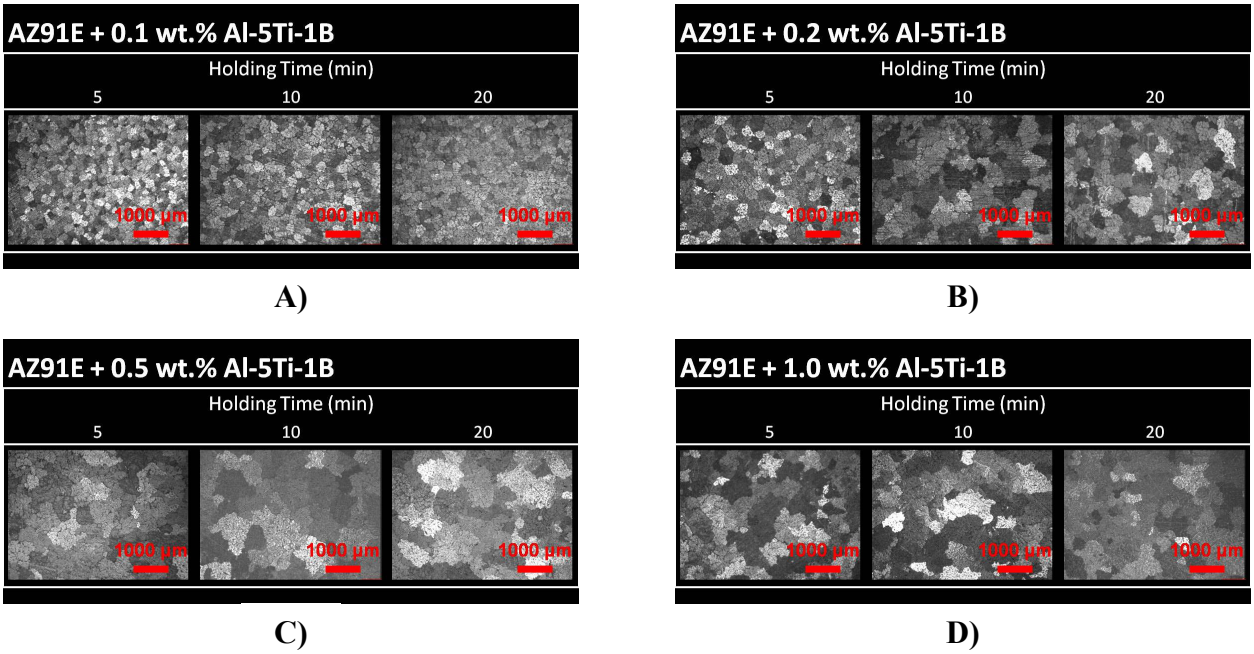

Figure 4-5: Optical Micrographs of AZ91E + Al-5Ti-1B Castings with Increasing Holding Time A) 0.1 wt.% Al-5Ti-1B B) 0.2 wt.% Al-5Ti-1B C) 0.5 wt.% Al-5Ti-1B D) 1.0 wt.% Al-5Ti-1B

A quantitative summary of the average grain sizes with error bars representing one standard deviation is shown in Figure 4-6. It is believed that TiB_2 particles within the grain refiners provided heterogeneous nucleating sites during solidification, as observed by Wang *et al.* [37] and Liu *et al.* [33].

The fading of the grain refiner could be explained by density differences between the Mg and TiB_2. For each casting, the liquid metal was ladled from the top of the crucible. As time progressed the denser TiB_2 particles (4.38 g/cm^3) [66] likely sunk to the bottom of the less dense (1.74 g/cm^3) Mg melt [1]. Therefore, at longer holding times, fewer TiB_2 particles were available

for nucleation. At addition levels of 0.5 and 1.0 wt.%, the poor grain refinement was attributed to TiB_2 particle agglomeration. Fine particles, such as TiB_2 tend to agglomerate to reduce their surface energy as observed by Mohanty *et al.* [66].

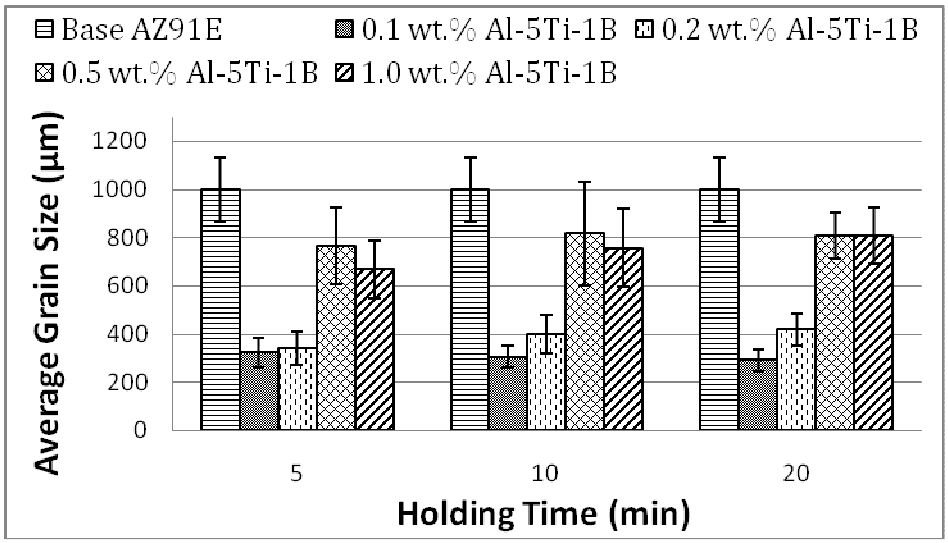

Figure 4-6: Influence of Al-5Ti-1B Addition Levels and Holding Time on the Grain Size of AZ91E

4.2.3 AZ91E + Al-1Ti-3B

The grain refinement was almost negligible with 0.1 and 0.2 wt.% Al-1Ti-3B addition (Figure 4-7A and B). However, the addition levels of 0.5 and 1.0 wt.% Al-1Ti-3B

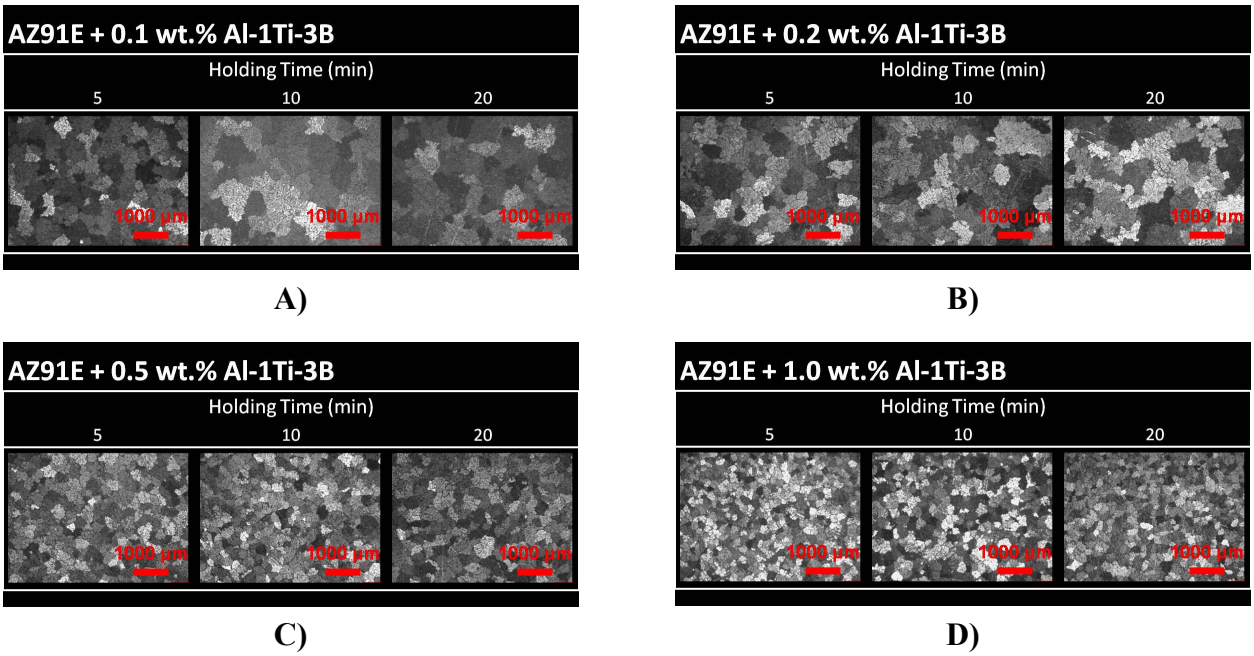

Figure 4-7: Optical Micrographs of AZ91E + Al-1Ti-3B Castings with Increasing Holding Time A) 0.1 wt.% Al-1Ti-3B B) 0.2 wt.% Al-1Ti-3B C) 0.5 wt.% Al-1Ti-3B D) 1.0 wt.% Al-1Ti-3B

(Figure 4-7C and D) provided significant grain refinement. The smallest average grain size after a holding time of five minutes was 361μm at an addition level of 1.0 wt.%. The grain refinement was attributed to AlB_2 and TiB_2 nucleating agents as observed by Suresh *et al.* [27] and Liu *et al.* [33] respectively. A summary of the average grain sizes with error bars representing one standard deviation is shown in Figure 4-8. The increase in holding time resulted in only a small increase in grain size with Al-1Ti-3B addition (Figure 4-7D), indicating that the Al-1Ti-3B grain refiner was resistant to fading. The significance of the change in grain size with holding time was examined with an analysis of variance (ANOVA) in Appendix A.3.

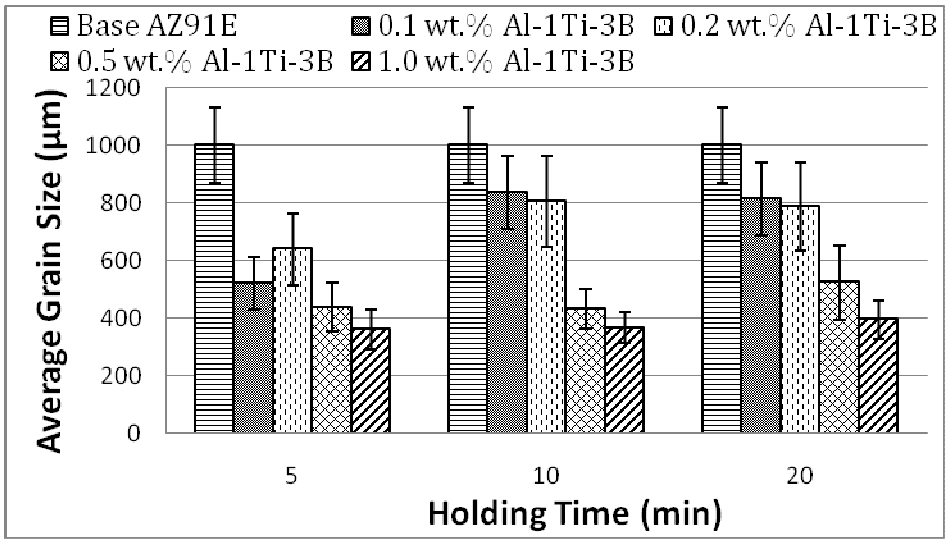

Figure 4-8: Influence of Al-1Ti-3B Addition Levels and Holding Time on the Grain Size of AZ91E

The results suggest that more Al-1Ti-3B was required to obtain similar grain sizes as those obtained when using small amounts of Al-5Ti-1B. A possible explanation for this is the smaller number of nucleating particles in the Al-1Ti-3B grain refiner. Since the Al-5Ti-1B grain refiner contained many nucleating particles as shown in Figure 4-1A, it was very effective even at low addition levels. The increase in grain size at 0.5 and 1.0 wt.% Al-5Ti-1B addition was attributed to TiB_2 agglomeration as observed by Mohanty *et al.* [66]. The residual K_2TiF_6 and KBF_4 salts observed in Figure 4-3A are wasted Ti and B additions that had the potential to become nucleating particles. The lost Ti and B could have hindered the grain refining performance of the Al-1Ti-3B grain refiner.

The grain size measurements indicated that both grain refiners are capable of providing significant grain refinement. The Al-5Ti-1B grain refiner was more effective at lower addition

levels with a minimum grain size of 323 μm with an addition level of 0.1 wt.% and the Al-1Ti-3B grain refiner had a minimum grain size of 361 μm with an addition level of 1.0 wt.%.

4.3 Thermal Analysis

Using the thermocouple setup depicted in Figure 3-2 (Section 3.1.4), measurements for the undercooling of the solidifying castings were taken as an indicator of grain refinement. A casting with zero or very little undercooling would indicate very marked grain refinement, while a casting showing undercooling similar to that of the unrefined AZ91E would indicate poor grain refinement. With grain refinement, the activation barrier ΔG^* (Section 2.1.1, [4]) decreases, resulting in a reduction of undercooling required by the melt for nucleation to occur. If the grain refinement in marked enough, no undercooling is required for nucleation.

Undercooling measurements were made by examining the dip in temperature on the cooling curves, as shown in Figure 4-9. The cooling curves for all the castings were plotted and each curve was measured individually. Undercooling measurements of the AZ91E casting without any refiner addition is presented first followed by castings treated with Al-5Ti-1B and Al-1Ti-3B, respectively. Of the grain refined castings, only the cooling curves corresponding to addition levels that provided the highest degree of grain refinement are presented in this section. The cooling curves for all the castings are in Appendix A.4.

The average undercooling in the base AZ91E alloy was 1 °C and is clearly visible at the 73 seconds in Figure 4-9. Undercooling measurements for the Al-5Ti-1B and Al-1Ti-3B grain refined castings were compared to that of the base AZ91E alloy as an indication of the degree of grain refinement. A very small undercooling (eg. 0.1 °C) would indicate significant grain refinement while a relatively large undercooling (0.9 °C) would relate to a small degree of grain refinement.

As observed in Figure 4-10 the addition of 0.1 wt.% Al-5Ti-1B resulted in a large reduction in undercooling for all holding times. This result is in agreement with the optical micrographs and grain size measurements.

Figure 4-9: Cooling Curve of AZ91E Alloy

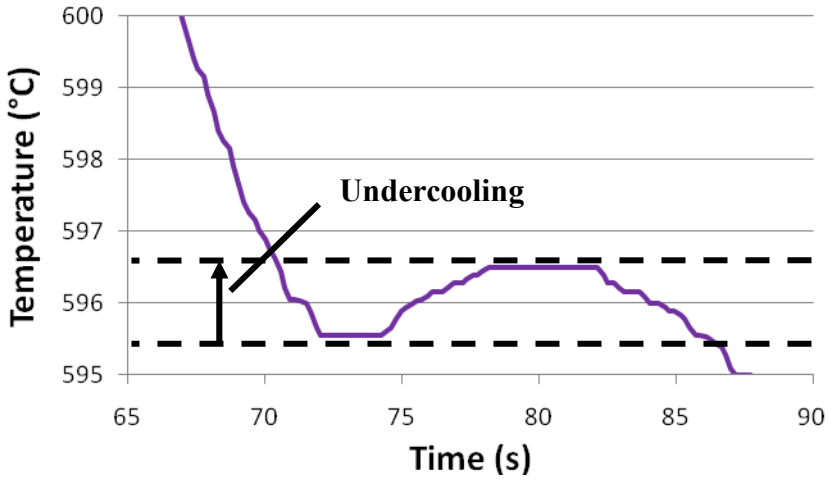

The measured average undercooling was 0.1, 0.2 and 0.1 °C for holding times of 5, 10 and 20 minutes respectively. A comparison to the 1 °C undercooling observed in the AZ91E alloy shows that 0.1 wt.% Al-5Ti-1B addition promoted nucleation and resulted in fine grains, as summarized in Figure 4-10. The undercooling data does show some inconsistency with a rise then fall of recorded undercooling from holding times of 10 and 20 minutes, respectively. This will be discussed further at the end of Section 4.3.

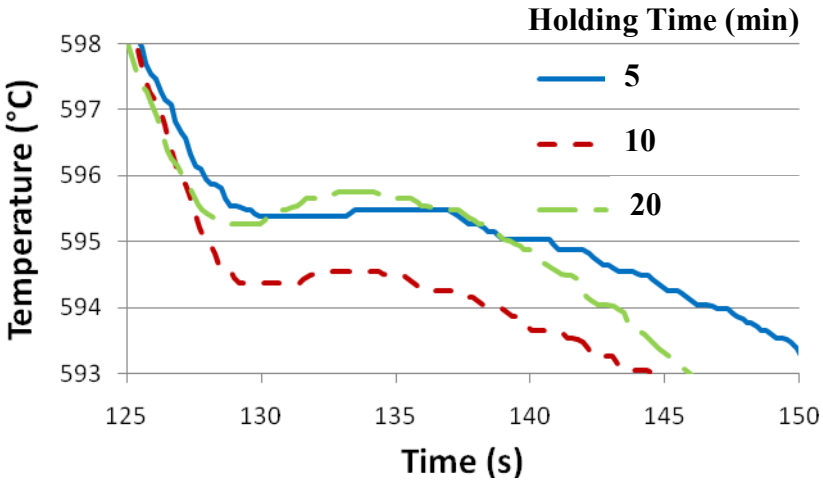

Figure 4-10: Cooling Curves of AZ91E + 0.1 wt.% Al-5Ti-1B

The cooling curves of the castings produced using 1.0 wt.% Al-1Ti-3B for all holding times are shown in Figure 4-11. The undercooling measurements recorded were 0.1, 0.3 and 0.1 °C for

holding times corresponding to 5, 10 and 20 minutes, respectively. Similar to the castings treated with 0.1 wt.% Al-5Ti-1B, there was inconsistent measurements resulting in an increase then decrease in undercooling with increasing holding time from 10 to 20 minutes.

It is interesting to note that both 0.1 wt.% Al-5Ti-1B and 1.0 wt.% Al-1Ti-3B additions provided approximately the same degree of grain refinement as well as similar undercooling values.

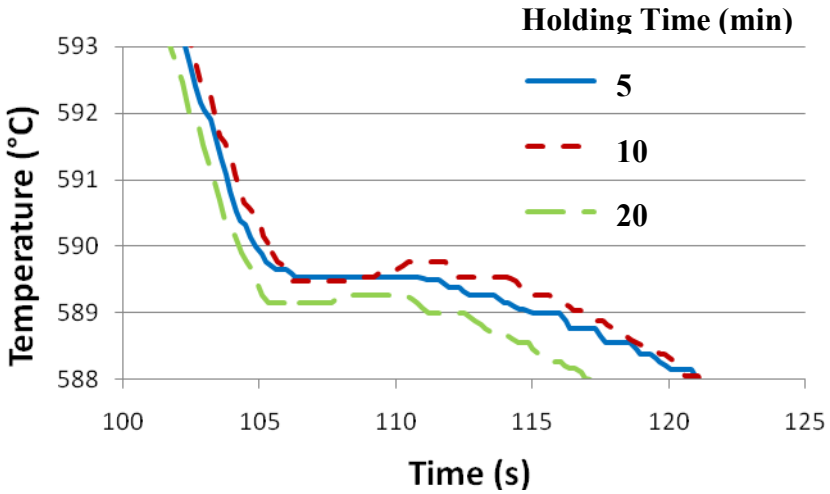

Figure 4-11: Cooling Curves of AZ91E + 1.0 wt.% Al-1Ti-3B

The average undercooling observed for all the casting trials is presented in Table 4-1. As discussed earlier there are some inconsistent values of undercooling observed for some of the casting trials. For example, the addition of 0.5 wt.% Al-1Ti-3B resulted in undercoolings of 0.3, 0.2 and 0 °C for 5, 10 and 20 minute holding times, respectively, indicating smaller grain sizes with increasing holding time. A comparison with the grain size measurements in Figure 4-8 indicates a small increase in grain size with increasing holding time.

A summary of the plateau temperatures of AZ91E, AZ91E + 0.1 wt.% Al-5Ti-1B and AZ91E + 1.0 wt.% Al-1Ti-3B is presented in Table 4-2. With Al-Ti-1B addition the plateau temperatures tend to fluctuate and can be explained as follows. The addition of 1.0 wt.% Al-1Ti-3B grain refiner increased the Al concentration within the melt by approximately 0.8 wt.%. The increased Al content reduced the nucleation temperature resulting in lower plateau temperatures compared to the unrefined alloy. With the addition of 0.1 wt.% Al-5Ti-1B, the Al concentration within the melt increased by less than 0.1 wt.%, resulting in only a small decrease in plateau temperatures as compared to the unrefined alloy. Additional information regarding the

change in nucleation temperature with the addition of Al to Mg is provided in the Mg-Al phase diagram in Appendix A.5.

Table 4-1: Average Undercooling During Solidification

Alloy	**Average Undercooling (°C)**		
AZ91E	1.0		
	Holding Time (min)		
	5	**10**	**20**
AZ91E + 0.1 wt.% Al-5Ti-1B	0.1	0.2	0.1
AZ91E + 0.2 wt.% Al-5Ti-1B	0.3	0.5	0.5
AZ91E + 0.5 wt.% Al-5Ti-1B	1.0	0.8	0.8
AZ91E + 1.0 wt.% Al-5Ti-1B	0.4	0.8	0.5
AZ91E + 0.1 wt.% Al-1Ti-3B	0.3	1.0	0.7
AZ91E + 0.2 wt.% Al-1Ti-3B	0.5	0.7	0.8
AZ91E + 0.5 wt.% Al-1Ti-3B	0.3	0.2	0
AZ91E + 1.0 wt.% Al-1Ti-3B	0.1	0.3	0.1

Table 4-2: Summary of Plateau Temperatures

Alloy	**Plateau temperature (°C)**
AZ91E	596.5
AZ91E + 0.1 wt.% Al-5Ti-1B (5 min)	595.5
AZ91E + 0.1 wt.% Al-5Ti-1B (10 min)	594.5
AZ91E + 0.1 wt.% Al-5Ti-1B (20 min)	595.7
AZ91E + 1.0 wt.% Al-1Ti-3B (5 min)	589.5
AZ91E + 1.0 wt.% Al-1Ti-3B (10 min)	589.5
AZ91E + 1.0 wt.% Al-1Ti-3B (20 min)	589.2

Despite the differences in plateau temperatures, the thermal analysis accurately predicted a large degree of grain refinement with small values of undercooling. An example can be seen with the addition of 0.1 wt.% Al-5Ti-1B and 1.0 wt.% Al-1Ti-3B. These two addition levels had the highest grain refinement represented by both grain size measurements and undercooling measurements. Therefore, thermal analysis can be used as an indicator of the efficiency of grain refinement.

4.4 Mechanism of Grain Refinement

Microstructure examination using both SEM and TEM was performed on the grain refined castings. Samples were examined in the same area that was used for the grain size measurements. The purpose of the microscopy was to identify the particles responsible for grain refinement and observe whether any reactions occurred within the melt. The results related to castings treated with Al-5Ti-1B are presented first, followed by the Al-1Ti-3B treated castings.

4.4.1 AZ91E + Al-5Ti-1B

Scanning electron microscopy analyses demonstrated no direct observation of TiB_2 particles within the centre of Mg grains. This was in contrast to the results obtained by Liu *et al.* [33]. As a result, the grain refinement was then attributed to TiB_2 particles restricting Mg grain growth, as observed by Wang *et al.* [38]. It was likely that the TiB_2 particles were rejected from the liquid metal front and pushed into the grain boundary regions becoming entrapped within the $Mg_{17}Al_{12}$ eutectic. Another possibility is that the TiB_2 particles act as nucleating sites and any excess particles (not going to the nucleating sites) restrict grain growth. To test the latter hypothesis, a sample containing a high concentration (5 wt.%) of Al-5Ti-1B was prepared. The sample was poured using the same experimental parameters as described in Section 3.2.1 with no holding time. As shown in Figure 4-12, large $TiAl_3$ and fine TiB_2 particles were found entrapped within the $Mg_{17}Al_{12}$ eutectic at the grain boundaries, which was in agreement with Wang *et. al.* [38]. The $TiAl_3$ particles also segregate to the grain boundaries but are not expected to aid in grain refinement. As a result of their large size, the $TiAl_3$ particles are unable to diffuse to the grain surface and build a solute layer required for grain growth restriction (Section 2.2). Without a slow diffusion of solute from the grain, the undercooled layer could not be built. Therefore, the addition of Al-5Ti-1B grain refiner introduces $TiAl_3$ and TiB_2 particles into the melt. Only the TiB_2 particles reduced the AZ91E grain size by grain growth restriction.

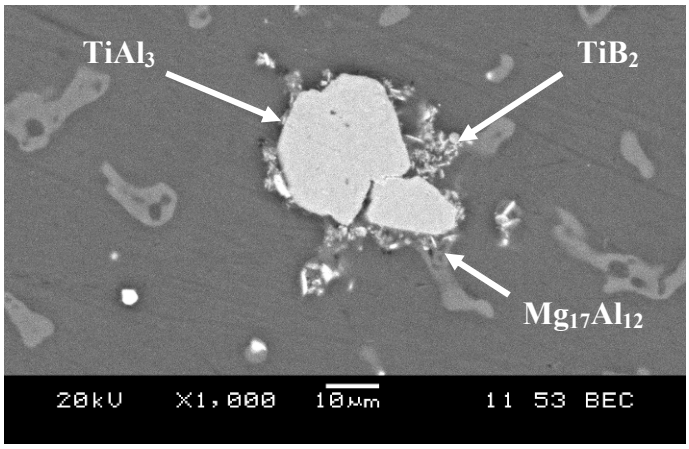

Figure 4-12: SEM Image of AZ91E + 5.0 wt.% Al-5Ti-1B Showing $TiAl_3$ and TiB_2 Particles entrapped within $Mg_{17}Al_{12}$ Eutectic

4.4.2 AZ91E + Al-1Ti-3B

An SEM image with corresponding EDX analysis of an Al based particle within the centre of the α-Mg grain is shown in Figure 4-13. The Al based particle is approximately 3.5 µm in length which is comparable to the sizes of particles observed in Figure 4-2 and the study by Fjellstedt *et al.* [64]. This particle is believed to be AlB_2. The AlB_2 particle within the centre of the grain indicates that it was the source of nucleation for the Mg grain.

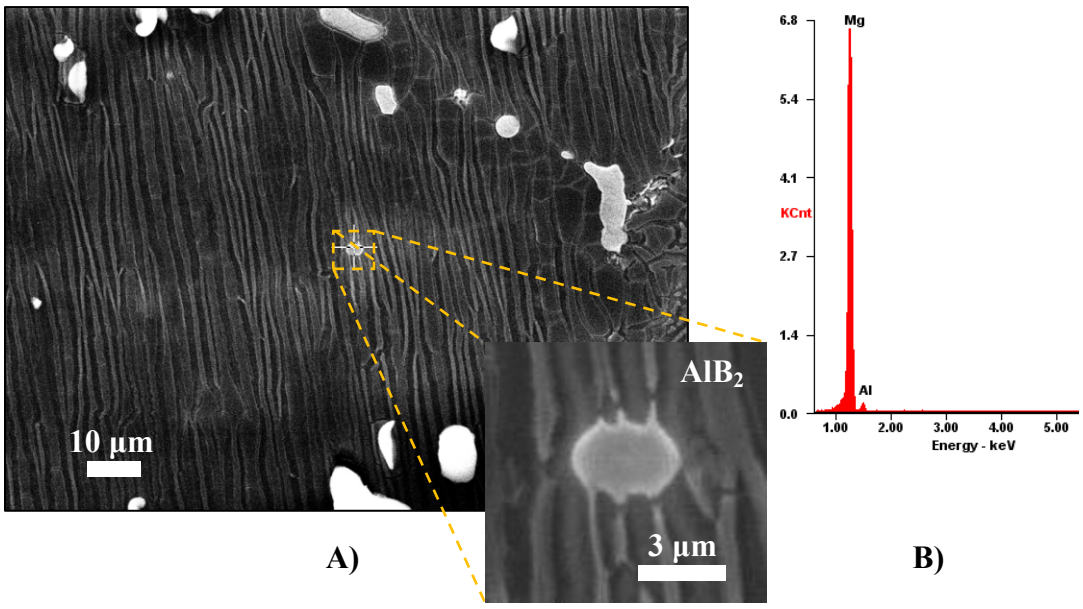

Figure 4-13: SEM Image of AZ91E + 1.0 wt.% Al-1Ti-3B after 5 Minutes of Holding A) Al Particle at the Centre of Grain B) Corresponding EDX Analysis

Similar to the casting treated with Al-5Ti-1B, the TiB_2 is believed to also aid in grain refinement by restricting grain growth, as shown in Figure 4-14. The image in Figure 4-14 was a high concentration (5 wt.%) Al-1Ti-3B sample used to confirm that the TiB_2 particles segregate to the grain boundaries in a manner similar to the Al-5Ti-1B sample in Figure 4-12.

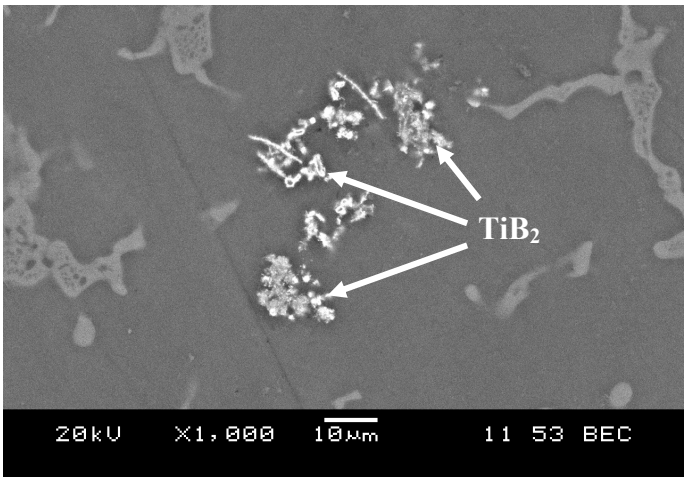

Figure 4-14: TiB_2 particles at Grain Boundary in AZ91E + 5 wt.% Al-1Ti-3B

The addition of the Al-1Ti-3B grain refiner also introduced solute Ti into the Mg alloy as observed in Figure 4-15. Small particles (~500 nm) containing Mg, Al, Ti, O and C were detected. The particles are believed to be titanium oxide formed during TEM sample preparation. The Mg and Al are from the matrix and C could be from contamination from the graphite mould walls.

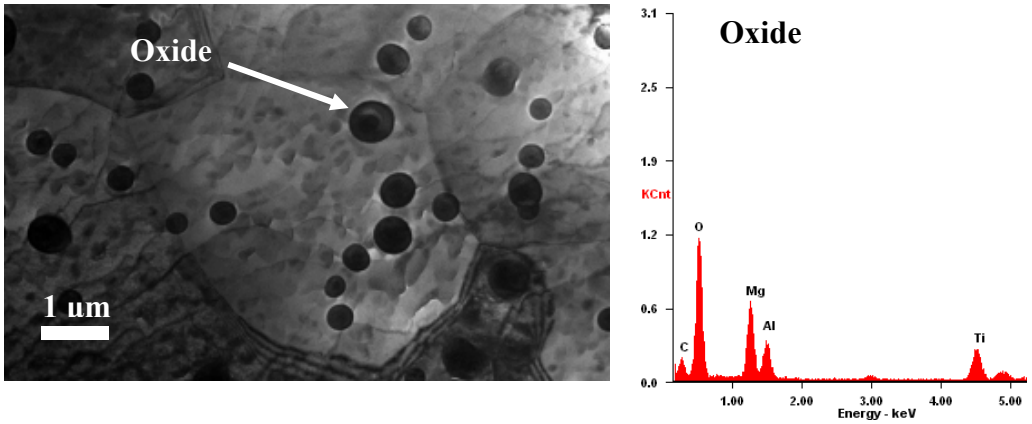

A) **B)**

Figure 4-15: TEM Image of AZ91E + 1.0 wt.% Al-1Ti-3B After 5 Minutes of Holding A) Ti Bearing Oxide Within and Around Grain Boundaries B) EDX Analysis of Ti Bearing Oxide Particle

It was expected that all the Ti within the K_2TiF_6 salt would react to form TiB_2, but the TEM image and corresponding EDX analysis in Figure 4-15 show that solute Ti can be observed within the AZ91E microstructure. During solidification the Ti particles would move towards the grain boundaries and restrict grain growth because of the near zero solubility of Ti in Mg at the melt temperature of 720 °C (Table 2-1, Section 2.4.5.3).

For the Al-5Ti-1B treated castings, the grain refinement was attributed to the grain growth segregation of TiB_2 particles to grain boundaries. The $TiAl_3$ particles became entrapped in the grain boundaries, but are unable to build a solute layer and restrict grain growth due to their large particle size. For the AZ91E castings treated with Al-1Ti-3B, both TiB_2 and AlB_2 particles aided in grain refinement. The TiB_2 particles provided grain growth restriction, while the AlB_2 particles provided nucleating sites. A summary of the results from the grain refinement and fading experiments is given in Table 4-3.

Table 4-3: Summary of Results from Grain Refinement and Fading Experiments

Alloy	Smallest Grain Size (5 min)	Undercooling (°C)	Mechanism of Grain Refinement
AZ91E	1000 µm	1	-
AZ91E + Al-5Ti-1B	323 µm, 0.1 wt.% addition	• 0.1, 0.2 and 0.1 for holding times of 5, 10 and 20 minutes respectively	• TiB_2 grain growth restriction
AZ91E + Al-1Ti-3B	361 µm, 1.0 wt.% addition	• 0.1, 0.3 and 0.1 for holding times of 5, 10 and 20 minutes respectively	• TiB_2 grain growth restriction • AlB_2 nucleating sites

Part II: Hot Tearing Susceptibility Experiments

The hot tear experiments were carried out in the permanent mould (Figure 3-4, Section 3.1.5.2), unlike the grain refinement experiments which were carried out in graphite moulds (Figure 3-1, Section 3.1.4). The results from Part I indicated that the optimal addition levels to achieve minimal grain size with the addition of Al-5Ti-1B and Al-1Ti-3B were 0.1 and 1.0 wt.%, respectively. For the hot tearing experiments, an addition level of 0.2 wt.% (instead of 0.1 wt.%) of Al-5Ti-1B was utilized. With a higher concentration of TiB_2 and $TiAl_3$ particles,

observation of their role in hot tearing was easier to investigate. The justification for the use of a higher concentration of Al-5Ti-1B is as follows.

As described in Section 4.4.1, the $TiAl_3$ particles were found in the grain boundaries of the AZ91E castings and the characteristics of the grain boundary regions was described as a factor influencing hot tear formation [30,31,48,49,54,56,57,60]. By increasing the concentration of $TiAl_3$ and TiB_2 particles without significantly increasing grain size, a better understanding about the role of the Ti based particles was obtained. The highly localized nature of hot tearing makes the presence of any particles near stress risers such as shrinkage pores, highly influential. The casting trials were designed to increase the likelihood of $TiAl_3$ and TiB_2 particles at hot spot regions. Thus, the effect of these particles on hot tearing was observed. If a lower concentration of Al-5Ti-1B was added (eg. 0.1 wt.%), the likelihood of observing the $TiAl_3$ and TiB_2 particles at the tear regions would decrease, making examination of their behaviour difficult.

4.5 Visual Examination of Hot Tears

Three compositions of permanent mould castings (AZ91E, AZ91E + 0.2 wt.% Al-5Ti-1B and AZ91E + 1.0 wt.% Al-1Ti-3B) were produced. The castings were examined for hot tears, upon removal from the permanent mould. Castings with long and wide non-branching cracks were considered as hot tearing susceptible, while castings with short and thin branching cracks were considered as hot tear resistant. A fourth set of castings was produced with the addition of commercial purity Al to AZ91E. Thus, the AZ91E + 1.0 wt.% Al-1Ti-3B casting increased the Al content within the melt by 0.8 wt.%. This Al enriched alloy provided a baseline to identify the effect of the additional Al content in the AZ91E + 1.0 wt.% Al-1Ti-3B castings.

4.5.1 Comparison of Unrefined and Refined Castings

Photographs of AZ91E permanent mould castings with and without the addition of Al-5Ti-1B and Al-1Ti-3B grain refiners are shown in Figure 4-16. The AZ91E casting in Figure 4-16A shows two large tears with relatively straight, brittle tear paths. With the addition of 0.2 wt.% Al-5Ti-1B grain refiner, thinner, less branched hot tears formed indicating a slight reduction in hot tear severity. A significant reduction in hot tearing was observed with the addition of 1.0 wt.% Al-1Ti-3B. The tears were very thin and short with many offshoots, common to ductile fracture surfaces.

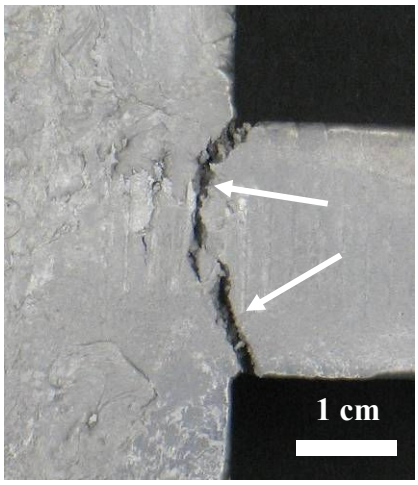

A)

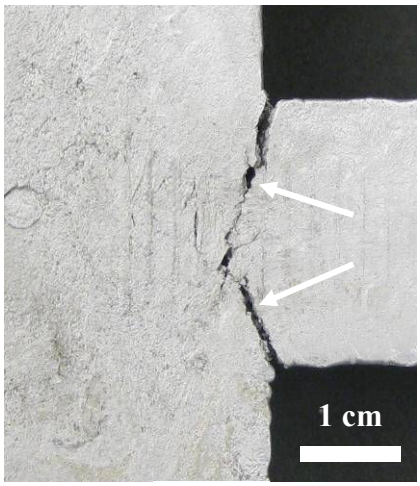

B)

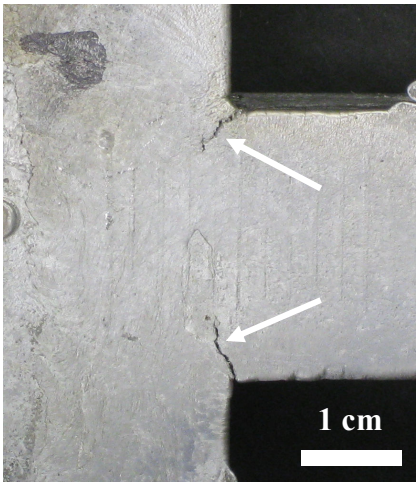

C)

Figure 4-16: Comparison of Hot Tearing Susceptibility of A) AZ91E B) AZ91E + 0.2 wt.% Al-5Ti-1B C) AZ91E + 1.0 wt.% Al-1Ti-3B

The results indicated that the addition of Al-5Ti-1B only slightly decreased hot tearing of AZ91E while Al-1T-i3B addition significantly reduced hot tearing. The AZ91E + 1.0 wt.% Al-1Ti-3B casting was then compared to a AZ91E + 0.8 wt.% Al casting to identify the effect of the additional Al content.

4.5.2 Effect of Pure Al on Hot Tearing Susceptibility

A comparison of the AZ91E castings treated with Al-1Ti-3B and pure Al, produced in this study, is shown in Figure 4-17.

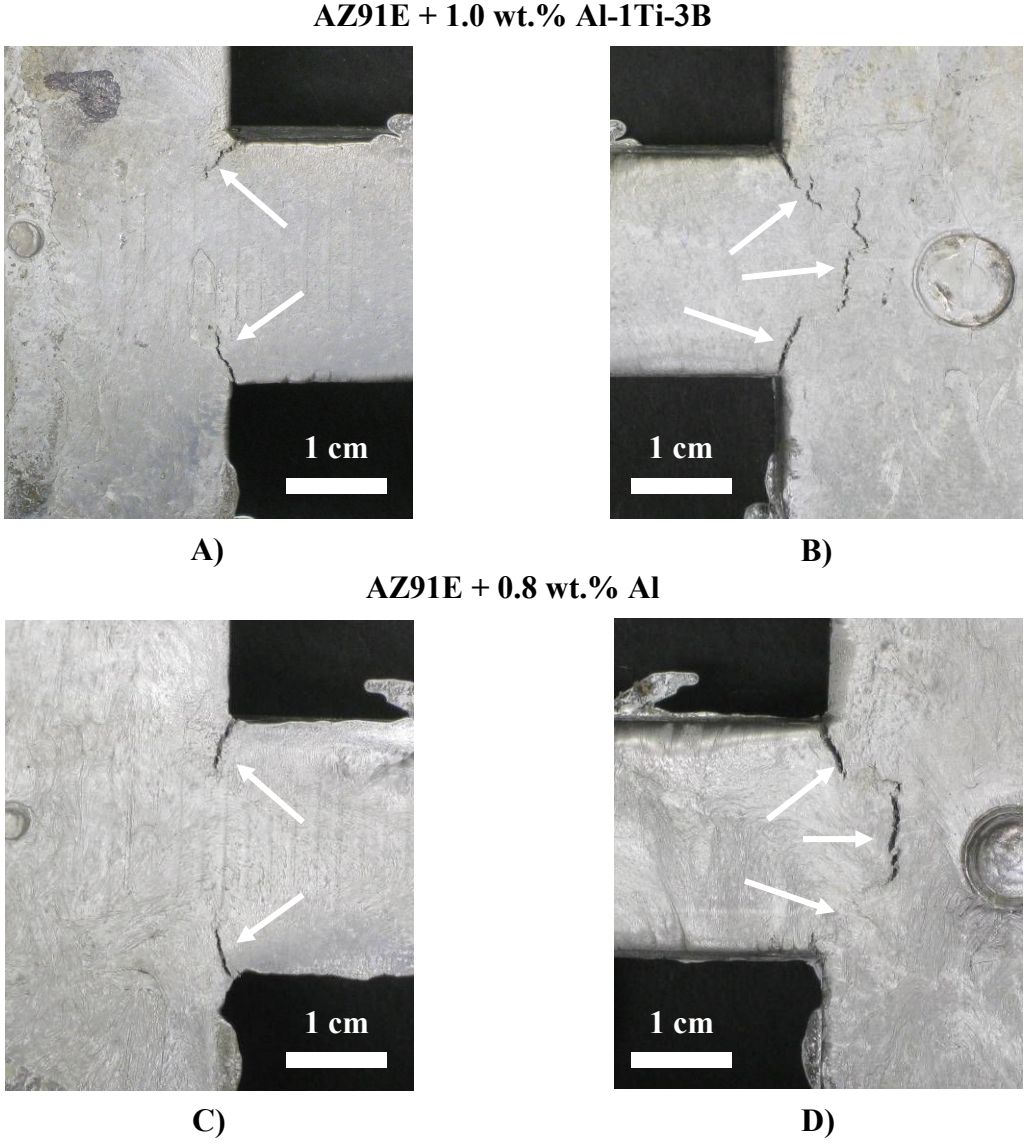

Figure 4-17: Comparison of Hot Tearing Susceptibility of A) AZ91E + 1.0 wt.% Al-1Ti-3B Front B) AZ91E + 1.0 wt.% Al-1Ti-3B Back C) AZ91E + 0.8 wt.% Al Front D) AZ91E + 0.8 wt.% Al Back

Both the AZ91 + Al-1Ti-3B and AZ91 + Al castings showed similar tear lengths, but the profile and thicknesses of the tears differed. As previously described in Section 4.5.1, the AZ91E + Al-1Ti-3B casting (Figure 4-17A-B) showed a small tear with many offshoots, common to ductile fracture surfaces. The AZ91E + Al casting (Figure 4-17C-D) contained hot tears that

were wider and less branched in nature than the AZ91E + Al-1Ti-3B casting. Cao and Kou [50] determined that the hot tearing susceptibility of Mg-Al-Ca alloys remained constant with increasing Al addition (4-6 wt.% Al). The differences in results could be attributed to the higher Al concentrations (~9 wt.%) and lack of Ca content in the AZ91E + 0.8 wt.% Al casting. Thus, it is observed that the addition of Al alone decreased the hot tearing susceptibility of AZ91E, but a contribution to hot tear reduction comes from the addition of Al-1Ti-3B. The difference in the hot tear morphologies between the addition of Al and Al-1Ti-3B stems from the grain refinement provided with Al-1Ti-3B addition which is further discussed in the next section.

4.6 Grain Size Measurements

Optical micrographs and grain size measurements of the permanent mould castings for the base AZ91E, AZ91E + 0.8 wt.% Al, AZ91E + 0.2 wt.% Al-5Ti-1B and AZ91E + 1.0 wt.% Al-1Ti-3B are shown in Figure 4-18 and Figure 4-19, respectively. The error bars in Figure 4-19 represent one standard deviation. The base AZ91E and AZ91E + 0.8 wt.% castings had non-uniform grain size distributions (Figure 4-18A-B). The average grain size of the base AZ91E was 113 μm. With the addition of 0.2 wt.% Al-5Ti-1B, the grain size distribution of AZ91E became less uniform, indicated by the larger standard deviation in grain size (Figure 4-18B). The average grain size also reduced slightly to 97 μm (14 % reduction) with Al-5Ti-1B addition. Significant grain refinement was observed when 1.0 wt.% Al-1Ti-3B was added to AZ91E, resulting in a uniform grain structure (Figure 4-18C) with average grain size of 72 μm (36 % reduction).

In comparison to the castings made with the graphite moulds, the permanent mould castings showed less grain refinement with Al-Ti-B additions. This can be attributed to the higher cooling rate in permanent mould casting. The steel permanent mould was only preheated to 180 °C, unlike in the graphite mould castings, where the mould was 750 °C. As a result, the higher cooling rates in permanent mould casting reduced the time duration for the added refiners to act as nucleating sites or grain growth restrictors.

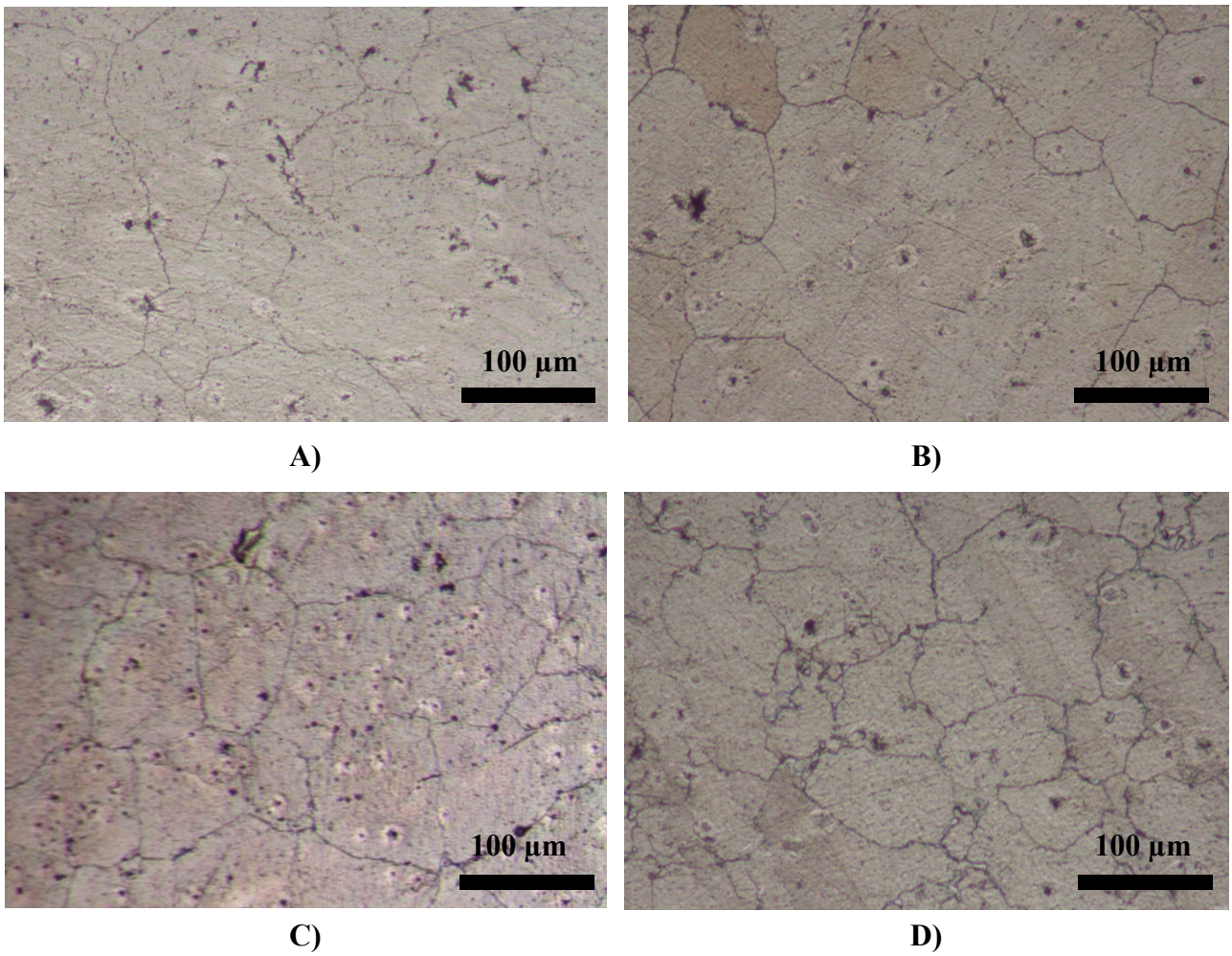

Figure 4-18: Optical Micrographs of Permanent Mould Castings A) AZ91E B) AZ91E + 0.8 wt.% Al C) AZ91E + 0.2 wt.% Al-5Ti-1B D) AZ91E + 1.0 wt.% Al-1Ti-3B

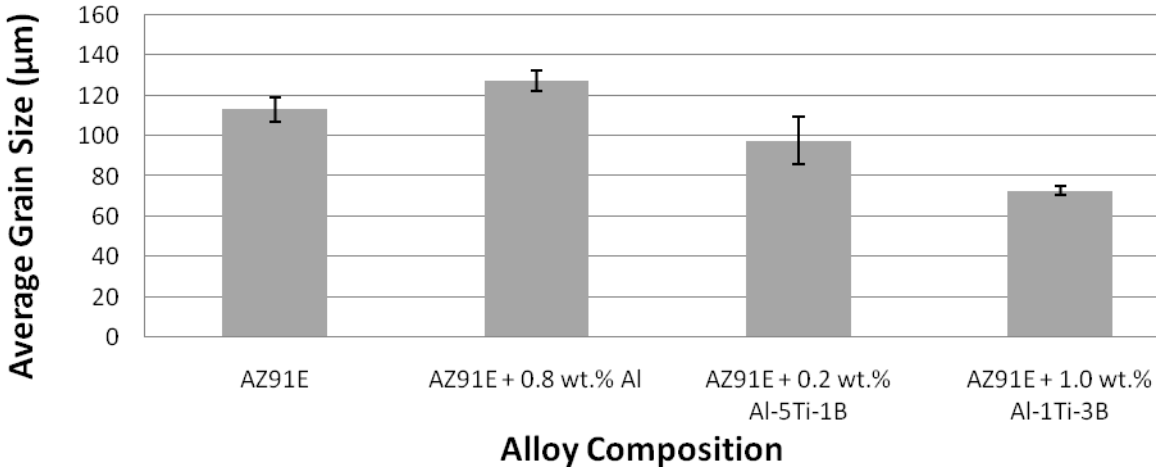

Figure 4-19: Effect of Al and Al-Ti-B Refiners on the Average Grain Size of AZ91E

The high hot tearing susceptibility observed with the addition of 0.2 wt.% Al-5Ti-1B in Section 4.5 can be partially explained by the lack of significant grain refinement. The grains in the casting with Al-5Ti-1B were still coarse and unable to distribute the strain during solidification of the melt. The casting treated with 1.0 wt.% Al-1Ti-3B showed significant grain refinement and was able to distribute the strain during solidification. More detailed discussion regarding the significance of the grain refinement with Al-Ti-B based refiner addition is provided in the ANOVA test in Appendix A.3. The addition of 1.0 wt.% Al-1Ti-3B to AZ91E also introduced an additional 0.8 wt.% Al into the melt. The effect of Al on grain refinement was investigated and found to have no effect on grain size when the Al concentration within the Mg alloy exceeds 5 wt.% [3,12]. In fact, the additional Al content increased the grain size to 127 μm (12 % increase, Figure 4-19). Therefore, the additional Al content does not aid in grain refinement. The grain size measurements validate the visual observations in Section 4.5.

4.7 Thermal Analysis

Thermal analysis was performed on the permanent mould samples to examine the solidification behaviour of the hot tear castings. The cooling rate and time duration during which the castings were in the semi-solid state (local solidification time, LST) were determined. These values were valuable to relate to the hot tearing susceptibility observations and grain size measurements. The thermocouples were placed in the centre of the casting bar at the locations indicated in Figure 3-5 in Section 3.1.5.4.

The cooling curves for the permanent mould castings are shown in Figure 4-20. The temperature data is for the thermocouple closest to the hot tear location (2.5 cm from downsprue). As noted by Campbell and Pellini [7,46], hot tears form during the semi-solid stage of solidification which makes the LST a valuable parameter to asses hot tearing susceptibility. From thermal analysis, the base AZ91E alloy had the longest LST with the castings treated with Al-5Ti-1B and Al-1Ti-3B having the second and third longest LST's respectively. A comparison with the visual observations of hot tears in Figure 4-16 in Section 4.5.1 shows that with a decrease in LST, the hot tearing susceptibility decreases. A similar result was obtained by Cao and Kou [50] where Mg-Al-Ca castings with short freezing ranges were the least susceptible to hot tearing.

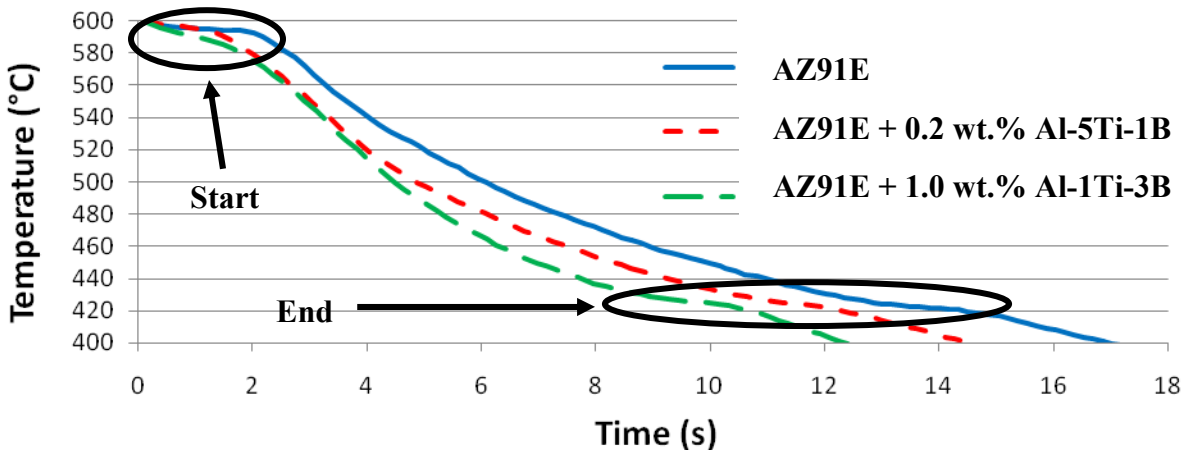

Figure 4-20: Cooling Curves of Permanent Mould Castings

A summary of the thermal observations is presented in Table 4-4. The thermal data in Table 4-4 indicates that with grain refinement, the semi-solid temperature range and the LST decrease, both contributing to a high cooling rate (CR). The addition of 1.0 wt.% Al-1Ti-3B promoted quick solidification, limiting the temperature and time for which hot tears formed. The high CR promoted grain refinement and resulted in the small grain sizes presented in Figure 4-19.

Table 4-4: Summary of Thermal Observations of Permanent Mould Castings

Sample	Semi-Solid Temperature Range (°C)	Local Solidification Time (s)	Total Solidification Time (s)	Cooling Rate (°C/s)	Superheat (°C)
AZ91E	595.6-422.1=173.5	13.1	14.5	13.2	28.2
AZ91E + 0.2 wt.% Al-5Ti-1B	595.3-423.0=172.3	10.8	12.9	15.8	28.3
AZ91E + 1.0 wt.% Al-1Ti-3B	589.6-422.1=167.5	9.4	11.4	17.8	36.0

Similar nucleation temperatures were observed for both the AZ91E and AZ91E + 0.2 wt.% Al-5Ti-1B castings (595.6 and 595.3 °C, respectively). The AZ91E +1.0 wt.% Al-1Ti-3B casting on the other hand, had a lower nucleation temperature of 589.6 °C. The lower nucleation temperature was a result of the additional Al content in the alloy, similar to the scenario observed

with the castings produced in the graphite moulds in Section 4.3. The additional Al content pushed nucleation to a lower temperature according to the Mg-Al phase diagram shown in Appendix A.5. The AZ91E + 1.0 wt.% Al-1Ti-3B treated casting also had a superheat of 36 °C, as compared to 28.2 and 28.3 °C for the AZ91E and AZ91E + 0.2 wt.% Al-5Ti-1B castings, respectively. This may have aided in reducing hot tearing by allowing more time for mould filling before solidification began.

4.8 Microstructure of Grain Refined Castings

This section first discusses the appearance of the hot tears in the untreated castings followed by the castings refined with Al-5Ti-1B. Finally, the microstructures of the castings with Al-1Ti-3B are presented.

4.8.1 AZ91E

The unrefined AZ91E castings were examined using SEM to observe the shape and path of the hot tears. The hot tear surface in Figure 4-21 shows that the main tear followed an irregular path that appeared dendritic in morphology. A smaller tear can also be observed, which preferred to advance through intergranular regions. The unrefined castings were also examined using TEM to observe any characteristics of deformation, notably dislocations, within the microstructure.

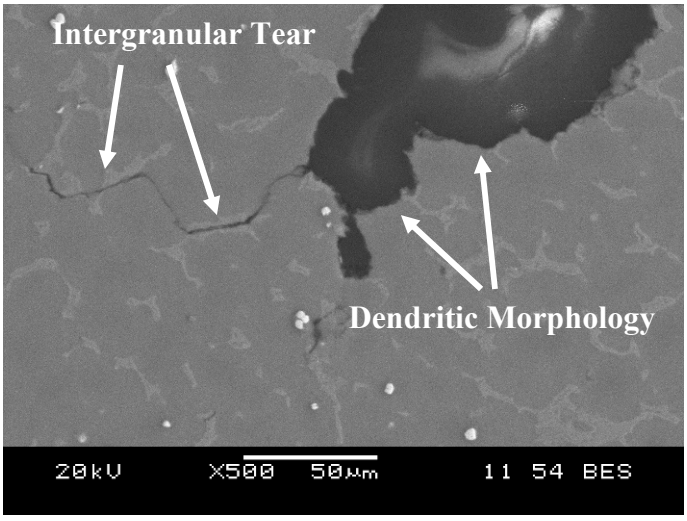

Figure 4-21: SEM Image of Hot Tear Surface in AZ91E Casting

The microstructures in Figure 4-22 show many dislocations along grain boundaries (Figure 4-22A), in dislocation pile-ups (Figure 4-22B) and against particles (Figure 4-22C). As outlined in the previous sections, the hot tears in the unrefined AZ91E castings formed during the semi-solid stage of solidification, as a result of a highly dendritic microstructure, lower CR and longer LST as compared to the refined castings. When the tear developed, the stress within the semi-solid AZ91E alloy was relieved and solidification progressed until the casting was completely solid. At the end of solidification, the casting was still at an elevated temperature (~420 °C) and as it cooled, it continually underwent constrained contraction. The dendritic grain morphology did not distribute strain evenly within the casting. The result was a deformation of the casting and the formation of dislocations as shown in Figure 4-22.

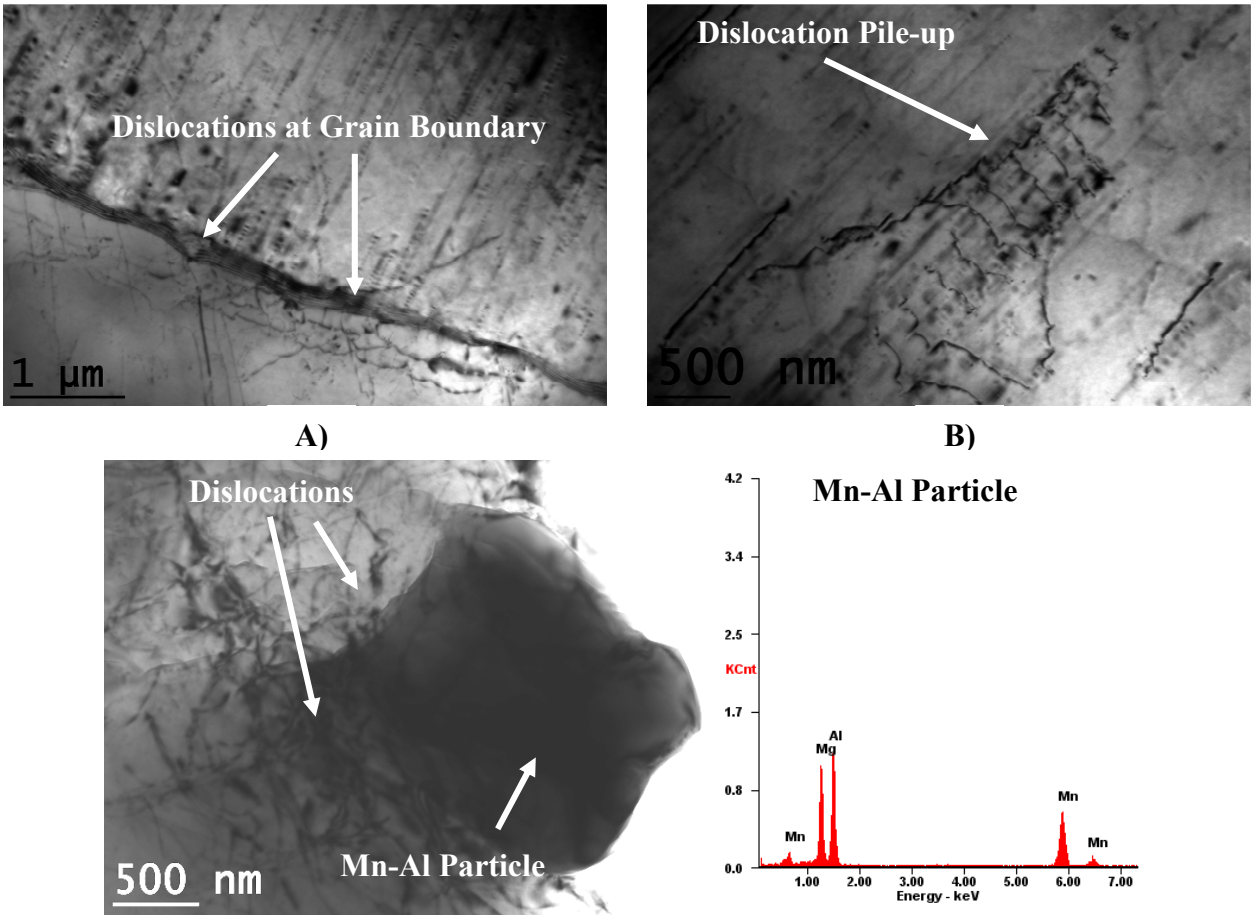

Figure 4-22: TEM Image of Dislocations in AZ91E Casting A) Dislocations at Grain Boundary B) Dislocation Pile-up C) Dislocations Around Mn-Al Particle with Corresponding EDX Analysis

The intergranular hot tears in the unrefined AZ91E casting resulted from the highly dendritic grain structure. The branched, dendritic grains were unable to provide adequate feeding between the dendrite arms. Lack of feeding in intergranular regions resulted in the formation of pores that expanded into tears. The following sections outline the change in hot tear microstructure with grain refinement.

4.8.2 AZ91E + Al-5Ti-1B

With the addition of Al-5Ti-1B grain refiner to AZ91E, the hot tears followed an intergranular path, as presented in Figure 4-23. To better observe the $TiAl_3$ and TiB_2 particles within the castings, some high concentration samples were produced (5 wt.% Al-5Ti-1B) following the procedure in Section 3.2.2. The castings refined using Al-5Ti-1B were examined to observe the interactions between $TiAl_3$, TiB_2 and the hot tear surface. In Figure 4-24A, a $TiAl_3$ particle in the vicinity of the hot tear was observed. The brittle and large (>30 μm) $TiAl_3$ particles near the tear region possibly suggests that this particle acted as a stress riser and promoted the growth of hot tears. In contrast, the TiB_2 particles observed Figure 4-24A were very fine and were thus not believed to act as stress risers. The $TiAl_3$ particle in Figure 4-24A

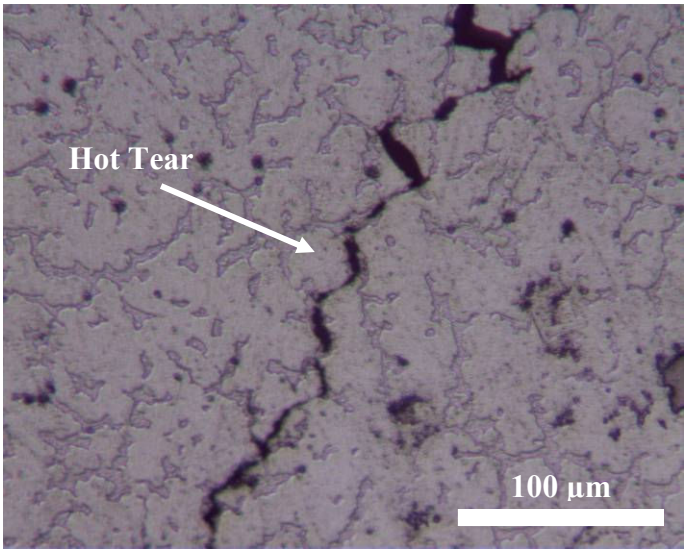

Figure 4-23: Optical Micrograph of Hot Tear in AZ91E + 5 wt.% Al-5Ti-1B Casting

showed a good bond with the $Mg_{17}Al_{12}$ eutectic phase, but in many instances porosity was observed alongside the $TiAl_3$-$Mg_{17}Al_{12}$ interface (Figure 4-24B). The large $TiAl_3$ particles may have blocked feeding channels during solidification and prevented flow of liquid metal resulting

in the formation of pores. A similar result was obtained by Zheng *et al.* [59] with the addition of rare-earth elements to Mg-Al alloys. The rare-earth addition caused the formation of $Al_{11}RE_3$ phases that blocked feeding channels, promoting hot tear formation. Another example of the poor interface between the $TiAl_3$ particles and AZ91E can be observed in Figure 4-24C. The shrinkage of the casting as it cooled may have promoted separation between the $TiAl_3$ and $Mg_{17}Al_{12}$ eutectic.

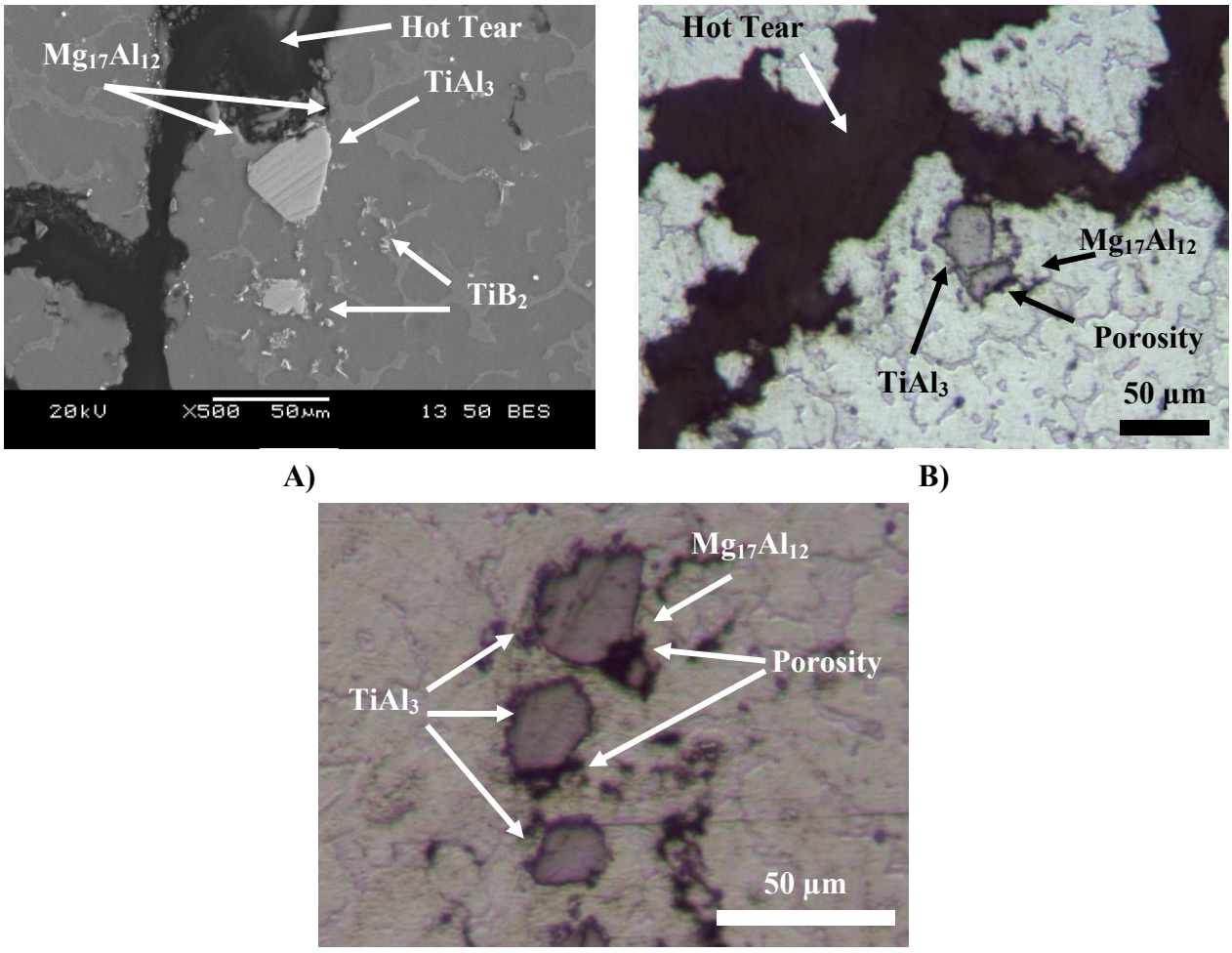

Figure 4-24: Microstructure of Hot Tears in AZ91E + 5 wt.% Al-5Ti-1B Castings A) SEM Image of $TiAl_3$ and TiB_2 Particles B) Optical Micrograph of $TiAl_3$ Particles Near Hot Tear C) Optical Micrograph of $TiAl_3$ Particles Alongside Shrinkage Porosity

The TiB_2 particles within the AZ91E castings appeared to help arrest the propagation of tears, as shown in Figure 4-25. The smaller, secondary tear shown in Figure 4-25 was propagating along the eutectic regions, but was stopped by the cluster of TiB_2 particles. The

small and hard TiB_2 particles did not interfere with metal feeding and were able to prevent the propagation of hot tears, reducing the hot tearing susceptibility of the casting.

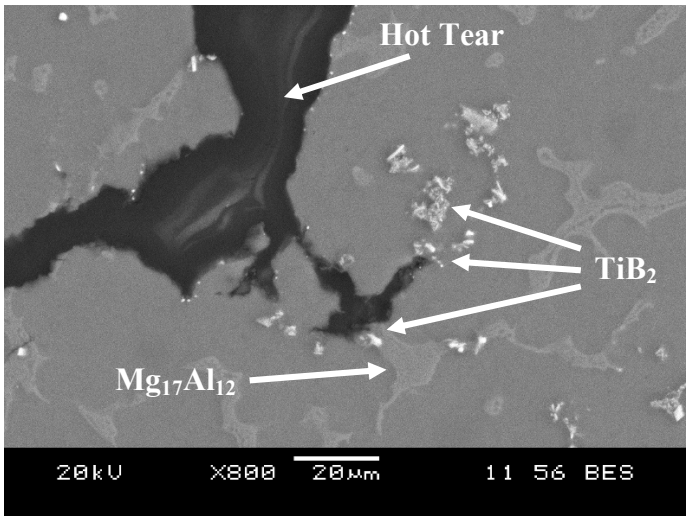

Figure 4-25: SEM Image of TiB_2 Particles Near Hot Tear in AZ91E + 5 wt.% Al-5Ti-1B Casting

The microstructure of the AZ91E + Al-5Ti-1B castings was also examined using TEM. In Figure 4-26, a Mn-Al particle similar to the Mn-Al particle in the unrefined AZ91E (Figure 4-22C) was observed. However, unlike the unrefined AZ91E casting, the AZ91E + 0.2 wt.% Al-5Ti-1B microstructure did not contain dislocation networks around the Mn-Al particle. This suggests that the uniform grain size resulting from the addition of Al-5Ti-1B enabled the casting to alleviate the imposed strain as it cooled in the permanent mould after solidification.

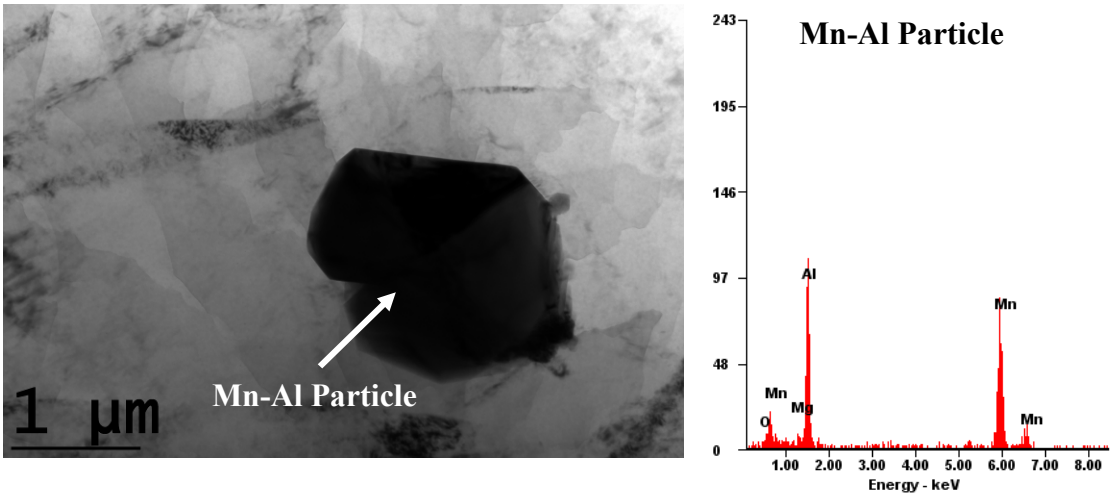

Figure 4-26: TEM Image of Mn-Al Particle in AZ91E + 0.2 wt.% Al-5Ti-1B Casting with Corresponding EDX Analysis

Further examination of the AZ91E + 0.2 wt.% Al-5Ti-1B casting revealed the presence of dislocation networks around a Mg rich particle (possibly MgO), as shown in Figure 4-27. However, the results indicated that the extent of deformation within the AZ91E + 0.2 wt.% Al-5Ti-1B casting was much lower than that of the unrefined AZ91E casting. This may have been due to the more uniform grain size that provided uniform strain over the semi-solid casting.

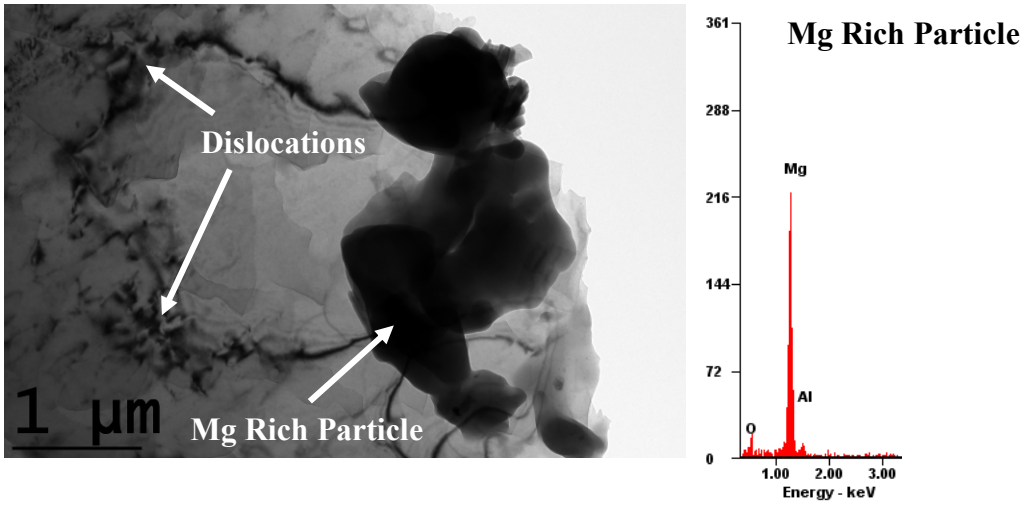

Figure 4-27: Dislocation Networks Near Mg Rich Particle in AZ91E + 0.2 wt.% Al-5Ti-1B Casting

With the addition of Al-5Ti-1B to AZ91E, $TiAl_3$ and TiB_2 particles were found in the eutectic regions of the casting and the hot tears remained intergranular. The $TiAl_3$ particles were found to have poor bonding with the eutectic regions which promoted pore formation in areas affected by solidification shrinkage. The coarse $TiAl_3$ particles may have also blocked feeding channels during solidification. The TiB_2 particles were very fine and appeared to arrest hot tear advancement without blocking feeding channels. Fewer dislocation networks were also found in the castings treated with Al-5Ti-1B. A two-fold effect on hot tearing susceptibility was observed with the addition of Al-5Ti-1B to AZ91E. The Al-5Ti-1B provided some grain refinement that reduced the formation of dislocation networks. Further, Al-5Ti-1B provided fine TiB_2 particles that prevented tear propagation. However, the large $TiAl_3$ particles bonded poorly to the eutectic phase and promoted the formation of pores. The result was only a marginal decrease in hot tearing susceptibility. The addition of Al-1Ti-3B was more effective at reducing hot tears and was attributed to the absence of $TiAl_3$ particles within the microstructure.

4.8.3 AZ91E + Al-1Ti-3B

The hot tear surface of AZ91E + 1.0 wt.% Al-1Ti-3B is presented in Figure 4-28. The hot tear was intergranular and very similar to the hot tear surface of the unrefined AZ91E casting in Figure 4-21.

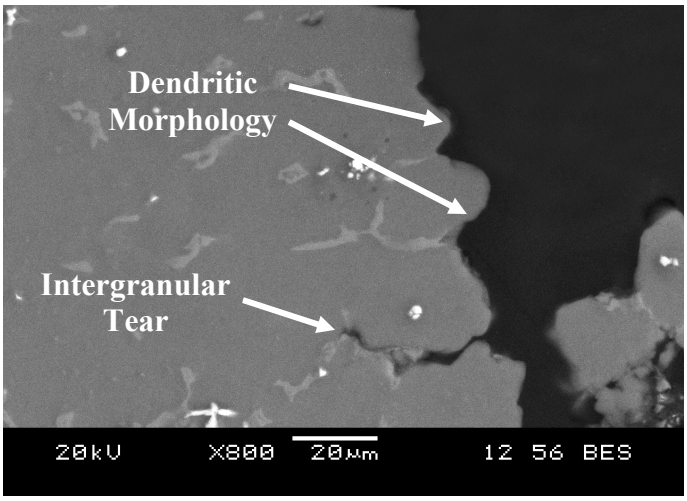

Figure 4-28: Hot Tear Surface of AZ91E + 1.0 wt.% Al-1Ti-3B Casting

The Al-1Ti-3B grain refiner contained TiB_2 and AlB_2 particles, but no $TiAl_3$ particles. The AlB_2 particles were found at the centre of grains, acting as heterogeneous nucleating sites (Figure 4-13). The presence of AlB_2 particles within the grains likely did not influence the intergranular hot tears. The TiB_2 particles segregated to grain boundaries providing grain growth restriction, as seen in the microstructure of Figure 4-14.

For the AZ91E + Al-5Ti-1B castings, the TiB_2 particles stopped the advancing hot tears (Figure 4-25). The TiB_2 particles had good bonding with the eutectic regions and were able to stop the advancing crack. Good bonding between TiB_2 and the eutectic regions was also observed in the AZ91E + Al-1Ti-3B castings (Figure 4-29). The areas surrounding the hot tear showed severe cracking. However, no porosity was observed adjacent to the TiB_2 particles.

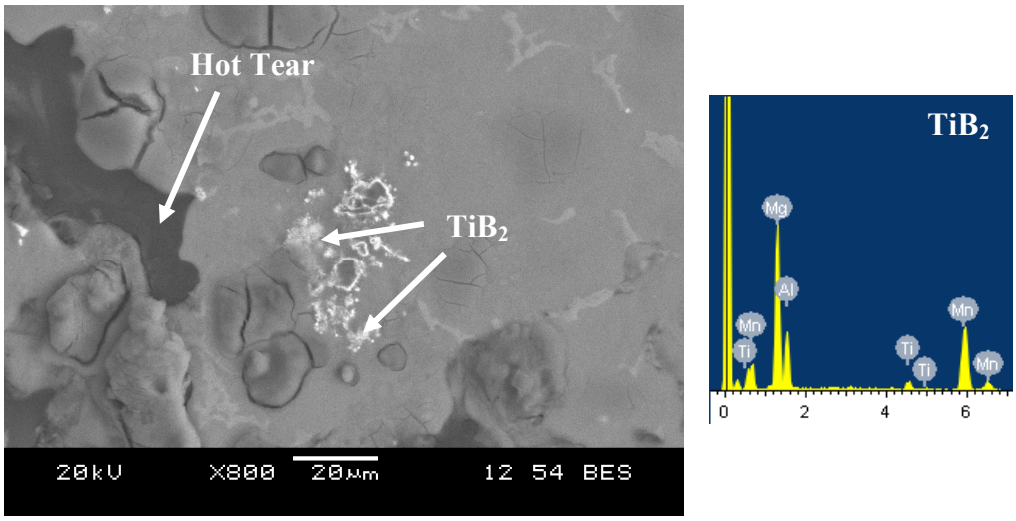

Figure 4-29: SEM Image of TiB_2 Particles in AZ91E + 1.0 wt.% Al-1Ti-3B Casting

The AZ91E + 1.0 wt.% Al-1Ti-3B castings were also examined using TEM. The TEM image in Figure 4-30 shows an Mn-Al particle in a AZ91E + 1.0 wt.% Al-1Ti-3B casting. The particle has a similar composition to the Mn-Al particles observed in AZ91E and AZ91E + 0.2 wt.% Al-5Ti-1B. Observation of Figure 4-30 showed that no dislocation networks formed, indicating that the casting was able to accommodate the thermal stresses generated during contraction in the permanent mould. The small, uniform grain size of the castings treated with Al-1Ti-3B helped distribute the thermal contraction and reduce the formation of any dislocation networks.

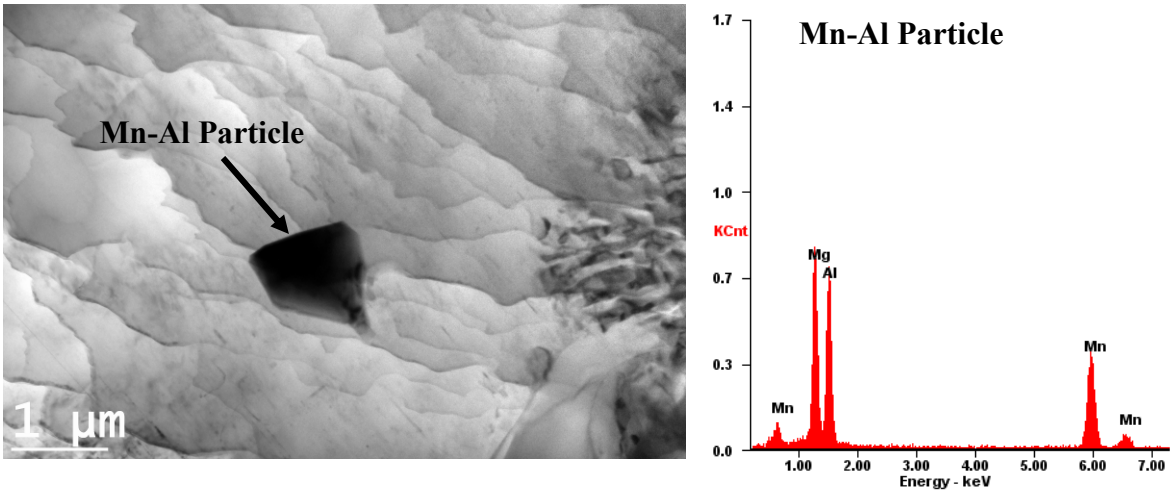

Figure 4-30: TEM Image of Mn-Al Particle in AZ91E + 1.0 wt.% Al-1Ti-3B

The castings refined with Al-1Ti-3B provided the smallest grain size which promoted liquid metal feeding and reduced hot tears. The TiB_2 particles appeared to have good bonding with the

eutectic which maintained the integrity of the casting, preventing the growth of hot tears. The AZ91E + 1.0 wt.% Al-1Ti-3B castings were also better able to accommodate the thermal contraction, preventing the formation of dislocation networks. A summary of the results of the hot tearing susceptibility experiments is given in Table 4-5.

Table 4-5: Summary of Results of Hot Tearing Susceptibility Experiments

Alloy	Hot Tear Severity	Grain Size (μm)	Thermal Analysis	Role of Particles near Hot Tears	Concentration of Dislocation Networks
AZ91E	Very High	113	- Longest LST - Lowest CR	-	High
AZ91E + Al-5Ti-1B	High	97	- Medium LST - Medium CR	**$TiAl_3$:** - Porosity surrounding particles - Blocked feeding channels **TiB_2:** - Prevented tear growth	Low
AZ91E + Al-1Ti-3B	Low	72	- Shortest LST - Highest CR	**TiB_2:** - Stopped tears - Good bonding with eutectic	Zero

CHAPTER 5 CONCLUSIONS

I: Grain Refinement and Fading Experiments

1. The Al-5Ti-1B grain refiner consisted of mostly fine (< 3 μm) TiB_2 particles and large (> 30 μm) $TiAl_3$ particles. The Al-1Ti-3B grain refiner contained AlB_2 (5-10 μm) and TiB_2 (< 3 μm) particles and no $TiAl_3$ particles.
2. In the unrefined AZ91E, the grain size was 1000 μm. The smallest average grain size obtained using the Al-5Ti-1B grain refiner was 323 μm (68 % reduction) at an addition level of 0.1 wt.%. The smallest average grain size obtained using the Al-1Ti-3B grain refiner was 361 μm (64 % reduction) at an addition level of 1.0 wt.%.
3. The mechanism of grain refinement with Al-5Ti-1B addition was grain growth restriction of TiB_2 particles. The addition of Al-1Ti-3B grain refined AZ91E through a combination of heterogeneous nucleation from AlB_2 and grain growth restriction by TiB_2 particles.
4. Both grain refiners exhibited a good resistance to fading during the holding times (5, 10 and 20 minutes) investigated, as shown by the grain size measurements and an ANOVA analysis.
5. The thermal analysis was effective for quick assessment of the degree of grain refinement.

II: Hot Tearing Susceptibility Experiments

1. The addition of Al-5Ti-1B provided a small reduction in hot tearing, while Al-1Ti-3B significantly reduced the hot tears. The hot tears for all the castings were intergranular in nature.
2. The average grain size of the permanent mould castings treated with Al-5Ti-1B was not significantly smaller than the baseline AZ91E alloy (113 μm), as shown by an ANOVA analysis. The average grain size of the Al-1Ti-3B treated castings was 72 μm. The significantly finer grain size (shown by an ANOVA analysis) of the Al-1Ti-3B treated castings helped reduce hot tearing by distributing strain during solidification. The AZ91E + Al-5Ti-1B and AZ91E + Al-1Ti-3B castings showed much fewer dislocation networks as compared to the untreated AZ91E casting. In effect, grain refinement resulted in uniform distribution of strain and minimization of hot tearing during solidification.

3. The permanent mould cast base AZ91E alloy had a cooling rate (CR) of 13.2 °C/s and local solidification time (LST) of 13.1 seconds. The castings treated with Al-1Ti-3B had a higher CR (17.8 °C/s) and shorter LST (9.4 seconds) relative to those treated with Al-5Ti-1B (CR: 15.8 °C/s , LST: 10.8 seconds).
4. The Al-5Ti-1B was unable to reduce hot tearing because of the presence of large $TiAl_3$ particles that had a poor interface with the eutectic and blocked feeding channels. The TiB_2 particles had a good interface with the eutectic and reduced tear growth in the Al-1Ti-3B castings.

III: Industrial Impact of the Conclusions

By examining the refining and fading behaviour of the added Al-5Ti-1B and Al-1Ti-3B grain refiners, better knowledge about the behaviour of the refiners in a foundry setting was obtained. Grain refinement on a foundry scale requires minimal fading to maintain productivity and reduce operating costs. This study demonstrated the effectiveness of Al-Ti-B refiners for Mg alloy melts. The current study also demonstrated that the addition of Al-1Ti-3B aids in reducing hot tearing susceptibility in permanent mould cast AZ91E alloy, thus enhancing the castability of the alloy.

CHAPTER 6 FUTURE WORK

The current study helps to determine the potential for Al-Ti-B grain refiners to grain refine Mg-Al alloys and reduce the hot tearing susceptibility of permanent mould castings. Further investigation is required to study the effect of grain refinement on yield strength, ultimate tensile strength and elongation. The Al-5Ti-1B and Al-1Ti-3B grain refiners were originally designed for Al alloys, and it is necessary to carry out optimization of Ti and B levels for Mg alloys.

6.1 Mechanical Testing

Determination of the change in yield strength, ultimate tensile strength and elongation for castings treated with Al-5Ti-1B and Al-1Ti-3B would be necessary in order to adapt Al-Ti-B refiners to the foundry industry. The purpose of grain refinement is to improve mechanical properties, and it is necessary to perform tensile testing to ensure that the added $TiAl_3$, TiB_2 and AlB_2 particles are not detrimental to strength and elongation.

6.2 Synthesis of Al-Ti-B, Al-B Grain Refiners

The different grain refining performance of the Al-5Ti-1B and Al-1Ti-3B refiners can be linked to the Ti and B content within their microstructure. The Ti:B ratios in Al-5Ti-1B and Al-1Ti-3B can be manipulated to result in different concentrations of $TiAl_3$, TiB_2 and AlB_2. It would be very interesting to synthesise Al-Ti-B grain refiners with various Ti:B ratios and examine the grain refining and relative hot tearing effects.

REFERENCES

1. Avedesian, M.M., Baker, H., *Magnesium and Magnesium Alloys*. 1999, Materials Park, OH: ASM International.
2. Davies, J.R., *Aluminum and Aluminum Alloys*. 1993, Materials Park, OH: ASM International.
3. Ramachandran, T.R., Sharma, P.K., Balasubramanian, K., *Grain Refinement of Light Alloys.* Proceedings of the 68th World Foundry Congress, 2008: p. 189-193.
4. Porter, D.A., *Phase Transformations in Metals and Alloys*. 1992, London: Chapman and Hall, Inc.
5. Callister, W.D., *Material Science and Engineering: An Introduction*. 2003, Hoboken, NJ: John Wiley and Sons, Inc.
6. Dieter, G.E., *Mechanical Metallurgy*. SI Edition ed. 1988, London: McGraw Hill.
7. Campbell, J., *Casting*. 1993, Woburn, MA: Butterworth-Heinemann.
8. Mitra, R., Mahajan, Y.R., *Interfaces in Discontinuously Reinforced Metal Matrix Composites: An Overview.* Bulletin of Materials Science, 1995. **18**: p. 405-434.
9. Lu, L., Dahle, A.K., St. John, D.H., *Grain Refinement Efficiency and Mechanism of Aluminum Carbide in Mg-Al Alloys.* Scripta Materialia, 2005. **53**: p. 517-522.
10. Murty, B.S., Kori, S.A., Chakraborty, M., *Grain Refinement of Aluminum and its Alloys by Heterogeneous Nucleation and Alloying.* International Materials Reviews, 2002. **47**(1): p. 3-29.
11. Stefanescu, D.M., Barice, W.J., Brown, R.B., Chong, D., Craig, D.B., *Casting*. ASM Handbook. Vol. 15. 1988, Materials Park, OH: ASM International.
12. Lee, Y.C., Liu, X.F., Yang, H., *The Role of Solute in Grain Refinement of Magnesium.* Metallurgical and Materials Transactions, 2000. **31A**: p. 2895-2906.
13. Lu, L., Dahle, A.K., Taylor, J.A., St.John, D.H., *Theoretical and Practical Considerations of Grain Refinement of Mg-Al Alloys.* Materials Science Forum, 2005. **488-489**: p. 299-302.
14. Emley, E.F., *Principles of Magnesium Technology*. 1966, London: Pergamon Press Ltd.
15. St. John, D.H., Ma,Q., Easton, M.A., Cao, P, Hildebrand, Z., *Grain Refinement of Magnesium Alloys.* Metallurgical and Materials Transactions, 2005. **36A**: p. 1669-1679.
16. Kabirian, F., Mahmudi, R., *Effects of Zirconium Additions on the Microstructure of As-cast and Aged AZ91 Magnesium Alloy.* Advanced Engineering Materials, 2009. **11**(3): p. 189-193.
17. Jin, Q., Eom, J., Lim, S., *Reply to Comments on "Grain Refining Mechanism of a Carbon Addition Method in a Mg-Al Magnesium Alloy".* Scripta Materialia, 2005. **52**: p. 421-423.
18. Motegi, T., *Grain-refining Mechanisms of Superheat-treatment of and Carbon Addition to Mg-Al-Zn Alloys.* Materials Science and Engineering, 2005. **A**: p. 408-411.
19. Kumar, R., Mahanty, R.K., *Grain Size Control of Magnesium.* British Foundryman, 1973. **66**: p. 39-42.
20. Schwam, D., Zhu, X., *The Effect of Cooling Rate on Grain Size of Magnesium Alloys Cast in a Permanent Mold.* AFS Transactions, 2008. **Vol. 112: 08-163**.
21. Ding, H., Liu, X., *The Grain Refinement Efficiency of Ni-C on Mg-Al Alloys.* Materials Letters, 2009. **63**: p. 635-637.
22. Easton, M.A., Schiffl, A., Yao, J.Y., Kaufmann, H., *Grain Refinement of Mg-Al(-Mn) Alloys by SiC Additions.* Scripta Materialia, 2006. **55**: p. 379-382.

23. Guang, H., Xiangfa, L., Haimin, D., *Grain Refinement of Mg-Al Based Alloys by a New Al-C Master Alloy.* Journal of Alloys and Compounds, 2009. **467**: p. 202-207.
24. Liu, Y., Liu, X., Xinfang, B., *Grain Refinement of Mg-Al Alloys with Al_4C_3-SiC/Al Master Alloy.* Materials Letters, 2004. **58**: p. 1282-1287.
25. Luo, A., *Heterogeneous Nucleation and Grain Refinement in Cast Mg(AZ91)/SiCp Metal Matrix Composites.* Canadian Metallurgical Quarterly, 1996. **35**(4): p. 375-383.
26. Qian, M., Cao, P., *Discussions on Grain Refinement of Magnesium Alloys by Carbon Inoculation.* Scripta Materialia, 2005. **52**: p. 415-419.
27. Suresh, M., Srinivasan, A., Ravi, K.R., Pillai, U.T.S., Pai, B.C., *Influence of Boron Addition on the Grain Refinement and Mechanical Properties of AZ91 Mg Alloy.* Materials Science and Engineering A, 2009. **525**: p. 207-210.
28. Lee, Y.C., Dahle, A.K., St.John, D.H., *Grain Refinement of Magnesium.* Magnesium Technology 2000, 2000: p. 211-218.
29. Du, J., Yang, J., Kuwabara, M., Li, W., Peng, J, *Improvement of Grain Refining Efficiency for Mg-Al Alloy Modified by the Combination of Carbon and Calcium.* Journal of Alloys and Compounds, 2009. **470**: p. 134-140.
30. Li, P., Tang, B., Kandalova, E.G., *Microstructure and Properties of AZ91D Alloy with Ca Additions.* Materials Letters, 2005. **59**: p. 671-675.
31. Cao, W., Zhang, C., Fan, T., Zhang, D., *In-situ Synthesis of TiB_2/Mg Composite by Flux-assisted Synthesis Reaction of the Al-Ti-B System in Molten Magnesium.* Key Engineering Materials, 2007. **351**: p. 166-170.
32. Li, J., Geng, H., Yang, Z., Wang, Y., Cui, F., Sun, C., *Effects of Y on Microstructure and Mechanical Properties of AZ91 Magnesium Alloy.* Foundry, 2005. **54**(1): p. 53-56.
33. Liu, S., Zhang, Y., Han, H., Li, B., *Effect of Mg–TiB2 Master Alloy on the Grain Refinement of AZ91D Magnesium Alloy.* Journal of Alloys and Compounds, 2009. **487**: p. 202-205.
34. Qiu, D., Zhang, M.X., Fu, H.M., Kelly, P.M., Taylor, J.A., *Crystallography of Recently Developed Grain Refiners for Mg-Al Alloys.* Philosophical Magazine Letters, 2007. **87**(7): p. 505-514.
35. Wang, H.Y., Jiang, Q.C., Zhao, Y.Q, Zhao, F., Ma, B.X., Wang, Y., *Fabrication of TiB_2-TiC Particulates Reinforced Magnesium Matrix Composites.* Material Science and Engineering A, 2004. **372**: p. 109-114.
36. Wang, Y., Wang, H.Y., Ma, B.X., Xiu, K., Jiang, Q.C., *Effect of Ti/B on Fabricating TiB_{2p}/AZ91 Composites by Employing a TiB_{2p}/Al Master Alloy.* Journal of Alloys and Compounds, 2006. **422**: p. 178-183.
37. Wang, Y., Zeng, X., Ding, W., *Effect of Al–4Ti–5B Master Alloy on the Grain Refinement of AZ31 Magnesium Alloy.* Scripta Materialia, 2006. **54**: p. 269-273.
38. Wang, Y., Wang, H.Y., Yang, Y.F., Jiang, Q.C., *Solidification Behaviour of Cast TiB_2 Particulate Reinforced Mg Composites.* Materials Science and Engineering A, 2008. **478**: p. 9-15.
39. Xu, C., Lu, B., Lü, Z., Liang, W., *Grain Refinement of AZ31 Magnesium Alloy by Al-Ti-C-Y Master Alloy.* Journal of Rare Earths, 2008. **26**(4): p. 604-608.
40. Zhang, M.X., Kelly, P.M., Qian, M., Taylor, J.A., *Application of Edge-to-edge Matching Model to Grain Refinement in Mg-Al Based Alloys.* Journal of Materials Science and Technology, 2005. **21**: p. 77-80.

41. Zhang, X., Wang, H., Liao, L., Teng, X., Ma, N., *The Mechanical Properties of Magnesium Matrix Composites Reinforced With (TiB_2 + TiC) Ceramic Particulates.* Materials Letters, 2005. **59**: p. 2105-2109.
42. Bai, J., Sun, Y.S., Xun, S., Xue, F., Zhu, T.B., *Microstructure and Tensile Creep Behaviour of Mg-4Al based Magnesium Alloys with Alkaline-earth Elements Sr and Ca Additions.* Materials Science and Engineering A, 2006. **A419**: p. 181-188.
43. Hirai, K.J., Somekawa, H.T., Takigawa, Y.N., Higashi, K.J., *Effects of Ca and Sr addition on Mechanical Properties of a Cast AZ91 Magnesium Alloy at Room and Elevated Temperature.* Materials Science and Engineering, 2005. **A403**: p. 276-280.
44. Vinod Kumar, G.S., Murty, B.S., Chakraborty, M., *Grain Refienment Response of LM25 Alloy Towards Al-Ti-C and Al-Ti-B Grain Refiners.* Journal of Alloys and Compounds, 2009. **472**.
45. Vinod Kumar, G.S., Murty, B.S., Chakraborty, M., *Development of Al-Ti-C Grain Refiners and Study of their Grain Refining Efficiency on Al and Al-7Si Alloy.* Journal of Alloys and Compounds, 2005. **396**: p. 143-150.
46. Pellini, W.S., *Strain Theory of Hot Tearing.* Foundry, 1952. **80**(11): p. 125-133.
47. Bracinni, M., Suéry, M., Stucky, M., *Influence of Grain Refinement on Hot-cracking in Aluminum-copper Alloys.* Fonderie-Fondeur d'Aujourd'hui, 2001. **208**: p. 12-24.
48. Lin, S., Aliravci, C., Pekguleryuz, M.O., *Hot-Tear Susceptibility of Aluminum Wrought Alloys and the Effect of Grain Refining.* Metallurgical and Materials Transactions A, 2007. **38A**.
49. Sadayappan, M., Sahoo, M., *Evaluation of the Hot Tearing Susceptibility of Selected Magnesium Casting Alloys in Permanent Molds.* AFS Transactions, 2007. **Vol. 111: 07-154**.
50. Cao, G., Kou, S., *Hot Tearing of Ternary Mg-Al-Ca Alloy Castings.* Metallurgical and Materials Transactions A, 2006. **37A**: p. 3647-3663.
51. Eskin, D.G., Suyitno, Katgerman, L., *Mechanical Properties in the Semi-solid State and Hot Tearing of Aluminum Alloys.* Progress in Materials Science, 2004. **49**: p. 629-711.
52. Metz, S.A., Flemings, M.C., *A Fundamental Study of Hot Tearing.* AFS Transactions, 1970: p. 453-460.
53. Suyitno, K., W.H., Katgerman, L., *Integrated Approach for Prediction of Hot Tearing.* Metallurgical and Materials Transactions A, 2009. **40A**.
54. Bichler, L., Elsayed, A., Lee, K., Ravindran, C., *Influence of Mold and Pouring Temperatures on Hot Tearing Susceptibility of AZ91D Magnesium Alloy.* International Journal of Metalcasting, 2008. **2**(1): p. 43-56.
55. Pekguleryuz, M.O., Vermette, P., *A Study on Hot-Tear Resistance of Magnesium Diecasting Alloys.* AFS Transactions, 2006.
56. Karunakar, D.B., Rai, R.M., Patra, S., Datta, G.L., *Effects of Grain Refinement and Residual Elements on Hot Tearing in Aluminum Castings.* International Journal of Advanced Manufacturing Technology, 2009: p. 851-858.
57. Datta, G.L., Karunakar, D.B., *A study on the Hot Tearing in Al-1wt.% Sn Cast Alloys.* Proceedings of the Institution of Mechanical Engineers, Part B: Journal of Engineering Manufacture, 2006. **220(7)**: p. 1131-1139.
58. D'Elia, F., Ravindran, C., *Effect of Ti-B Grain Refiner on Hot Tearing in Permanent Mold Cast B206 Aluminum Alloy.* AFS Transactions, 2009. **Vol. 113: 09-055**.

59. Zheng, W., Li, S., Tang, B., Zeng, D., Guo, X., *Effect of Rare Earths on Hot Cracking Resistant Property of Mg-Al Alloys.* Journal of Rare Earths, 2006: p. 346-351.
60. Elsayed, A., Lee, K., Ravindran, C., *Effect of Ca and Mn Additions on the Castability and Mechanical Properties of AZ91D Mg Alloy Permanent Mold Castings.* AFS Transactions, 2009. **Vol. 113: 09-085**.
61. Kori, S.A., *Studies on the Grain Refinement and Modification of Some Hypoeutectic and Eutectic Al-Si Alloys*, in *Metallurgical and Materials Engineering*. 2000, Indian Institute of Technology - Kharagpur. Ph.D Thesis.
62. D'Elia, F., *A Study on Grain Refinement and Hot Tearing in Permanent Mould Cast Aluminum Alloys*, in *Mechanical and Industrial Engineering*. 2009, Ryerson University: Toronto. p. 96. M.A.Sc. Thesis.
63. Bichler, L., *Phenomenological Studies of Hot Tearing During Solidification of Magnesium Alloys*, in *Mechanical and Industrial Engineering*. 2009, Ryerson University: Toronto. p. 367. Ph.D Thesis.
64. Fjellstedt, J., Jarfors, A.E.W., Svendsen, L., *Experimental Analysis of the Intermediary Phases AlB_2, AlB_{12} and TiB_2 in the Al-B and Al-Ti-B Systems.* Journal of Alloys and Compounds, 1999. **283**: p. 192-197.
65. Kellie, J., Wood, J., *Reaction Processing in the Metals Industry.* Materials World, 1995. **3**(1): p. 10-12.
66. Mohanty, P.S., Guthrie, R.I.L., Gruzleski, J.E., *Studies on the Fading Behaviour of Al-Ti-B Master Alloys and Grain Refinement Mechanism Using LiMCA.* Light Metals: Proceedings of Sessions, TMS Annual Meeting (Warrendale, Pennsylvania) 1995: p. 859-868.

APPENDICES

A.1 Al-1Ti-3B Grain Refiner Preparation Sample Calculation

A sample calculation for the preparation of 1000 g of Al-1Ti-3B grain refiner is described below [61]. The following materials are required:

- Potassium titanium fluoride (K_2TiF_6)
- Potassium fluoroborate (KBF_4)
- Commercial Purity Al

Addition of Ti (K_2TiF_6):

- 1g Ti is equivalent to 5.012 g of K_2TiF_6
- 1000 g of Al-1Ti-3B grain refiner contains 10 g of Ti
- 10 g of Ti is equivalent to 10 X 5.012 g = 50.12 g of K_2TiF_6

Assume 20 % loss:

- Required amount of K_2TiF_6 is 1.2 X 50.12 g = 60.1 g

Addition of B (KBF_4):

- 1 g of B is equivalent to 11.646 g of KBF_4
- 1000 g of Al-1Ti-3B grain refiner contains 30 g of B
- 30 g of B is equivalent to 30 X 11.646 g = 349.38 g of KBF_4

Assume 20 % loss:

- Required amount of KBF_4 is 1.2 X 349.38 g = 419.2 g

Al content:

- 1000 g of Al-1Ti-3B grain refiner contains 960 g of Al

Assume loss of 3.4 % (Al_2O_3 and $KAlF_4$ formation)

- Required amount of Al is 1.034 X 960 g = 992.6 g of Al

Therefore, the charge required to produce 1000g of Al-1Ti-3B is:

- **60.1 g of K_2TiF_6**
- **419.2 g of KBF_4**
- **992.6 g of Al**

A.2 Grain Refiner Addition Sample Calculation

A sample calculation for the preparation of 1000 g of AZ91E + 1.0 wt.% Al-1Ti-3B is described below. An equation for the amount of Al-1Ti-3B addition required to obtain a concentration of 1.0 wt.% can be described as:

$$\frac{x}{x+1000\ g} = 1.0\ \% \div 100$$

With x being amount in grams of Al-1Ti-3B addition. Rearranging for x yields:

$$(1-0.01)x = 10\ g$$

Solving for x results in:

$$x = 10.10\ g$$

Therefore, the addition of 10.10 g of Al-1Ti-3B to 1000 g of AZ91E will result in an AZ91E + 1.0 wt.% Al-1Ti-3B alloy.

A.3 Analysis of Variance (ANOVA) of Grain Size Measurements

An ANOVA examination of the grain size measurements in Parts I and II was undertaken to determine the maximum confidence level for which the following three null hypotheses could be tested:

1) The mean grain sizes with increasing addition level remain the same (Part I).
2) The mean grain sizes with increasing holding time remain the same (Part I).
3) The mean grain sizes of the permanent mould castings treated with Al-5Ti-1B and Al-1Ti-3B are the same as the base AZ91E casting (Part II).

Part I: Grain Refinement and Fading Experiments

AZ91E + Al-5Ti-1B

This case represents a two factor experiment with no replications. Addition level and holding time were the two factors under consideration. The raw data are presented in Table A-1.

Table A-1: Two Factor Experiment (Part I: AZ91E + Al-5Ti-1B)

Holding Time (min) / Addition Level (wt.%)	5	10	20	Holding Time Mean
0	1000 +/- 131	1000 +/- 131	1000 +/- 131	1000
0.1	323 +/- 59	306 +/- 44	291 +/- 43	307
0.2	341 +/- 67	400 +/- 80	420 +/- 65	387
0.5	767 +/- 158	817 +/- 213	810 +/- 95	798
1.0	668 +/- 118	756 +/- 160	810 +/- 117	745
Addition Level Mean	620	656	666	647

Table A-2: Analysis of Variance (Part I: AZ91E + Al-5Ti-1B)

Source of Variation	Sum of Squares	Degree of Freedom (v)	Mean-Square Value	F (v_1, v_2)
Between Addition Levels	1020117	4	255029	211 (4,8)
Between Holding Times	5981	2	2990	2.475 (2,8)
Residual	9666	8	1208	
Total	1035766	14		

For the null hypothesis, the mean grain size with increasing addition level remains the same:

F = 211, with $v_1 = 4$ and $v_2 = 8$.

Gives $P_{max} > 99.9$ % ($P_{max} > 90$ %, reject null hypothesis)

Therefore, the addition level has a very significant effect on grain size for the AZ91E + Al-1Ti-3B castings.

For the null hypothesis, the mean grain size with increasing holding time remains the same:

F = 2.475, with $v_1 = 2$ and $v_2 = 8$.

Gives $P_{max} \sim 83$ % ($P_{max} < 85$ %, accept null hypothesis)

Therefore, the holding time does not have a significant effect on grain size for the AZ91E + Al-5Ti-1B castings.

AZ91E + Al-1Ti-3B

This case represents a two factor experiment with no replications. Addition level and holding time are the two factors under consideration. The raw data are presented in Table A-3.

Table A-3: Two Factor Experiment (Part I: AZ91E + Al-1Ti-3B)

Holding Time (min) / Addition Level (wt.%)	5	10	20	Holding Time Mean
0	1000 +/- 131	1000 +/- 131	1000 +/- 131	1000
0.1	522 +/- 91	835 +/- 128	814 +/- 126	724
0.2	638 +/- 124	806 +/- 157	787 +/- 152	744
0.5	436 +/- 84	430 +/- 69	523 +/- 128	463
1.0	361 +/- 67	366 +/- 54	394 +/- 65	374
Addition Level Mean	591	687	704	661

Table A-4: Analysis of Variance (Part I: AZ91E + Al-1Ti-3B)

Source of Variation	Sum of Squares	Degree of Freedom (v)	Mean-Square Value	F (v_1, v_2)
Between Addition Levels	741129	2	185282	31.35 (4,8)
Between Holding Times	36868	3	18434	3.11 (2.8)
Residual	47270	6	5908	
Total	825268	11		

For the null hypothesis, all the addition level means are the same:

F = 31.35, with $v_1 = 4$ and $v_2 = 8$.

P_{max} > 99.9 % (P_{max} > 90 %, reject null hypothesis)

Therefore, the addition level has a very significant effect on grain size for the AZ91E + Al-1Ti-3B Castings.

For the null hypothesis, all the holding time means are the same:

F = 3.11, with $v_1 = 2$ and $v_2 = 8$.

P_{max} ~ 90 % (P_{max} ~ 90 %, no decision can be made)

Therefore, no decision can be made regarding the significance of holding time on grain size for the AZ91E + Al-1Ti-3B castings. It is expected that any effect of holding time on grain size is very small, indicating a good resistance to fading.

Part II: Hot Tearing Susceptibility Experiments

AZ91E and AZ91E + 0.2 wt.%Al-5Ti-1B

This case represents a one factor experiment. Only Al-5Ti-1B addition is under consideration. The raw data are presented in Table A-5.

Table A-5: One Factor Experiment (Part II: AZ91E + 0.2 wt.% Al-5Ti-1B)

Trial / Addition Level (wt.%)	1	2	Average Grain Size
0	117	109	113 +/- 5
0.2	105	89	97 +/- 11
Total Mean			105

Table A-6: Analysis of Variance (Part II: AZ91E + 0.2 wt.% Al-5Ti-1B)

Source of Variation	Sum of Squares	Degree of Freedom (v)	Mean-Square Value	F (v_1, v_2)
Between Addition Levels	240	1	240	2.78 (1,2)
Residual	172	2	86	
Total	413	3		

For the null hypothesis, all the addition level means are the same:

F = 2.78, with $v_1 = 1$ and $v_2 = 2$.

P_{max} ~ 75 % (P_{max} < 85 %, accept null hypothesis)

Therefore, the addition of 0.2 wt.% Al-5Ti-1B did not significantly decrease the grain size.

AZ91E and AZ91E + 1.0 wt.%Al-1Ti-3B

This case represents a one factor experiment. Only Al-1Ti-3B addition is under consideration. The raw data are presented in Table A-7.

Table A-7: One Factor Experiment (Part II: AZ91E + 1.0 wt.% Al-1Ti-3B)

Trial / Addition Level (wt.%)	1	2	Average Grain Size
0	117	109	113 +/- 5
1.0	74	72	73 +/- 2
Total Mean			93

Table A-8: Analysis of Variance (Part II: AZ91E + 1.0 wt.% Al-1Ti-3B)

Source of Variation	Sum of Squares	Degree of Freedom (v)	Mean-Square Value	F (v_1, v_2)
Between Addition Levels	1557	1	1557	86.65 (1,2)
Residual	35	2	17	
Total	1593	3		

For the null hypothesis, all the addition level means are the same:

F = 86.65, with $v_1 = 1$ and $v_2 = 2$.

P_{max} ~ 98.4 % (P_{max} > 90 %, reject null hypothesis)

Therefore, the was a significant effect on grain size with the addition of 1.0 wt.% Al-1Ti-3B.

A.4 Cooling Curves

Cooling curves for all the addition levels of Al-5Ti-1B and Al-1Ti-3B for Part I are presented below.

Part I: Grain Refinement and Fading Experiments

AZ91E + Al-5Ti-1B:

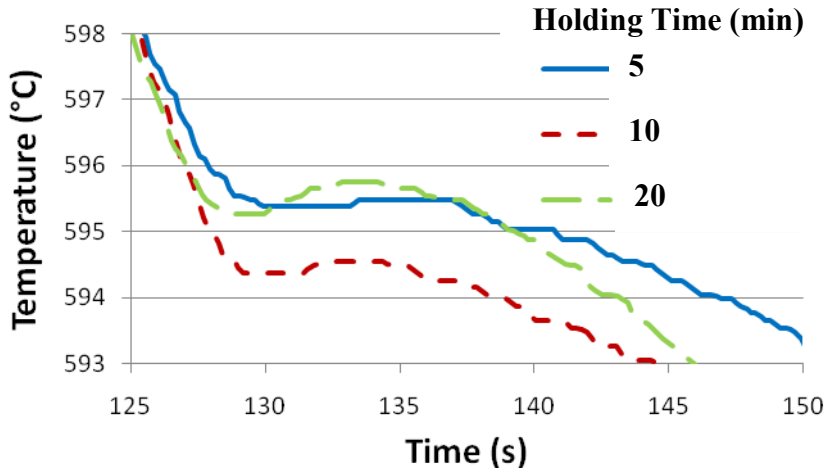

Figure A-1: Cooling Curve of AZ91E + 0.1 wt.% Al-5Ti-1B

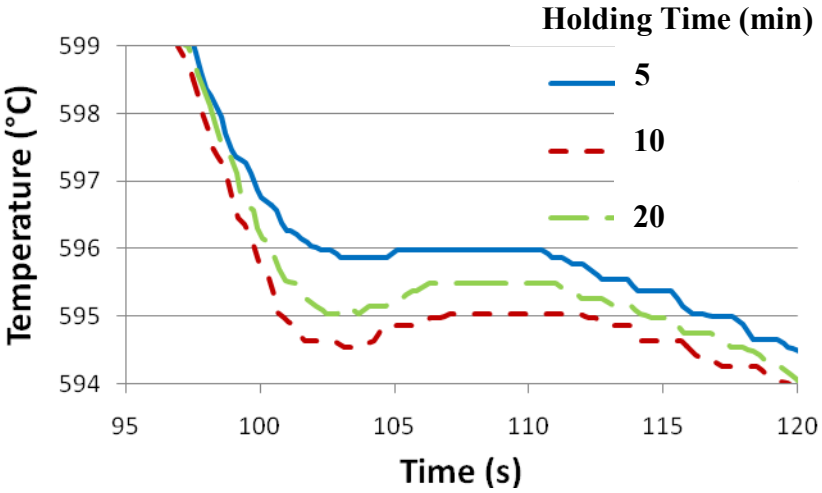

Figure A-2: Cooling Curve of AZ91E + 0.2 wt.% Al-5Ti-1B

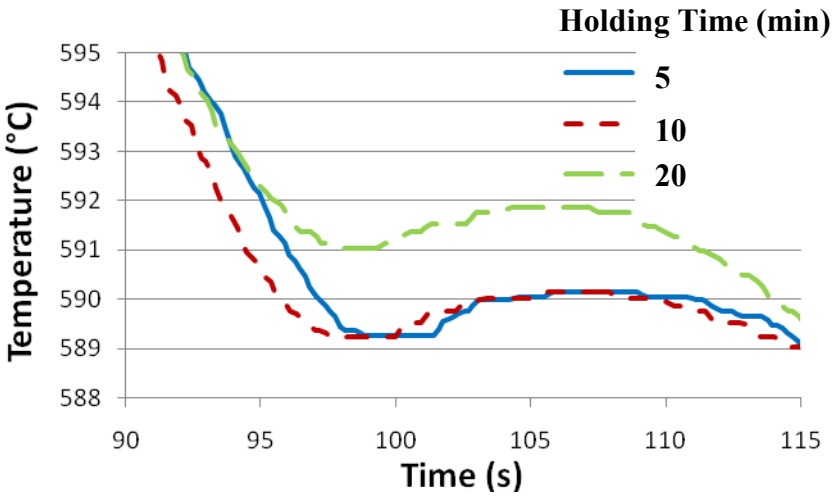

Figure A-3: Cooling Curve of AZ91E + 0.5 wt.% Al-5Ti-1B

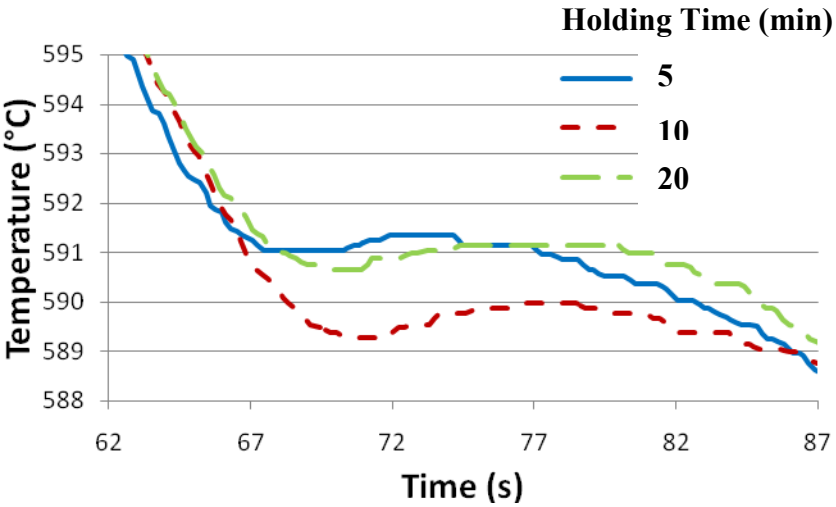

Figure A-4: Cooling Curve of AZ91E + 1.0 wt.% Al-5Ti-1B

AZ91E + Al-1Ti-3B:

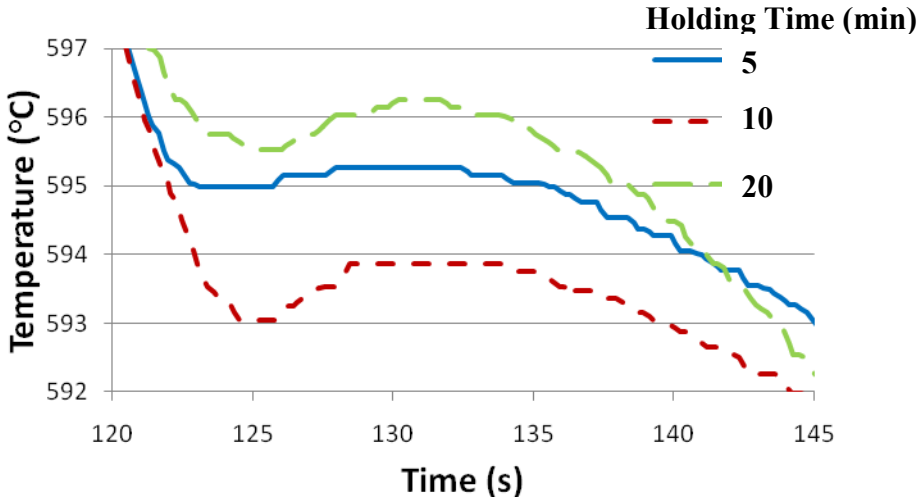

Figure A-5: Cooling Curve of AZ91E + 0.1 wt.% Al-1Ti-3B

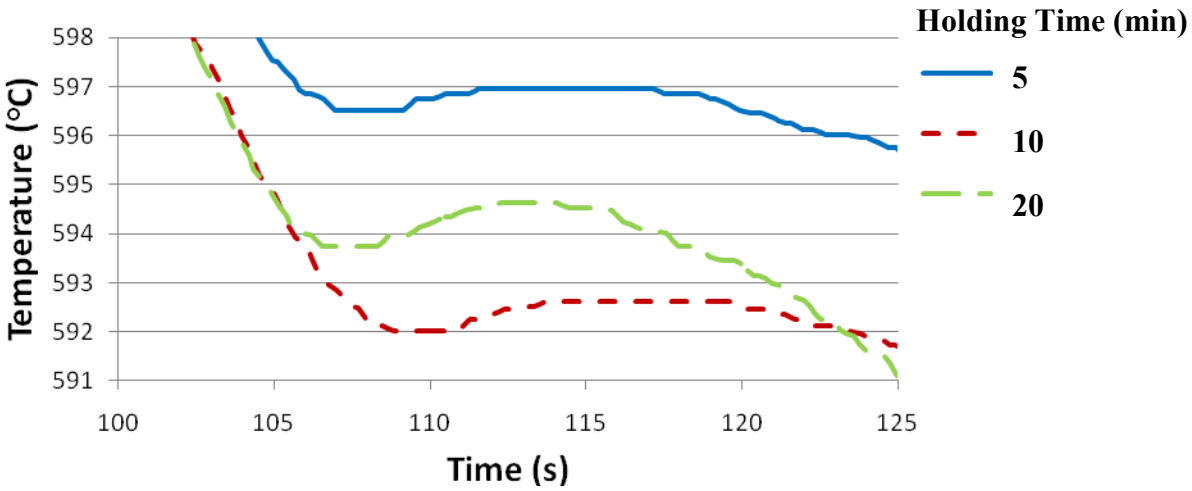

Figure A-6: Cooling Curve of AZ91E + 0.2 wt.% Al-1Ti-3B

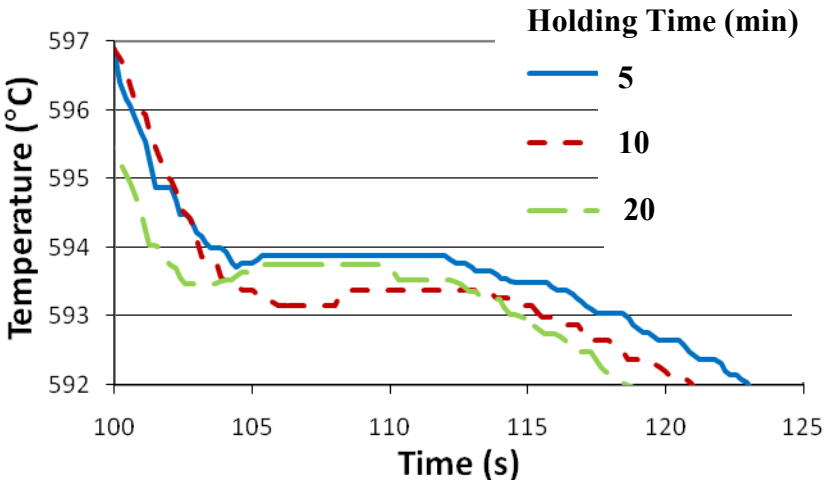

Figure A-7: Cooling Curve of AZ91E + 0.5 wt.% Al-1Ti-3B

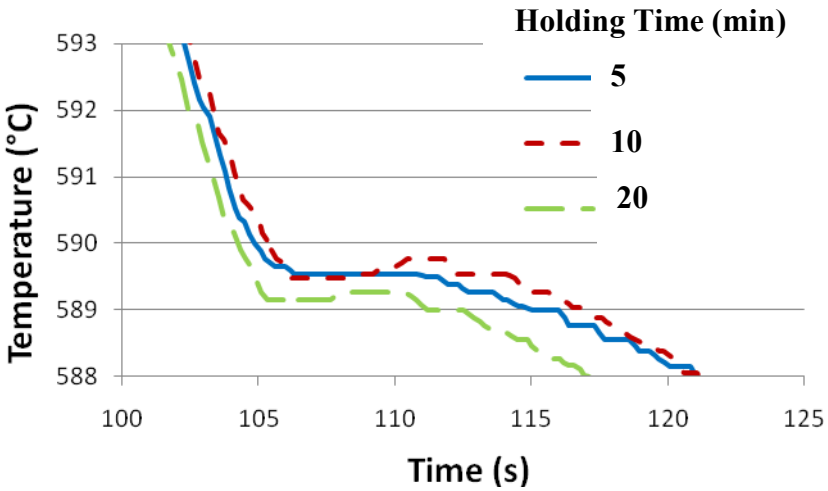

Figure A-8: Cooling Curve of AZ91E + 1.0 wt.% Al-1Ti-3B

Part II: Hot Tearing Susceptibility Experiments

The cooling curves for the permanent mould castings for all the locations along the casting bar are presented below. The first cooling curve is the permanent mould casting of AZ91E. The next two cooling curves are for AZ91E + 0.2 wt.% Al-5Ti-1B and AZ91E + 1.0 wt.% Al-1Ti-3B, respectively.

AZ91E

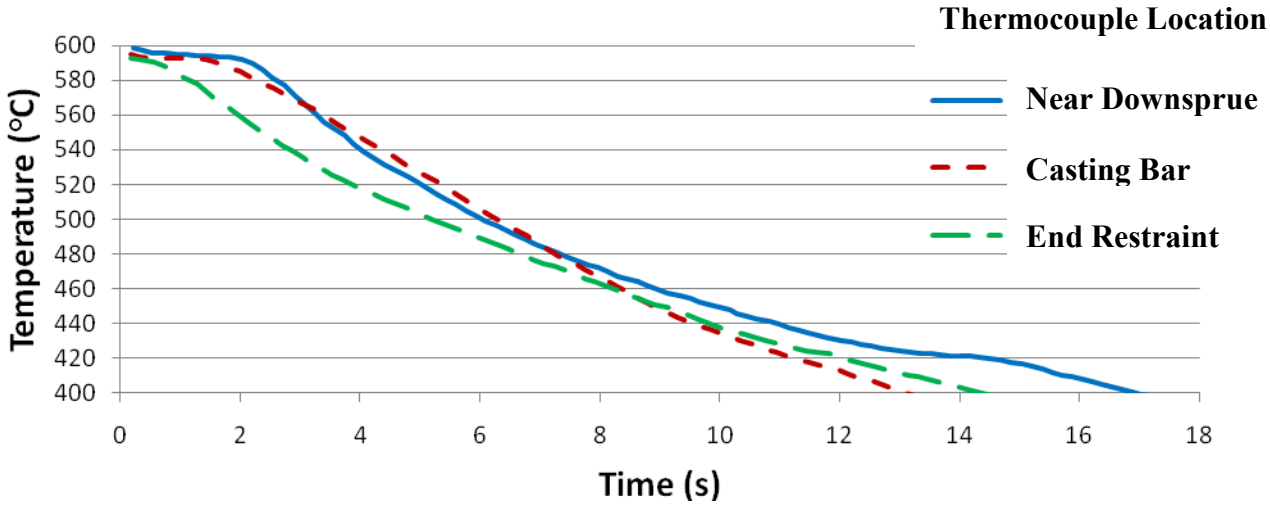

Figure A-9: Cooling Curve of Permanent Mould Cast AZ91E

AZ91E + 0.2 wt.% Al-5Ti-1B

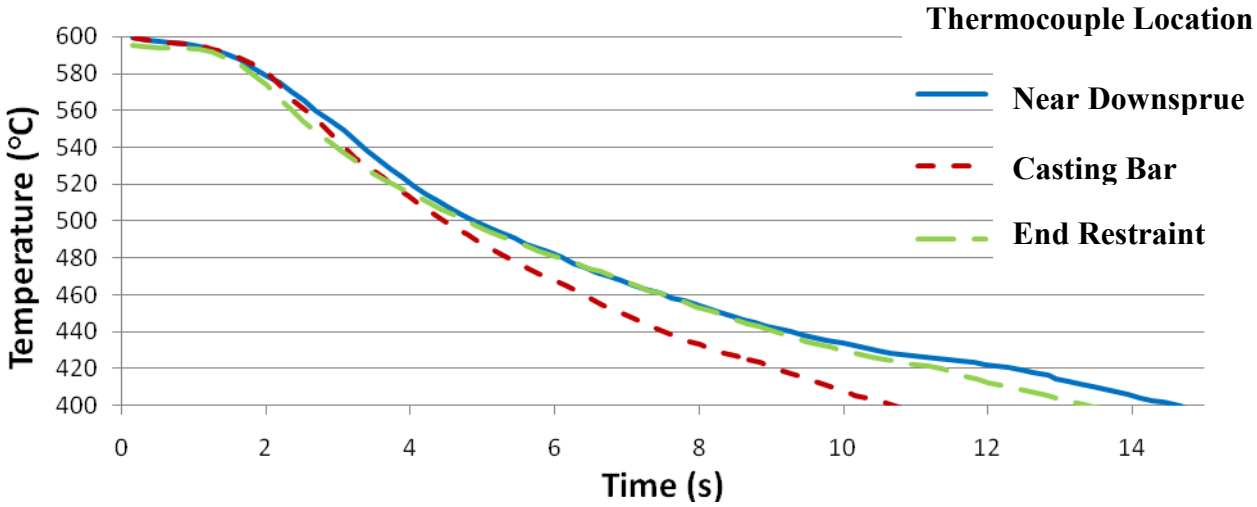

Figure A-10: Cooling Curve of Permanent Mould Cast AZ91E + 0.2 wt.% Al-5Ti-1B

AZ91E + 1.0 wt.% Al-1Ti-3B

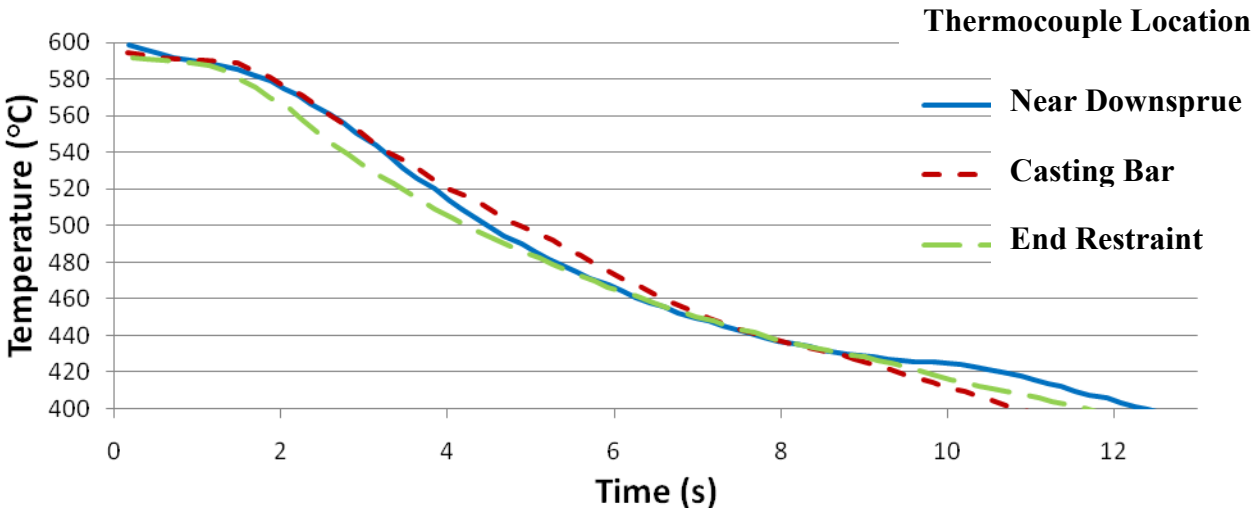

Figure A-11: Cooling Curve of Permanent Mould Cast AZ91E + 1.0 wt.% Al-1Ti-3B

A.5 Mg-Al Phase Diagram

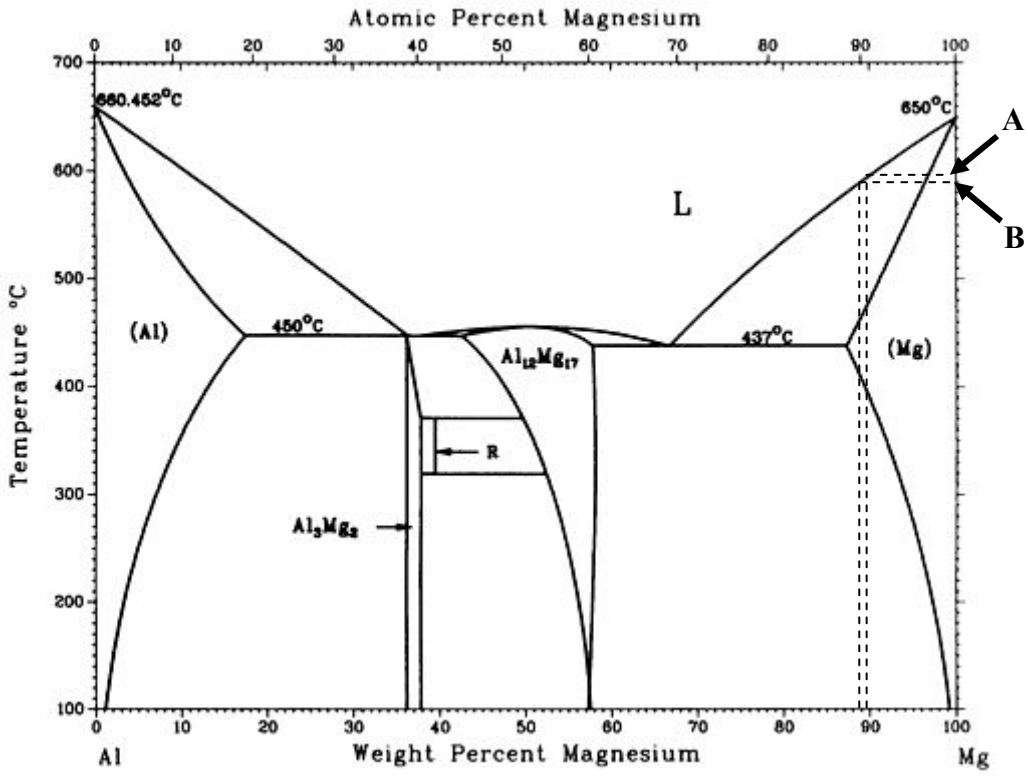

Figure A-12: Mg-Al Phase Diagram [1]

Description of Points:

A: Nucleation temperature of AZ91E,

- 596.2 °C under equilibrium conditions

B: Nucleation temperature of AZ91E + 1.0 wt.% Al-5Ti-1B, AZ91E + 1.0 wt.% Al-1Ti-3B and AZ91E + 0.8 wt.% Al

- 590 °C under equilibrium conditions